

Dynamic organization and interactions of plasmalemmal  
SNARE proteins studied in plasma membrane sheets and  
live cells

Dissertation  
zur  
Erlangung des Doktorgrades (Dr. rer. nat.)  
der  
Mathematisch-Naturwissenschaftlichen Fakultät  
der  
Rheinischen Friedrich-Wilhelms-Universität Bonn

vorgelegt von  
Nagaraj D. Halemani  
aus  
Bangalore India

Bonn 2010

Angefertigt mit Genehmigung der Mathematisch-  
Naturwissenschaftlichen Fakultät der Rheinischen Friedrich-Wilhelms-  
Universität Bonn

1. Gutachter: Prof. Dr. rer. nat. Thorsten Lang

2. Gutachter: Prof. Dr. rer. nat. Christoph Thiele

Tag der Promotion: 09. März 2011

Erscheinungsjahr: 2012

## **Abstract**

All Eukaryotic cells and their internal organelles are surrounded by membranes. Many cellular functions involve transport of material between membrane bound compartments initiated by a fusion step of respective membranes. One example is regulated exocytosis during which cellular secretion at the plasma membrane is spatially restricted and temporally controlled. This complex process requires a multitude of molecular players, for instance, neuronal SNARE (Soluble N-ethylmaleimide-sensitive-factor Attachment Receptor) proteins, namely, SNAP-25 and syntaxin 1 on the pre-synaptic membrane and synaptobrevin from the vesicular membrane. All three SNARE proteins come together to form a four helical bundle to drive the fusion of two opposing membranes and thereby mediate the release of vesicular contents into the synaptic cleft.

Assembly of SNARE proteins occurs in a sequential manner, beginning with the formation of an initial intermediate involving interaction between the plasma membrane SNAREs, SNAP-25 and syntaxin 1. A wide variety of studies have reported a possible set of initial intermediate complexes regulated by accessory proteins. But the exact nature of the physiological intermediates in the SNARE assembly pathway has been elusive.

In this work, the existence of such initial intermediates has been studied – FRAP (Fluorescence Recovery After Photobleaching) has been applied to study protein interactions in live cells complemented by biochemical studies using plasma membrane sheets and analysis of their spatial organization by super resolution microscopy. In addition, it has been tested how divalent cations influence the organization of membrane proteins. The two SNARE proteins, SNAP-25 and syntaxin 1, known to be organized into separate clusters, were found to be subjected to regulation by non specific electrostatic interactions mediated by the divalent cation calcium. More importantly, the neuronal SNAREs syntaxin 1 and SNAP-25 interact at the interface of their respective protein clusters to form an initial intermediate, involving only the N-terminal SNARE motif of SNAP-25 and SNARE motif of syntaxin 1, independent of any neuronal co-factors. The intermediate complex seems to be fully zippered all along the SNARE motifs and highly dependent on the position and orientation of the SNARE motifs involved.

The observed complex is different from the ones reported by numerous *in vitro* studies. The existence of such an intermediate complex in live cells is a consequence of specific organization of the two SNARE proteins into clusters on the plasma membrane with different mechanisms which results in an excess of active SNAP-25 relative to syntaxin 1.

Our study highlights the importance of studying membrane proteins and their interactions in their native environment as the membrane seems to exert a multi component regulation on its constituent proteins.

## Table of Contents

<b>1. Introduction</b>	01
<b>Prologue</b>	01
<b>1.1. Biological membranes - structure and composition</b>	01
<b>1.2. Membrane fusion</b>	03
1.2.1. Molecular components of membrane fusion	06
1.2.2. SNAREs – Diversity and their fusion specificity	07
1.2.3. A special case - Neuronal exocytosis	08
1.2.4. Membrane microdomains - SNARE protein clusters	08
<b>1.3. The neuronal SNAREs</b>	09
1.3.1. SNAP-25 (Q <sub>b</sub> Q <sub>c</sub> – SNARE)	11
1.3.2. Syntaxin 1 (Q <sub>a</sub> – SNARE)	12
1.3.3. Synaptobrevin 2 (R – SNARE)	13
1.3.4. The SNARE-cycle	14
1.3.4. 1. SNARE complex assembly and disassembly	14
1.3.4. 2. The SNARE interacting proteins	16
<b>1.4. Putative intermediate SNARE-complexes on the pathway to membrane fusion</b>	18
1.4.1. Binary SNARE interactions	18
1.4.1.1. Syntaxin 1- synaptobrevin interaction	18
1.4.1.2. SNAP-25 - synaptobrevin interaction	18
1.4.1.3. Syntaxin 1 - SNAP-25 interaction	19
1.4.2. Ternary SNARE-interactions	20
<b>1.5. Aims of the studies</b>	23
1.5.1. Structure and dynamics of SNAP-25 (Q <sub>b</sub> Q <sub>c</sub> ) and syntaxin 1 (Q <sub>a</sub> ) interaction in live cells	23
1.5.2. Membrane organization of SNAP-25 and syntaxin 1	23

<b>2. Materials and Methods</b>	24
<b>2.1. Cloning - Plasmid DNA constructs</b>	24
2.1.1. SNAP-25 constructs	24
2.1.2. Syntaxin constructs	25
<b>2.2. Cell culture</b>	25
2.2.1. Coating of glass coverslips	25
2.2.2. Cell culture and propagation of PC12 and BHK cells	26
2.2.3. Transient transfection of PC12 and BHK cells	26
<b>2.3. Plasma membrane sheet assay</b>	27
2.3.1. Generation of plasma membrane sheets	27
2.3.2. Incubation of plasma membrane sheets with nanomolar calcium	27
2.3.3. Immunostaining of plasma membrane sheets	28
2.3.4. Recombinant syntaxin1A binding using BHK cell plasma membrane sheets	29
2.3.5. Fluorescence microscopic imaging of plasma membrane sheets	29
2.3.6. Fluorescence microscopy - Image analysis	30
<b>2.4. FRAP (Fluorescence Recovery After Photobleaching) on live Cells</b>	31
2.4.1. Sample preparation	31
2.4.2. Confocal microscopy for FRAP	31
2.4.3. FRAP data analysis	32
<b>2.5. STED - (Stimulated Emission Depletion) Microscopy</b>	33
2.5.1. STED sample preparation	33
2.5.1.1. Sample preparation for SNAP-25 cluster morphology and co-localisation studies	33
2.5.1.2. Sample preparation for syntaxin1 cluster morphology after cholesterol depletion	34
2.5.2. STED microscopic imaging	35

2.5.3. STED image analysis for SNAP-25 cluster morphology and co-localisation studies	36
<b>2.6. Depolarisation of bovine chromaffin cells</b>	<b>36</b>
2.6.1. Sample preparation - stimulation and immunostaining of bovine chromaffin cells	36
2.6.2. Confocal microscopic imaging	37
2.6.3. Analysis of confocal images of bovine chromaffin cells	38
<b>3. Results</b>	<b>39</b>
3.1. Generation of GFP-SNAP-25 plasmid DNA constructs	39
3.2. Biochemical analysis of GFP-SNAP-25 expression in PC12 cells	41
3.3. Setting up the FRAP assay	43
<b>3.4. Studying the Q - SNARE interactions through FRAP and membrane sheet binding studies</b>	<b>44</b>
3.4.1. Structure and dynamics of Q-SNARE-interactions – a Q <sub>a</sub> Q <sub>b</sub> -SNARE complex formation as revealed by FRAP studies	45
3.4.1.1. N-terminal SNARE motif is required for complex formation	45
3.4.1.2. Co-overexpressed syntaxin1 decreases SNAP-25 mobility manifold	46
3.4.1.3. Position of the N-terminal SNARE motif is important for efficient syntaxin interaction	50
3.4.1.4. Most of the N-terminal SNARE motif is required for SNAP-25 mobility restriction	52
3.4.1.5. Alpha helical conformation of the N-terminal SNARE motif is required for SNAP-25 mobility restriction	55
3.4.1.6. Correlation of expression levels and maximal recovery and half time	58
3.4.1.7. Restricted SNAP-25 mobility through non-cognate SNARE interactions using syntaxin 4 as an example	60

3.4.1.8. The restricted SNAP-25 mobility through syntaxin 1 interactions does not require any neuronal co-factors	62
3.4.2. Syntaxin 1- SNAP-25 interactions studied in native plasma membrane sheets	64
3.4.2.1. Soluble syntaxin 1 readily reacts with N-terminal SNARE motif of SNAP-25	65
3.4.2.2. Soluble syntaxin 1 binds N-terminal SNARE motif efficiently only when it is at the N-terminus of SNAP-25	67
<b>3.5. Nanoscale organisation of SNAP-25 and syntaxin 1 in the plasma membrane</b>	69
3.5.1. SNAP-25 cluster morphology is independent of its SNARE motifs	69
3.5.2. SNAP-25 and syntaxin1 form distinct but close clusters	72
3.5.3. SNAP-25 and syntaxin 4 clusters are more distant than the SNAP-25 and syntaxin 1 clusters	74
3.5.4. Overlap between SNAP-25 and syntaxin 1 upon SNARE complex formation	77
3.5.5. Effect of cholesterol depletion on syntaxin1 cluster morphology	83
<b>3.6. Ca<sup>2+</sup> induced remodelling of membrane proteins</b>	85
3.6.1. Influence of Mg <sup>2+</sup> ions and the incubation process on the organization of membrane proteins	87
3.6.2. Direct modulation of membrane protein organization by Ca <sup>2+</sup>	88
3.6.3. Calcium induced remodelling of membrane proteins under physiological conditions	91
<b>4. Discussion</b>	94
4.1. SNARE protein organization on the plasma membrane	94
4.2. Calcium induced remodelling of membrane proteins	96



4.3. Structure and dynamics of syntaxin 1 (Q <sub>a</sub> ) and SNAP-25 (Q <sub>b</sub> Q <sub>c</sub> ) interaction in live cells	97
4.3.1. Q <sub>a</sub> Q <sub>b</sub> SNARE complex formation predominates in live cells	97
4.3.2. The Q <sub>a</sub> Q <sub>b</sub> SNARE complex in live cells is most likely zippered all along its length	100
4.3.3. Do syntaxin clusters represent sites of Q-SNARE complex formation?	101
4.4. FRAP as a method to measure protein-protein interactions in live cells	102
4.5. Conclusions	104
<b>5. Bibliography</b>	<b>105</b>
<b>6. List of Abbreviations</b>	<b>125</b>
<b>7. List of Figures</b>	<b>128</b>
<b>8. List of Tables</b>	<b>131</b>
<b>9. Curriculum Vitae (in brief)</b>	<b>132</b>
<b>10. Appendix</b>	<b>133</b>

## **1. Introduction**

### **Prologue**

Cells are the basic structural and functional units of life, separated from their surroundings by a semi permeable membrane. Eukaryotic cells differ from prokaryotic cells by having their internal organelles bound by a membrane which serves a diverse set of functions through its unique structure. These membrane bound organelles communicate with each other in a spatial and temporal fashion to carry out the cellular functions like protein and lipid trafficking in and out of the cell. The entire process of inter organelle communication begins from identification and tethering to each other eventually proceeding to fusion of two membranes and mixing of their content material. Extensive studies in the last few decades enabled the identification of the events in the process and a better understanding of the associated molecular players is slowly emerging. An evolving conceptual understanding of the dynamical nature of the biological membranes has far reaching implications as far as understanding the life in general is concerned.

### **1.1. Biological Membranes - Structure and Composition**

Biological membranes are basically matrices of lipid bilayers with freely diffusing membrane proteins (Singer and Nicolson, 1972) (see Figure 1 a). Plasma membrane is composed of various species of phospholipids and sphingolipids (van Meer et al., 2008). The amphipathic phospholipids self orient into exterior hydrophilic heads and interior hydrophobic tails formed by diacylglycerol (DAG) chains. Some of the major glycerophospholipids in the membrane are: phosphatidylcholine (PC) phosphatidylethanolamine (PE), phosphatidylinositol (PI), phosphatidylserine (PS). Sphingolipids such as sphingomyelin and glycosphingolipids contain ceramide as hydrophobic backbone. The sphingolipids accommodate cholesterol molecules within thereby rendering the membrane more fluid (van Meer et al., 2008).

Biological membranes though appear to be the most simple of all cellular structures, our understanding of their precise composition, molecular organization and their functional significance is still an ongoing effort. Although the Singer and Nicolson's fluid mosaic model of biological membranes put forth the general organization of proteins and lipids

within membranes, the model continues to undergo reassessment till today (Laude and Prior, 2004). For instance, the fluid mosaic model of membrane as originally proposed by Singer and Nicolson is laterally homogeneous and shows monomeric proteins freely diffusing in the sea of lipids. But, a bulk of evidence from comparison of diffusion coefficients of molecules in plasma membrane and artificial membranes/liposomes suggest that molecules in the plasma membrane do not enjoy free diffusion. The diffusion coefficients of the measured molecules in the plasma membrane were several orders of magnitude lower than that observed for the artificial membranes (Kusumi et al., 2005; Owen et al., 2009; Ritchie and Spector, 2007). The restricted diffusion has been shown to be due to lateral heterogeneity in the membrane organization created as a result of myriad of interactions between constituent lipids and proteins in time and space together with the underlying actin cytoskeletal network (Jacobson et al., 2007; Kusumi et al., 2005; Lommerse et al., 2004) According to the current model, biological membranes are heterogeneous structures with variable thickness and higher protein content than previously suggested (reviewed in (Engelman, 2005)) (see Figure 1 b). The organization of membrane components into micro domains like lipid rafts (Simons and Ikonen, 1997) and protein clusters (Lang, 2007; Lang and Rizzoli, 2010) and sub membranous cytoskeletal based ‘picket fences’ (Kusumi et al., 2005; Kusumi et al., 1993) contribute to the membrane heterogeneity. A brief overview on membrane microdomains with respect to membrane proteins, SNAREs (Soluble *N*-ethylmaleimide-sensitive factor Attachment protein Receptors) is provided in section 1.2.4.

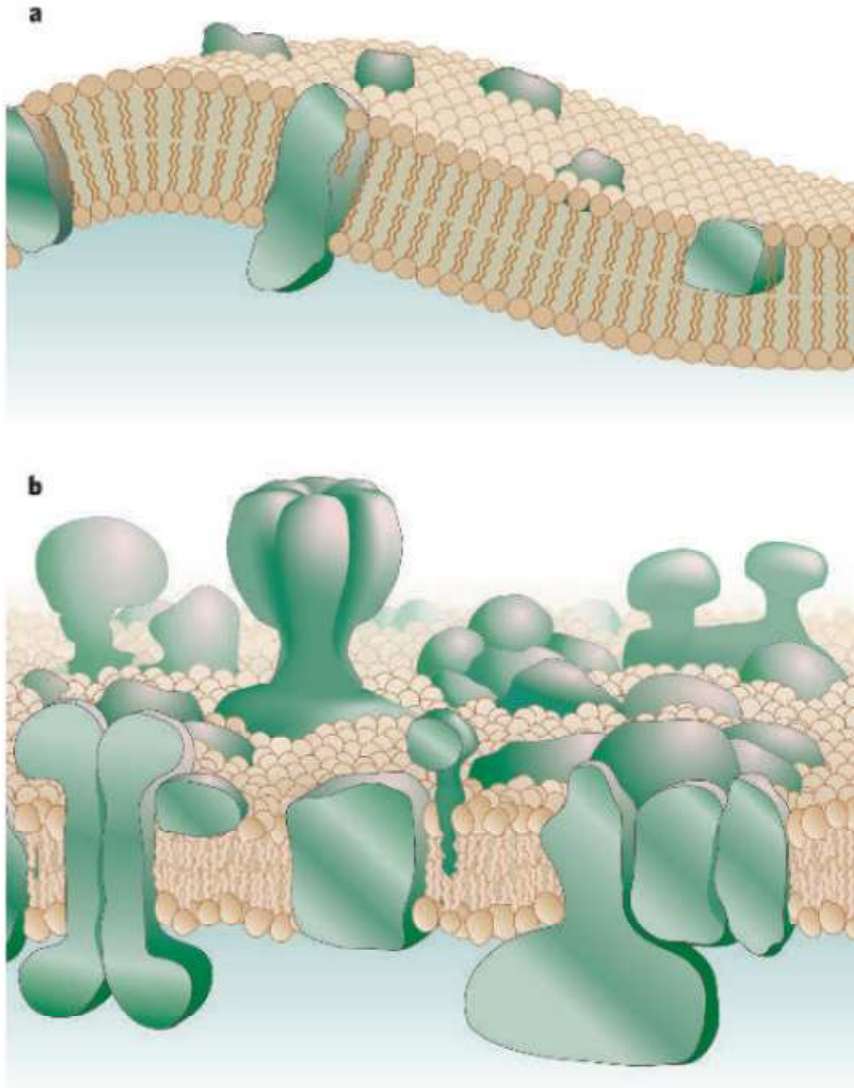


**Figure 1. Models for membrane structure.**

**a.** The Singer and Nicholson 'fluid mosaic model' depicts that the biological membranes are two-dimensional homogeneous structures with random diffusion of constituent proteins and lipids.

**b.** The current version of the model depicts a heterogeneous nature of membranes dominated by patches of proteins and variable thickness of the bilayer. [Figure taken from Engelman, \(2005\).](#)

## 1.2. Membrane fusion

Membrane enclosed organelles in eukaryotic cells exchange material through trafficking vesicles which bud from the precursor organelles and subsequently fuse with the target membrane. The two reactions, budding and fusion are carried out by highly conserved multi protein complexes in close interplay with the constitutive lipids (reviewed in (Jahn and Scheller, 2006; Lang, 2008)). Membrane fusion involves close apposition of

the two bilayers and their subsequent deformation and merger, achieved by the dynamic conformational changes in the membrane brought about by the lipids, proteins and the interplay between the two. By exploiting the very nature of lipids to spontaneously assemble, through hydrophobic effect, into bilayer structures such as liposomes and supported bilayers it was possible to dissect the sequence of events leading to bilayer mixing (Zimmerberg and Gawrisch, 2006) (see Figure 2 a).

Biological membrane fusion follows a series of steps, beginning with a contact of the two membranes destined to fuse. Once the membranes are brought into close proximity, the two apposing proximal leaflets establish a connection while the distant ones remain undisturbed with stalk like appearance, forming a hemifusion intermediate. The lateral expansion of the hemifusion intermediate gives rise to a fusion pore which leads to complete merger of the two leaflets thereby establishing an aqueous connection (Zimmerberg and Gawrisch, 2006; Jahn et al., 2003) (see Figure 2 a & b).

There are atleast three distinct examples of biological membrane fusion supposed to share some of the above mentioned features – 1) fusion of enveloped viruses such as influenza and HIV with host cell membrane, 2) cell-to-cell fusion as in fertilization and muscle syncytia formation and 3) intracellular fusion reactions like in protein trafficking, exocytosis and mitochondrial remodelling (Chernomordik and Kozlov, 2008; Jahn et al., 2003).

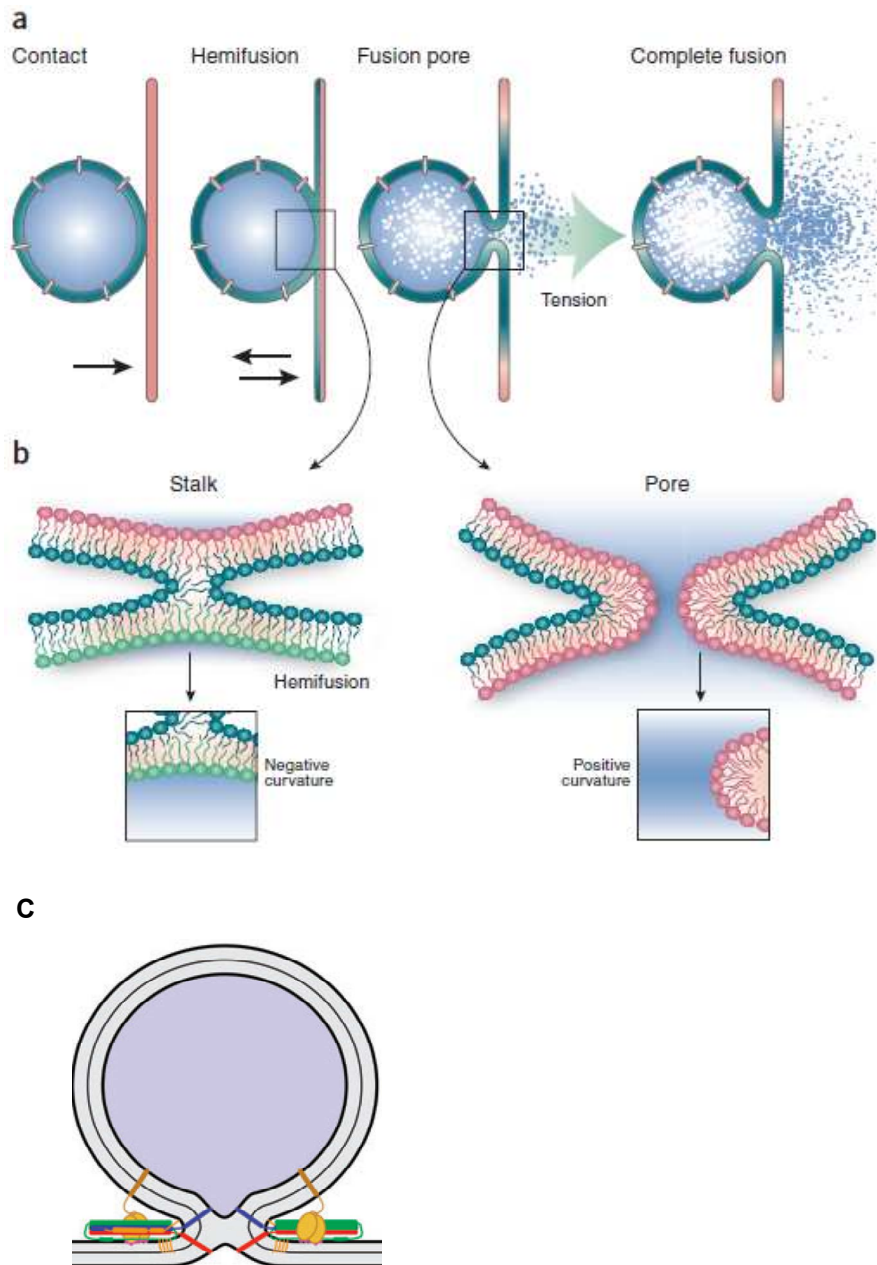


**Figure 2. Stages of membrane fusion.**

Biological membrane fusion is likely to proceed through intermediates, (a) hemifusion with stalk formation which through its lateral expansion results in (b) fusion pore formation. (c) SNARE mediated fusion between a secretory vesicle membrane and plasma membrane in neurosecretory cells. Synaptobrevin (blue) on vesicle membrane and SNAP-25 (green) / syntaxin (red) on target membrane assemble into a four helical *trans*-SNARE complex in the intermediate hemifusion state. With the entry of calcium, synaptotagmin (yellow) mediates the complete merger of the membranes resulting in the formation of a fusion pore which allows vesicular content release. See the text for details. Figure taken (a and b) from Zimmerberg and Gawrisch, (2006) and (c) from Sorensen, (2009).

### 1.2.1. Molecular components of membrane fusion

Membrane fusion involves at least three different steps – tethering/docking, priming, and fusion, brought about by a diverse set of constitutive lipids and proteins which overcome repulsive forces between two opposing bilayers (Chernomordik and Kozlov, 2008). Changes in membrane curvature brought about by effective molecular shapes of lipids influence membrane fusion. For instance, LPC (Lysophosphatidylcholine) and polyphosphoinositides tend to create a negative curvature on the membrane surface whereas PE (Phosphatidylethanolamine) and DAG (diacylglycerol) create a positive curvature (Chernomordik and Kozlov, 2008) (see Figure 2 b inset).

Apart from the role of lipids in the dynamics of fusion pore formation, the fusion specificity is mediated by a diverse family of proteins. Protein families and their respective cofactors involved in the different fusion steps are: Rab proteins, SM (Sec1/Munc18) and SNAREs (Soluble *N*-ethylmaleimide-sensitive factor Attachment protein Receptors) (Pfeffer, 1999; Jahn et al., 2003). Rab proteins constitute a family of conserved GTPases which are localized to different compartments. Rab GTPases and Rab effectors, through their interactions with tethering complexes, are involved in the regulation of tethering/ docking of vesicles to the target membrane (Pfeffer, 1999). Rab proteins are intimately linked to SNAREs (Novick and Zerial, 1997; Zerial and McBride, 2001) and by selectively localizing to certain compartments, both Rab and SNARE proteins in combination are believed to confer transport specificity (Mayer, 2001; Mayer, 2002). Once the membranes are brought closer, SNAREs acting in concert with SM proteins, drive the fusion process thereby resulting in the merging of two bilayers (see Figure 2 c). According to the SNARE hypothesis the SNARE proteins in opposing membranes (synaptobrevin on vesicle membrane and SNAP-25/syntaxin on the plasma membrane in neurosecretory cells) form a highly stable complex releasing free energy to overcome the energy barrier for the membrane fusion (Jahn and Scheller, 2006). Synaptobrevin on vesicle membrane and SNAP-25/syntaxin (t-SNAREs) on plasma membrane assemble into a *trans*-SNARE complex of four parallel helices (see Figures 2c and 8 A) that brings the two membranes together. However, the exact mechanism of how the energy released during SNARE complex formation is transmitted to the membranes is still being debated. A more recent X-ray crystal structure study of neuronal SNARE complex (that included linkers and TMRs of syntaxin 1 and synaptobrevin 2) (Stein et al., 2009) has shown that stiff helical bundles

from the regions involved in complex formation, continue all the way into the membranes and suggest a direct coupling of energy between the SNARE motifs and the transmembrane domains during membrane fusion ( Stein et al., 2009; Guzman et al., 2010) (see Figure 8 A). Although a reconstituted proteoliposome fusion assay demonstrated that SNAREs can act as minimal machinery for membrane fusion (Weber et al., 1998), they alone are not sufficient for the *in vivo* membrane fusion. SM (Sec1/Munc18) proteins are a family of cytosolic proteins that are involved in the regulation of membrane fusion steps (see also section 1.3.4.2). Through their interactions with syntaxins and t-SNARE complexes, SM proteins regulate SNARE complex formation and probably are involved in vesicle docking (Malsam et al., 2008; Sorensen, 2009).

### **1.2.2. SNAREs – Diversity and their fusion specificity**

SNARE proteins belong to a superfamily of small proteins with 25 members in yeast *S. cerevisiae*, 36 members in humans and 54 members in *A. thaliana* (Jahn and Scheller, 2006). They invariably contain a 60-70 residue long SNARE motif, arranged in heptad repeats spaced such that the adoption of an alpha-helical structure places all the relevant side chains on the same face of the helix (Ungar and Hughson, 2003). Most SNAREs are membrane anchored through transmembrane domain or lipid anchors.

Many SNAREs are selectively localized to specific subcellular compartments. For example, syntaxin -1, 2 & 4, SNAP-25, SNAP-23 are localized to the plasma membrane, synaptobrevin at the synaptic vesicles, and syntaxin-5 and VAMP4 in the Golgi apparatus (reviewed in (Hong, 2005)). However, their distribution is not strictly confined to these sites as the SNAREs involved in a particular pathway recycle between the compartments (Jahn and Scheller, 2006).

It is generally accepted that a specific combination of SNAREs participating in a particular fusion step of the secretory pathway contributes to the fusion specificity in the cell (Zerial and McBride, 2001). However, SNAREs can functionally replace each other to a varying degree since deletion of certain SNAREs in chromaffin cells (Borisovska et al., 2005; Delgado-Martinez et al., 2007) or depletion of endosomal SNAREs (Bethani et al., 2009) did not prevent the respective membrane fusion step. Recently, it has been suggested that intracellular fusion specificity is achieved through *trans*- configuration of



the cognate SNAREs in the opposing membranes probably assisted by accessory proteins like SM (Sec1/Munc18) proteins and lateral segregation of SNAREs at contact sites of fusing organelles (Bethani et al., 2007). Although there is currently no general explanation for the fusion specificity of cellular compartments, it is conceivable that there are numerous layers of regulation starting from tethers to SNAREs (Malsam et al., 2008).

### **1.2.3. A special case – Neuronal exocytosis**

Neuronal exocytosis at the synapse is an exquisitely regulated form of membrane fusion and attempts to understand the complexity of the process and its precise spatial and temporal regulation has shed light on the general mechanism of membrane fusion. Synaptic vesicles are docked at the active zone in the presynaptic membrane awaiting an action potential. Exocytosis is triggered within one millisecond of the  $\text{Ca}^{2+}$  ion influx that follows arrival of an action potential (Sudhof, 2004). Formation of neuronal SNARE complexes is central in the neuronal exocytosis and it is believed that many other proteins acting either simultaneously or sequentially interact with this complex to regulate its assembly at distinct steps towards membrane fusion. Munc18-1 is a SM (Sec1/Munc18) protein which plays a very important regulatory role in vesicle docking and SNARE complex assembly (Brunger, 2005; Toonen et al., 2006; Zilly et al., 2006; Sorensen, 2009). In the later stages of neuronal exocytosis particularly during the  $\text{Ca}^{2+}$ -triggered step of release, synaptotagmin-1 and complexin are known to be directly involved in the regulation of SNARE complex mediated membrane fusion (Rizo and Rosenmund, 2008). However, the precise nature of their interactions with the SNAREs and SNARE complex still remains unresolved. For further description and functional roles of the neuronal SNAREs, SNARE cycle and SNARE interacting proteins, please see the section 1.3.

### **1.2.4. Membrane Microdomains – SNARE protein clusters**

As mentioned in the section 1.1, a diverse array of interactions among membrane lipids and proteins create lateral heterogeneity in the plasma membrane. Predominant structures that compartmentalize the plasma membrane include lipid rafts (Simons and

Ikonen, 1997) and membrane cytoskeleton based picket fences (Kusumi et al., 1993). Lipid rafts, more appropriately called membrane rafts, are small (10-200 nm), heterogeneous, highly dynamic, sterol- and sphingolipid enriched domains (Pike, 2006). Membrane rafts are often found to be segregated with membrane protein clusters (Laude and Prior, 2004) and serve as platforms for cell signaling (Simons and Toomre, 2000) and are involved in the regulation of membrane protein trafficking and secretory vesicle biogenesis (Tooze et al., 2001). Studies have demonstrated that the SNARE proteins are associated with lipid rafts (Chamberlain et al., 2001; Chamberlain and Gould, 2002; Chintagari et al., 2006; Lafont et al., 1999) or cholesterol rich membrane domains (Lang et al., 2001) which seem to be important for membrane fusion and exocytosis. However, SNARE proteins and their homologs exhibit different levels of raft association in different cell types (reviewed in (Salaun et al., 2004a)).

Apart from the lipid raft association, membrane proteins can spatially segregate into clusters using membrane actin cytoskeleton fences (Kusumi et al., 2005) or homophilic and heterophilic protein interactions (reviewed in (Lang, 2007)). Super resolution STED (Stimulated Emission Depletion) microscopy revealed that the SNARE proteins SNAP-25 (Willig, 2006) and syntaxin1 (Sieber et al., 2006) form clusters of sizes 60-80 nm and their signals overlap with each other to certain degree (Lang et al., 2001). Although initial studies showed that the integrity of these clusters was cholesterol dependent, later studies, particularly for syntaxin, demonstrated that apart from cholesterol, clustering is mediated by specific homooligomerization involving SNARE motifs of syntaxin (Sieber et al., 2006). Mechanism of SNAP-25 clustering is not studied in detail although it is thought that SNAP-25 through its palmitoyl membrane anchors is targeted to lipid rafts in the plasma membrane (Salaun et al., 2005b).

### **1.3. The neuronal SNAREs**

The best characterized SNARE proteins are those mediating neurotransmitter release (exocytosis) from presynaptic vesicles (Sollner et al., 1993b). The three proteins involved in this reaction are syntaxin 1A (Bennett et al., 1992), SNAP-25 (25 kDa synaptosome associated protein) (Oyler et al., 1989) and synaptobrevin 2, also known as vesicle associated membrane protein (VAMP 2) (Baumert et al., 1989). In particular, syntaxin1A and synaptobrevin 2 are attached to the membrane by a C-terminus single

membrane spanning domain and SNAP-25 is attached to the membrane by palmitoylation of four cysteine residues in the central region of the protein (Hess et al., 1992).

The SNARE protein complex is represented by elongated coiled coils of four intertwined, parallel alpha helices, with each helix being contributed by a different SNARE motif. The center of the SNARE complex bundle contains 15 stacked hydrophobic layers of interacting side chains and one central ionic '0' layer (Jahn and Sudhof, 1999). Formation of this structure, starting from the N-termini, may directly precede fusion (Hanson et al., 1997). X-ray crystallography studies of crystal structures of two distantly related (neuronal and endosomal) SNARE complexes reveal a marked degree of conservation (Antonin et al., 2002; Sutton et al., 1998).

SNAREs were originally classified into two groups: v-SNAREs, which are associated with vesicle membranes, and t-SNAREs, which are associated with target membranes. Synaptobrevin 2 is a v-SNARE while syntaxin 1A and SNAP-25 are t-SNAREs (Sollner et al., 1993a). However, it was found that v-SNARE and t-SNARE can coexist on vesicles or target membranes as in homotypic fusion. Therefore to avoid confusion, SNARE proteins were reclassified as R-SNARE (arginine containing SNAREs, e.g., synaptobrevin2) and Q-SNARE (glutamine containing SNAREs, e.g. syntaxin 1A and SNAP-25), based on a highly conserved glutamine (Q) or arginine (R) residue in their central '0' ionic layer of respective SNARE complex (Fasshauer et al., 1998).

Neuronal SNAREs are vulnerable to proteolytic cleavage by certain clostridial neurotoxins (CNT) from the bacterial species *Clostridium tetani* and *botulinum* (Schiavo et al., 1992). The light-chain proteases of CNTs specifically cleave the SNARE proteins at different locations, thus disrupting neurotransmission and causing flaccid or spastic paralysis occurring in botulism and tetanus diseases (Schiavo et al., 1992). The target sites for botulinum neurotoxin (BoNT) serotypes A-G and tetanus neurotoxin (TeNT) were all found to cluster in the SNARE motifs (Blasi et al., 1993; Schiavo et al., 1993) (see Figure 3). The CNTs cleave only free SNAREs not SNAREs in complex and therefore have been extensively used to dissect the precise roles of SNARE proteins in neuronal exocytosis (reviewed in (McNew, 2008)).

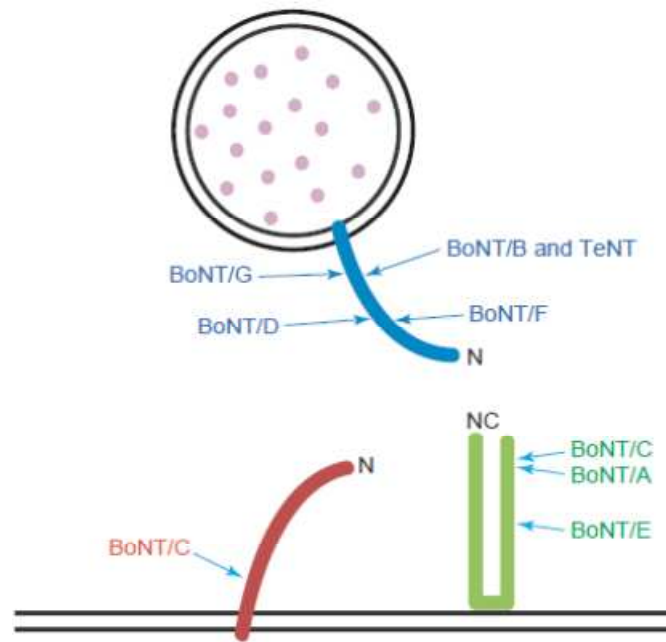


**Figure 3. Proteolytic cleavage of neuronal SNAREs.**

The several serotypes of botulinum neurotoxin (BoNT) and tetanus toxin (TeNT) cleave the SNARE core domains at various locations indicated by the arrows. Synaptobrevin (blue), Syntaxin (red) and SNAP-25 (green). [Figure taken from Breidenbach and Brunger, \(2005\).](#)

### 1.3.1. SNAP-25 (Q<sub>b</sub>Q<sub>c</sub> – SNARE)

SNAP-25 is a hydrophilic protein of 206 amino acids that associates with the plasma membrane through palmitoyl anchors that are thioester linked to four closely spaced cysteine residues at the linker region of the protein. It has two SNARE motifs each at N- and C- terminus connected by a linker region (see Figure 4).



**Figure 4. The primary structure digram for SNAP-25.**

SNAP25 has two SNARE motifs SN1 and SN2 at the N and C terminal positions respectively connected with a linker region that contains a cluster of four cysteines that are palmitoylated for membrane association. [Figure taken from Brunger et al., \(2009\).](#)

SNAP-25 is targeted to the plasma membrane by a stretch of 36 amino acids (85–120) in the linker region (Gonzalo et al., 1999). The flanking hydrophobic amino acids along with palmitoylation of all four cysteine residues (C85, C88, C90 and C92) through palmitoyl transferase DHHC17 are necessary for SNAP25 membrane association (Greaves et al., 2009; Lane and Liu, 1997; Veit et al., 1996). Studies from SNAP-25 knock out neurons have shown that SNAP-25 is absolutely required for calcium triggered release (Bronk et al., 2007). Cleaving the C-terminal residues of SNAP-25 using Botulinum toxin A or E markedly reduces the calcium triggered release but increasing calcium partially overcomes this deficit (Finley et al., 2002; Sakaba et al., 2005). In neurons, SNAP-25 has two isoforms, called SNAP-25 a and b, that are generated by alternative splicing of exon 5 resulting in nine amino acid substitutions at the C-terminal end of the N-terminal SNARE motif and the first part of the linker that includes one of the palmitoylated cysteines at position 90 (Bark and Wilson, 1994; Hess et al., 1992). Developmental regulation of SNAP-25 expression in the nervous system leads to predominance of SNAP-25a during early development and SNAP-25b in the adult. However, SNAP-25a is the main isoform in adult adrenal, pituitary and PC12 cells (Bark et al., 1995; Boschert et al., 1996). Although the physiological significance of the isoforms in the synaptic vesicle exocytosis remains obscure, a study on chromaffin cells from SNAP-25 *null* mice, suggest that the two isoforms exhibit differential ability in their regulation of the size of the releasable vesicle pools, isoform b being more potent in supporting the secretion (Delgado-Martinez et al., 2007; Sorensen et al., 2003).

### 1.3.2. Syntaxin 1 (Q<sub>a</sub> – SNARE)

Syntaxin1, originally identified by a monoclonal antibody as a retinal antigen named HPC-1 (Barnstable et al., 1985) is a 35 kDa membrane protein with a single transmembrane domain. Syntaxin 1 contains a SNARE motif and a H<sub>abc</sub> domain (see Figure 5). The N-terminal H<sub>abc</sub> domain, a three helix bundle, folds back and is bound intramolecularly to the coiled-coil domain of the SNARE motif in the closed conformation (Dulubova et al., 1999; Misura et al., 2000). Munc 18-1 binds to this four helix structure in the closed conformation but can also bind to the syntaxin N-terminal peptide allowing the formation of the *trans* complexes with SNAP-25 and synaptobrevin (reviewed in (Sudhof and Rothman, 2009)).

There are 15 mammalian syntaxin genes, and four of the expressed proteins (syntaxins 1–4) are localized to the plasma membrane and function in exocytic pathways. Each of the syntaxins 1 to 4 can be expressed as alternatively spliced isoforms. These plasma membrane syntaxins are differentially expressed with distinct spatial distribution (Salaun et al., 2004b). Syntaxin 1 has two isoforms, which are called syntaxin 1a and syntaxin 1b and are 84% identical in their amino acid sequence and are differentially distributed in the central and peripheral nervous system (Aguado et al., 1999). Syntaxin 4, expressed as the major isoform in non neuronal tissues and along with SNAP-23 and cellubrevin, is involved in constitutive exocytosis, (Hong, 2005).

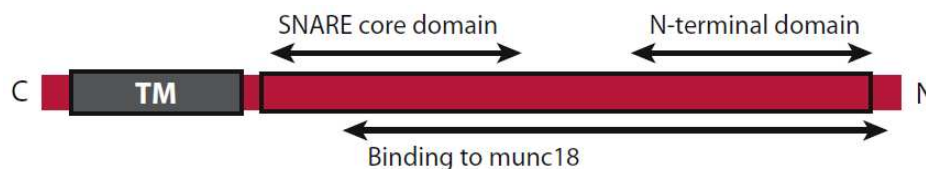


**Figure 5. The primary structure diagram for syntaxin1.**

Syntaxin has a N-terminal  $H_{abc}$  domain which forms three helical bundle followed by a core SNARE domain and a transmembrane domain for membrane insertion. A large portion of N – terminal region is involved in an interaction with munc-18. N - N-terminus sequence, TM – Transmembrane domain, C - C-terminus sequence. [Figure taken from Brunger et al., \(2009\).](#)

### 1.3.3. Synaptobrevin (R – SNARE)

The synaptic vesicle fusion protein synaptobrevin (or VAMP, for vesicle-associated membrane protein) 2 is a small 18 kDa protein with a single membrane-spanning domain. It consists of 116 amino acids in mammals and is made up of four domains (Sudhof et al., 1989) (see Figure 6). The proline rich cytoplasmic N-terminus, a highly conserved SNARE core domain of 63 amino acids, a well-conserved 20 amino acid transmembrane domain followed by a divergent C-terminus. The two synaptobrevin isoforms, synaptobrevin 1 and synaptobrevin 2 are differentially distributed in the nervous system (McMahon et al., 1993).

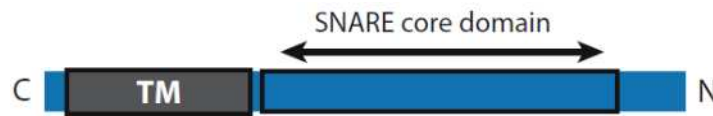


**Figure 6. The primary structure diagram for synaptobrevin.**

Synaptobrevin has a small N-terminal domain followed by a core SNARE domain, a transmembrane domain for membrane insertion and a small C-terminal domain. N - N-terminus sequence, TM – Transmembrane domain, C - C-terminus sequence. [Figure taken from Brunger et al.,\(2009\).](#)

### **1.3.4. The SNARE cycle**

SNAREs are known to undergo a regulated cycle of assembly and disassembly in order to perform their task and ready to be available for the next round of fusion. Some of the steps involved in the SNARE cycle and its regulation are discussed below.

#### **1.3.4.1. SNARE complex assembly and disassembly**

SNAREs on the plasma-membrane are highly abundant and clustered and have been associated with cholesterol and lipid rafts (Chamberlain et al., 2001; Lang et al., 2001). These clustered SNAREs are constitutively active and ready to form complexes with their partners (Lang et al., 2002). SNARE complex formation follows an orderly and sequential assembly pathway. Many studies have indicated that the foremost intermediate in the assembly is a  $Q_{abc}$  complex which can be stabilized by interacting proteins like Munc-18 and is ready to receive synaptobrevin from the synaptic vesicle. The resulting complex is held in its state by synaptotagmin and complexin until the entry of  $Ca^{2+}$  triggers the final stage of the fusion and neurotransmitter release (reviewed in (Jahn and Scheller, 2006)). SNARE complexes are known to be stable under conditions as extreme as 80°C, 8 M urea or 2% SDS (Fasshauer et al., 2002). Therefore, after fusion *cis* - SNARE complexes that reside in the fused membrane are dissociated in an energy requiring process.

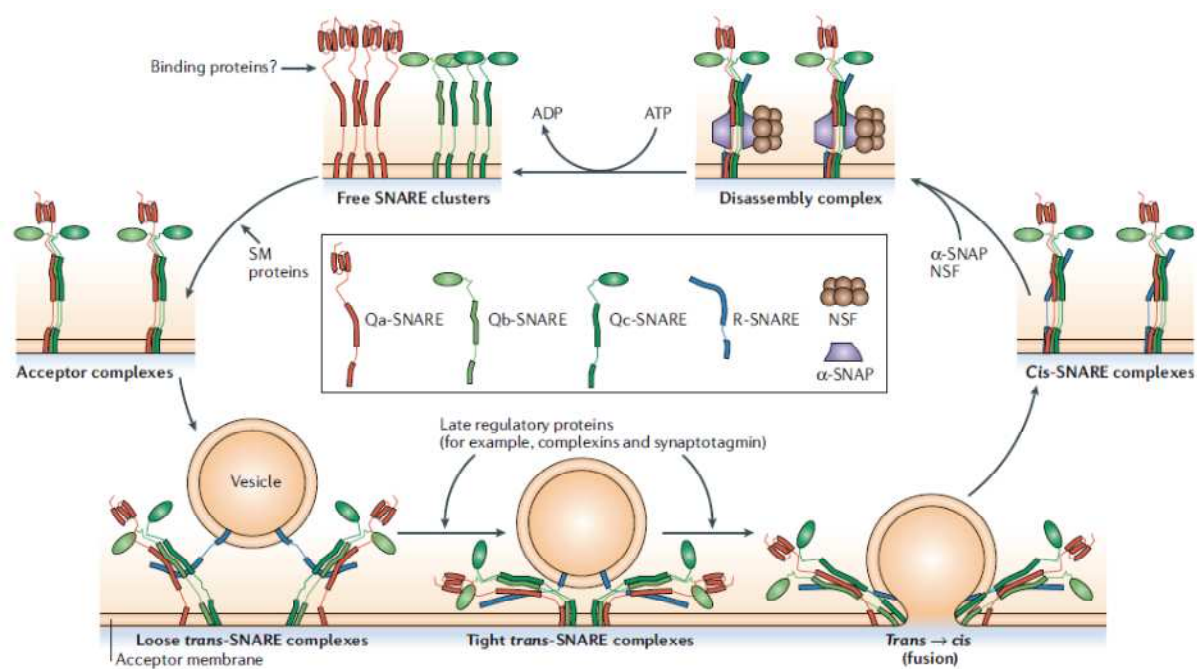


**Figure 7. The SNARE conformational cycle during vesicle docking and fusion.**

On membranes, SNAREs are organized into clusters which form acceptor complexes possibly stabilized by SM (Sec1/Munc18) proteins. Synaptobrevin from an approaching vesicle interacts with the acceptor complex to form a four helical *trans*-complex and this status could be regulated by accessory proteins like complexins and synaptotagmins. Once the fusion occurs, SNARE complexes relax into *cis*-state which can be disassembled by NSF and αSNAPs. Later, individual SNAREs are sorted by endocytic recycling. [Figure taken from Jahn and Scheller, \(2006\).](#)

SNARE complex disassembly by NSF (*N*-ethylmaleimide-sensitive factor) - a hexameric ATPase and alpha SNAPs (soluble NSF attachment proteins) is essential to maintain a steady state pool of free SNAREs for further rounds of fusion and fusion competence (Sollner et al., 1993a) (see Figure 7). Three alpha SNAP molecules bind to the middle of the SNARE complex and recruit NSF for complex dissociation (Marz et al., 2003). Moreover it is thought that the process also prevents the accumulation of dead-end by-products that are derived from the highly reactive SNAREs (reviewed in (Jahn and Scheller, 2006)).



#### **1.3.4.2. The SNARE interacting proteins**

While it is known that the SNAREs function as minimal fusion machinery, many regulatory factors have been identified which serve to ensure that SNARE complex assembly occurs in a precise spatio-temporal pattern. Some of the SNARE regulatory proteins are briefly discussed below.

##### **Munc18-1**

Munc18-1 knockout mice exhibit a complete abolition of neurotransmitter release suggesting its central role in synaptic vesicle exocytosis (Verhage et al., 2000). However, several attempts to elucidate its precise role in the same has yielded conflicting results and views complicating the entire picture. Munc18-1 is a cytosolic protein, interacts with syntaxin 1 through mutually non-exclusive two distinct modes of interaction (termed mode 1 and mode 2/3) at distinct binding sites (reviewed in (Smyth et al. 2010)). In mode 1, munc18-1 forms a complex with the closed conformation of syntaxin 1 which is incompatible with the SNARE complex formation (Misura et al., 2000). Mutations disrupting the closed conformation of syntaxin maintain a permanently open conformation and abolish interaction with munc18 (Dulubova et al., 1999). In mode 2/3, munc18-1 binds to a highly conserved motif at the N-terminus of syntaxin 1 (Dulubova et al., 2007; Rickman et al., 2007). Munc18-1 and syntaxin interactions are involved in secretory vesicle docking (Toonen et al., 2006). However, recent studies suggest that munc18-1 also binds and stabilizes syntaxin-1–SNAP-25 heterodimers so as to facilitate SNARE complex formation with synaptobrevin (Weninger et al., 2008; Zilly et al., 2006).

##### **Munc13**

Munc13 is a 200 kDa protein that is essential for synaptic vesicle exocytosis as its knock out results in complete abrogation of spontaneous and evoked release (reviewed in (Rosenmund et al., 2003)). Through their interactions with the syntaxin 1 N-terminal region *unc13* and *munc13* play a role in the conformational transition of syntaxin and it has been shown that a constitutively open syntaxin mutant partially rescues neurotransmitter release in *unc13* null mutants in *C. elegans* (Richmond et al., 2001). However, it was also shown that the *munc13* does bind to membrane anchored SNARE complexes (Guan et al., 2008) and to syntaxin-1–SNAP-25 heterodimers (Weninger et

al., 2008). It is possible that Munc13 in concert with Munc18-1 is involved in the formation of the syntaxin-1–SNAP-25 heterodimer and promotes vesicle priming (reviewed in (Rizo and Rosenmund, 2008)).

### **CAPS**

The protein CAPS (Ca<sup>2+</sup>-dependent Activator Protein for Secretion) shares a similar sequence with C-terminal domain of munc13-1 that is involved in syntaxin 1 binding and is implicated in vesicle priming (Grishanin et al., 2004). Recently, reconstituted liposome fusion assays demonstrated that CAPS promote formation of *trans*-SNARE complexes through syntaxin interactions (James et al., 2009).

### **Synaptotagmin**

Membrane protein synaptotagmin 1 acts as a Ca<sup>2+</sup> sensor in the neurotransmitter release (Fernandez-Chacon et al., 2001). Synaptotagmin 1 is a synaptic vesicle protein with two C2 domains, the C2A and C2B domains that adopt  $\beta$ -sandwich structures and bind three and two Ca<sup>2+</sup> ions, respectively. It has been shown that Ca<sup>2+</sup> bound synaptotagmin 1 promotes SNARE-mediated liposome fusion by simultaneously binding to phospholipid membranes and SNARE complexes (reviewed in (Rizo and Rosenmund, 2008)). Synaptotagmin 1 binds and stabilizes membrane-anchored syntaxin 1 - SNAP-25 heterodimers in a Ca<sup>2+</sup> independent manner (Weninger et al., 2008) and this interaction mediates synaptic vesicle docking (de Wit et al., 2009). Ca<sup>2+</sup> independent interaction of synaptotagmin 1 with t-SNARE (syntaxin 1 - SNAP-25) complexes acts as a ‘clamp’ for the membrane fusion and upon the entry of calcium switches to ‘accelerator’ of fusion (Chicka et al., 2008).

### **Complexin**

Complexin is a soluble protein that binds to the SNARE complex and also acts as a ‘clamp’ to stop the fusion process at the very last step of exocytosis until the entry of calcium (McNew, 2008). Recent data demonstrates that complexin-I binds and stabilizes syntaxin-1–SNAP-25 heterodimers (Weninger et al., 2008).

#### **1.4. Putative intermediate SNARE complexes on the pathway to membrane fusion**

Neurotransmitter release at the synapse is a highly regulated process involving a series of steps from docking of vesicles to priming and subsequent fusion. Therefore, as SNARE proteins are known to be involved in all these steps it is conceivable that their assembly pathway proceeds through an orderly and sequential reaction. Hence, characterizing the intermediates in the SNARE complex assembly that leads to fusion has been a very important aspect of understanding the release cascade and efficiency. SNARE motifs are largely unstructured (except for syntaxin) and their transition into helical structure coincides with their entry into either binary or ternary SNARE complexes (Fasshauer et al., 1997a; Fiebig et al., 1999).

##### **1.4.1. Binary SNARE interactions**

###### **1.4.1.1. Syntaxin 1- synaptobrevin interaction**

CD spectroscopy studies reported the occurrence of certain but weak interaction between the SNAREs syntaxin and synaptobrevin (Fasshauer et al., 1997b). Moreover modified synaptic vesicles or proteoliposomes with synaptobrevin fused to planar lipid bilayer membranes containing only syntaxin 1, in a  $\text{Ca}^{2+}$  independent manner (Bowen et al., 2004; Liu et al., 2005; Woodbury and Rognlien, 2000). However, this interaction is supposed to be not sufficient for membrane fusion *in vivo*. In SNAP-25 knockout mice,  $\text{Ca}^{2+}$  triggered release is abolished though vesicle docking and spontaneous fusion persisted (Washbourne et al., 2002) supporting the importance of SNAP-25 in  $\text{Ca}^{2+}$  dependent membrane fusion.

###### **1.4.1.2 SNAP-25 – synaptobrevin 2 interaction**

In an attempt to describe sequential SNARE assembly, studies from semi intact PC12 cells (Chen et al., 2001) conclude that an initial interaction between SNAP-25 and synaptobrevin primes the secretory vesicles before syntaxin joins them to form a fully zippered complex in  $\text{Ca}^{2+}$  triggered release. However there is little evidence from *in vitro* studies to support such a claim as there is very small increase in alpha helicity upon mixing the two proteins (Fasshauer et al., 1997b) and also a weak interaction observed on supported bilayers (Weninger et al., 2008).

### 1.4.1.3. Syntaxin 1 - SNAP-25 interaction

The syntaxin 1- SNAP-25 binary complex on the plasma membrane is the most likely candidate for being an initial intermediate in the neuronal SNARE assembly pathway. The binary complex acts as a binding site for synaptobrevin 2 from the synaptic vesicle and thus came to be known as 'acceptor complex'. Biochemical and biophysical characterization of the neuronal t-SNARE interactions revealed a binary complex with a molar ratio of 2:1 (two syntaxins to one SNAP-25) (Fasshauer et al., 1997b) in contrast to a 1:1 stoichiometry of yeast homologues (Fiebig et al., 1999; Rice et al., 1997). But *in vivo*, yeast t-SNAREs can form a 2:1 complex (Marash and Gerst, 2001). However, the neuronal t-SNARE 2:1,  $(Q_a)_2Q_bQ_c$  complex stoichiometry can be avoided by the addition of synaptobrevin which forms a stable ternary complex (Fasshauer et al., 1997b). Site-directed spin-labeling electron paramagnetic resonance (EPR) measurements suggest that the structure of the 2:1 complex is a coiled coil structure of a parallel four-helix bundle resembling that of the ternary complex (Zhang et al., 2002) contradicting the previous studies showing that the complex has either a disordered mid section (Xiao et al., 2001) or an unstructured C-terminal region (Margittai et al., 2001). In any case the 2:1 syntaxin 1 - SNAP-25 complex represents a non-physiological dead end intermediate as it does not react with synaptobrevin (Fasshauer et al., 1997b). The more reactive 1:1 intermediate is transient and unstable (Fasshauer and Margittai, 2004) and such a dynamic intermediate state goes undetected easily in the conventional solution measurements as they rely on signal averaging over many molecules (Sakon and Wening). Moreover, the orientation of the proteins under study is different in solution than when membrane bound. In recent years, an elegant study has overcome these technical limitations by seeding the syntaxin 1 molecules at extremely low concentrations (about 100 molecules in  $450 \times 90 \mu\text{m}$  area) on a supported bilayer and performed single molecule FRET (smFRET) assays on 1:1 binary interactions between adherent syntaxin 1 and added SNAP-25 (Wening et al., 2008). The smFRET studies report signals from single pair detecting the intermediate states during dynamic transitions and thereby identify different subpopulations of molecular conformation (Sakon and Wening, 2010). The study enabled them to observe a three helix bundle of 1:1 syntaxin 1 - SNAP-25 heterodimer  $(Q_aQ_bQ_c)$  which dynamically equilibrates between two helical configurations involving the syntaxin SNARE motif and one of the two SNARE motifs of SNAP-25 representing a  $Q_aQ_b$  or a  $Q_aQ_c$  complex. Interestingly,

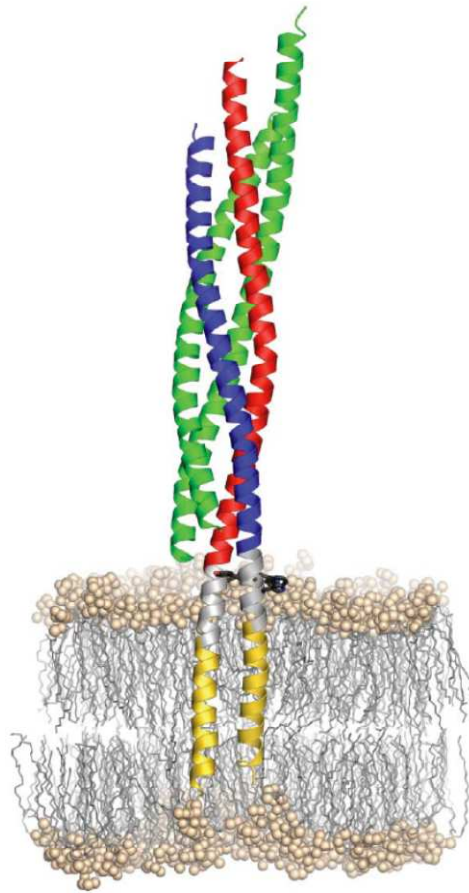
these two intermediate states are abolished by the addition of accessory proteins such as Munc13-1, Munc18-1, complexin and synaptotagmin I, thereby shifting the equilibrium state towards the three helix  $Q_aQ_bQ_c$  bundle. Interestingly, in support of these observations, FLIM-FRET (Fluorescence Lifetime Imaging FRET) studies on live cells revealed the existence of two subpopulations of heterodimer t-SNARE conformation representing a  $Q_aQ_bQ_c$  or  $Q_aQ_b$  complex (Rickman et al., 2010). Also, using an intramolecular FRET probe for SNAP-25, several studies have reported the formation of the binary complex ( $Q_aQ_bQ_c$ ) in live cells (An and Almers, 2004; Takahashi et al., 2010; Wang et al., 2008) CD spectroscopy studies revealed the formation of two helix coiled coil structure involving the N-terminus of SNAP-25 and syntaxin 1 ( $Q_aQ_b$ ) (Fasshauer et al., 1997b), but the crystallized complex consisted of two antiparallel aligned binary complexes which could be a kinetically trapped product (Misura et al., 2001) and unlikely to occur in live cells. *In vivo* ensemble FRET studies in live neuroendocrine cells suggested the presence of a binary complex between syntaxin 1 and the N-terminal SNARE motif of SNAP-25 (An and Almers, 2004) as a precursor for the exocytic core complex. However, such complex formation was found to be induced upon calcium influx suggesting an involvement of other factors which is rather a relatively late event in the SNARE assembly pathway. The FRET readout was affected by the fluorophore concentrations within the cells and was possible only in certain molecular conformations. Moreover, the data also indicated the presence of 2:1 complex and did not address the structural and dynamic aspects of the observed  $Q_aQ_b$  complex.

#### 1.4.2. Ternary SNARE interactions

As discussed above the binary syntaxin 1/SNAP-25  $Q_aQ_bQ_c$  complex with a 1:1 stoichiometry is more likely to be the functional on-pathway intermediate serving as a genuine binding site for synaptobrevin. The resulting ternary SNARE complex is a parallel four helix bundle, extremely stable - resists SDS denaturation and thermal denaturation upto 80°C (Hayashi et al., 1994). The ternary SNARE complex assembly is a directed process starting from the N-termini and proceeding towards the C-termini as evident from several studies. N-terminal truncations of the either SNAP-25 or syntaxin 1 inhibited the assembly more than the C-terminal truncations and were independent of

the N- or C- terminal truncations of synaptobrevin suggesting again that the binary t-SNARE complex formation precedes the entire process (Fasshauer and Margittai, 2004). A monoclonal antibody against the N-terminal portion of SNAP-25 inhibits complex formation further supporting the idea of N-terminal zippering (Xu et al., 1999). SNARE motifs domains undergo major structural transitions – from unstructured to helical configuration – to form a ternary SNARE complex which consists of a parallel four-helix bundle (Sutton et al., 1998) (see Figure 8). Liposome fusion assays - in which recombinant t-SNARE and v-SNARE proteins are reconstituted into two sets of liposomes separately and lipid mixing was monitored over timescale, provided ample evidence in support for the requirement of ternary SNARE complex formation for membrane fusion. The bulk liposome fusion assays, apart from corroborating the already known structural dynamics, filled many gaps and have overcome some key deficiencies of the solution assays in understanding of the ternary SNARE complex formation. Promiscuity of SNARE interactions that has been observed in solution (Fasshauer et al., 1999; Yang et al., 1999) was refuted by liposome fusion studies using different combinations of SNAREs, underscoring the importance of particular SNARE pairing (Parlati et al., 2002). Similarly, importance of membrane anchors of the SNARE proteins in the membrane fusion (McNew et al., 2000; Melia et al., 2002) and physiological lipid composition, protein-to-lipid ratio (Mima et al., 2008) was realized. In a recent study of liposome fusion assay, it has been shown that one SNARE complex is sufficient for membrane fusion overriding the previous estimates of around 3 to 15 complexes (van den Bogaart et al., 2010). But the electrophysiological measurements of chromaffin cell secretion suggested that atleast 3 SNARE complexes are required for the fast fusion typically observed in neuronal or neuroendocrine cells (Mohrmann et al., 2010).

A)



B)

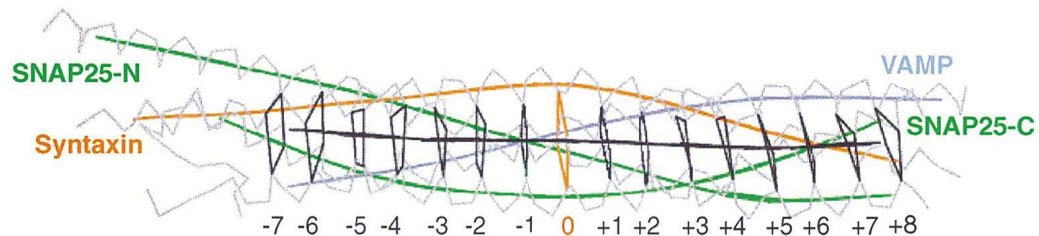


**Figure 8. The neuronal ternary SNARE complex.**

**A).** Model of the X-ray crystal structure of the neuronal SNARE complex in *cis* (post-fusion) state with the C-terminal region inserted into phospholipid bilayer membrane. The C-terminal region includes linkers (grey) and transmembrane regions (yellow) of syntaxin and synaptobrevin. Note the helical continuity into linkers and transmembrane regions. Aromatic residues within the linker region (black) are shown as a landmark. The syntaxin coil is in red, VAMP in blue, and SNAP- 25 N- and C- terminal coils in green. [Figure taken from Stein et al., \(2009\).](#)

**B)** X-ray crystal structure of the four helical bundle of neuronal SNARE complex as determined by Sutton et al., (1998) showing the 15 hydrophobic interaction layers (in black) are marked

from -7 to +8, with the ionic layer (in red) at 0. Colour coding for SNARE motifs as in (A).

## **1.5. Aims of the studies**

### **1.5.1. Structure and dynamics of the SNAP-25 (Q<sub>bc</sub>) and syntaxin (Q<sub>a</sub>) interaction in live cells**

Over the years, the sequence of SNARE assembly pathway has been deciphered through a series of biochemical and biophysical studies employing recombinant SNARE domains in solution and full length SNAREs reconstituted in proteoliposomes. They all indicated that the assembly pathway is a sequence of interactions that naturally follow towards a kinetically and thermodynamically favorable complex. A consensus was that a syntaxin 1 - SNAP-25 complex with a 1:1 stoichiometry, i.e. a Q<sub>a</sub>Q<sub>b</sub>Q<sub>c</sub> -SNARE complex, is likely the functional on-pathway intermediate and serves as a true binding site for synaptobrevin. Few live cell studies also supported the presence of such complexes in the cells and even the formation of the foremost intermediate Q<sub>a</sub>Q<sub>b</sub> complex but they all lacked detailed structural and dynamic analysis of such complexes. Therefore in order to characterize the SNARE complex intermediate in live cells in a more detailed manner employing a quantitative microscopic imaging technique - FRAP (Flourescence Recovery After Photobleaching), which in general can be applied to study the mobility of membrane proteins and protein-protein interactions. In addition, exogenously added recombinant protein binding assays using native plasma membrane sheets and standarad biochemical approaches were used to further support the data from the live cell FRAP assays.

### **1.5.2. Membrane organization of SNAP-25 and syntaxin 1**

The studies were also aimed at investigating the morphological characterization of surface distribution of SNAP-25 clusters and their spatial relation to syntaxin clusters using super resolution STED (Stimulation Emission Depletion) microscopy and studying the influence of divalent cations on SNARE protein organization.



## 2. Materials and Methods

### 2.1. Cloning - Plasmid DNA constructs

#### 2.1.1. SNAP-25 constructs

Plasmid DNA constructs for transient overexpression under the CMV promoter were produced by standard molecular biological methods (Sambrook, 2001). A monomeric variant of GFP (mGFP), carrying the single amino acid substitution A206K to prevent dimerization (Zacharias et al., 2002) was fused N-terminally to the sequence of full length rat SNAP-25B (AB003992) or SNAP-25B constructs in a vector based on pEGFP-C1 (Clontech, Mountain View, CA) (GenBank accession No. U55763). All fusion proteins contained a linker of 5 amino acids (RSRAL) between mEGFP and the N-terminus of SNAP-25B. The constructs were cloned into BglII and KpnI restriction sites of the multiple cloning site in the vector. All constructs were expressed under the control of the CMV promoter.

SNAP25-wt [mEGFP + SNAP25B-(1-206)]

SNAP25-N<sub>L</sub>0 [mEGFP + SNAP25B-(1-142 + 203-206)]

SNAP25-0<sub>L</sub>C [mEGFP + SNAP25B-(1-13 + 80-206)]

SNAP25-0<sub>L</sub>0 [mEGFP + SNAP25B-(1-13 + 80-142 + 203-206)]

SNAP25-N<sub>L</sub>N [mEGFP + SNAP25B-(1-142 + 14-79 + 203-206)]

SNAP25-C<sub>L</sub>C [mEGFP + SNAP25B-(1-13 + 143-202 + 80-206)]

SNAP25-0<sub>L</sub>N [mEGFP + SNAP25B-(1-13 + 80-142 + 14-79)]

SNAP25-Δ -7 to -5 [mEGFP + SNAP25B-(1-25 + 37-206)]

SNAP25-Δ -7 to -2 [mEGFP + SNAP25B-(1-25 + 47-206)]

SNAP25-Δ -7 to +3 [mEGFP + SNAP25B-(1-25 + 65-206)]

For amino acid substitution constructs Stratagene QuickChange Primer design Program (<http://www.stratagene.com/qcprimerdesign>) was used for designing primers with optimal length, melting temperatures and GC content. Stratagene's QuickChange® Site-Directed Mutagenesis Kit (Stratagene, Agilent technologies, La Jolla, CA) was used for the PCR amplification of the mEGFP-SNAP-25B vector plasmid using the pair of primers containing the desired mutations/substitutions in the N-terminus SNARE motif.

The resulting constructs were:

SNAP25-M32P,V36P [mEGFP + SNAP25B-(1-206 carrying the mutations M32P and V36P], SNAP25-I60P, M64P [mEGFP + SNAP25B-(1-206 carrying the mutations I60P and M64P], SNAP25-G43P,T46P [mEGFP + SNAP25B-(1-206 carrying the mutations G43P and T46P] (not further followed) and SNAP25-G43D [mGFP + SNAP25B-(1-206 carrying the mutations G43D].

Coding sequences of all constructs have been verified by sequencing using for SNAP-25B the according rat sequences as references.

### **2.1.2. Syntaxin constructs**

The C-terminally CFP tagged syntaxin 1A obtained from Maria Drumniski (Dept. of Neurobiology, Max Planck Institute for Biophysical Chemistry, Göttingen) - (Syx1A-CFP [Syx1A-(1-288) + CFP]) was cloned into BglII and KpnI sites and syntaxin 4 (Syx4-CFP [Syx4-(1-298) + CFP]) into the NheI and SacII sites. Both the constructs are based on the expression vector pECFP-N1 (Clontech, Mountain View, CA). A 12 amino acids linker (LVPRARDPPVAT) connects the corresponding syntaxin to ECFP. Coding sequences of all constructs have been verified by sequencing using for syntaxin 1A and syntaxin 4 the according rat sequences as references.

## **2.2. Cell culture**

### **2.2.1. Coating of glass coverslips**

Glass coverslips (Menzel Gläser, Braunschweig, Germany) were cleaned in absolute ethanol and sterilised by brief flaming. 500 µl of a 100 µg/ml poly-L-lysine hydrobromide (molecular weight >300 kDa, Sigma, Cat. No: P-1524) dissolved in sterile water was placed evenly onto each coverslip and incubated for 30-45 min at RT. This was followed by a washing step with sterile water for about 20 min and then the coverslips were air dried at RT for at least 2 hours before using them for plating the cells.

### 2.2.2. Cell culture and propagation of PC12 and BHK cells

Rat pheochromocytoma (PC12 cells, clone 251) (Heumann et al., 1983) were maintained in 75 cm<sup>2</sup> tissue culture flasks containing 25 ml of medium – DMEM with high (4.5 g/l) glucose (Cambrex, New Jersey, USA) supplemented with 10 % horse serum (Biochrom, Berlin), 5 % foetal calf serum (PAA laboratories, Cölbe, Germany), 4 mM L-Glutamine (Cambrex, New Jersey, USA) and 60 U/ml penicillin and 60 µg/ml streptomycin (Cambrex, New Jersey, USA). The cells were incubated at 37°C, 10% CO<sub>2</sub> and 90% relative humidity in sterile incubators and allowed to grow for 2-3 days to attain a confluence before splitting into fresh flasks. Media was removed followed by a wash with PBS (2.7 mM KCl, 1.5 mM KH<sub>2</sub>PO<sub>4</sub>, 137 mM NaCl, 8 mM Na<sub>2</sub>HPO<sub>4</sub>, pH 7.3). Cells were detached from the substrate with 3 ml trypsin/EDTA (Cambrex, New Jersey, USA) for 2-3 min. Trypsin was then inhibited by the addition of 20 ml of growth media. The suspension was centrifuged at 1000 rpm for 5 min at RT. Media was removed and the cell pellet was re-suspended in fresh growth media and titrated for about 10-15 times. The re-suspended cells were then either split into fresh flasks (1:2 or 1:4 ratio) or taken for transfection and plated onto coated glass coverslips for experiments.

For BHK (Baby Hamster Kidney) cells essentially the same protocol was used for cell culture except that the growth media, DMEM was supplemented with high (4.5 g/l) glucose, 10 % tryptose phosphate broth (Gibco, Paisley, UK), 5 % foetal calf serum 2 mM L-Glutamine and 60 U/ml penicillin and 60 µg/ml streptomycin. The cells were grown at 37°C, 5% CO<sub>2</sub> and 90% relative humidity in sterile incubators. The cells were allowed to grow for 1-2 days to attain a confluence and then either split into fresh flasks (1:10 or 1:20 ratio) or taken for transfection and plated onto coated glass coverslips for experiments.

### 2.2.3. Transient transfection of PC12 and BHK cells

For transfection, the pelleted cells were re-suspended and titrated in cytomix buffer (120 mM KCl, 10 mM K<sub>2</sub>HPO<sub>4</sub>, 10 mM KH<sub>2</sub>PO<sub>4</sub>, 0,15 mM CaCl<sub>2</sub>, 2 mM EGTA, 5 mM MgCl<sub>2</sub>, 25 mM HEPES, pH 7.6, sterile filtered). A total of 400 µl of cell suspension including 30–50 µg of plasmid DNA were mixed in an electroporation cuvette (2 mm electrode gap, Biorad, Munich). An electric pulse was applied using a Biorad

Genepulser II (settings: potential difference – 1.15 kV, resistance – 50  $\Omega$ , capacitance - 50  $\mu$ F). The cell suspension was then diluted immediately with 2-3 ml growth media and 500  $\mu$ l of the same was plated onto poly-Lysine coated coverslips and used for experiments 20 – 60 hrs after transfection. In co-transfection experiments, 30–60  $\mu$ g of each of the corresponding plasmids were added to an electroporation cuvette.

### **2.3. Plasma membrane sheet assay**

#### **2.3.1. Generation of plasma membrane sheets**

For preparation of membrane sheets, transfected or untransfected cells (PC12 or BHK) were grown on poly-L-lysine coated coverslips for 24-36 hours. The cells were then subjected to sonication as previously described (Avery et al., 2000) using a 2.5 mm sonication tip (Sonifier 450, Branson Ultrasonics corp. Danbury, USA) with the following settings: duty cycle 10%, output control around 2, duty cycle on hold. For sonication, each coverslip was placed into the ice cold sonication buffer (120 mM potassium glutamate, 20 mM potassium acetate, 20 mM HEPES pH 7.2 and containing, if not indicated otherwise, 10 mM EGTA) at a tip distance of about 10 to 12 mm and exposed to a 100 ms pulse.

#### **2.3.2. Incubation of plasma membrane sheets with nanomolar calcium**

Membrane sheets from PC12 cells prepared as described above (by using ice-cold sonication buffer: 120 mM potassium glutamate, 20 mM potassium acetate, 2 mM EGTA and 20 mM HEPES pH 7.2) were incubated at 37°C in potassium glutamate (K-Glu) buffer (120 mM potassium glutamate, 20 mM potassium acetate and 20 mM HEPES pH 7.2) + 3% BSA with the addition of varying concentration of free calcium or no calcium and with or without 2 mM  $MgCl_2$ /2 mM ATP, for 5 or 10 minutes as indicated. To obtain free calcium concentrations in the nanomolar range a calcium/EGTA buffer system (using the formula – free  $[Ca^{2+}] = K_d EGTA * [CaEGTA/K_2EGTA]$  with  $K_d$  EGTA at pH 7.2 = 150 nM), was used (Tsien and Pozzan, 1989). For instance, to achieve about 225 nM free calcium in the solution 6:4 parts of  $CaCl_2$ /EGTA : EGTA were mixed (see Table 1). For no calcium condition 2 mM of EGTA was added to the solution. The coverslips were then briefly washed in sonication

buffer (with 2 mM EGTA) and fixed in 4% PFA in PBS for about 60-90 minutes before carrying out immunostaining.

<b>CaEGTA(2mM) EGTA (2mM)</b>	<b>:</b>	<b>Free [Ca<sup>2+</sup>] (nM)</b>
1:9		17
2:8		38
3:7		64
4:6		100
5:5		150
6:4		225
7:3		350
8:2		600
8.5:1.5		850
9:1		1350

**Table 1. Free calcium in the buffer solution.**

2 mM stocks of CaCl<sub>2</sub>/EGTA and EGTA were mixed in different proportions to obtain specific concentration of free Ca<sup>2+</sup> in the incubating solution. See the text for details.

### 2.3.3. Immunostaining of plasma membrane sheets

After sonication, membrane sheets (from PC12 or BHK cells) were either incubated or directly fixed for about 60 – 90 min at room temperature in 4 % paraformaldehyde in PBS, washed with PBS, quenched for 20 min in PBS containing 50 mM NH<sub>4</sub>Cl and washed with PBS. The samples were then incubated with primary antibodies (1:100 or 1:200 in PBS + 3% BSA) for about 60 minutes at room temperature and washed three times in PBS for 5-10 min each, followed by 60 min incubation with respective secondary antibody conjugated to fluorescent dyes (1:200 or 1:400 in PBS + 3% BSA). Then the samples were washed 3 times in PBS for 5-10 min each. The glass-coverslips were mounted in a microscopy chamber filled with PBS containing 1-(4- trimethylammonium phenyl)-6-phenyl-1,3,5-hexatriene *p*- toluenesulfonate (TMA-DPH) (Molecular Probes, Eugene, Oregon, United States) for the visualization of phospholipid-membranes.

As primary antibody, mouse monoclonal antibodies were used for the detection of syntaxin 1A/B (HPC-1), SNAP-25 (Cl. 71.1, which recognizes AA 20-40, Cat. No. 111001, Synaptic Systems, Germany), synaptophysin (Cl. 7.2, Cat. No. 101011,

Synaptic Systems, Germany) and human transferrin-receptor (Zymed, USA). Rabbit polyclonal antibodies were used for the detection of Munc18-1 (Cat. No. 116002, Synaptic Systems, Germany) and SNAP-23 (Cat. No. 111202, Synaptic Systems, Germany). As secondary antibodies goat anti-rabbit-Cy3 and goat anti-mouse-Cy3 (Dianova, Hamburg, Germany) were used.

For the STED microscopy sample preparation, rabbit polyclonal antibodies for the detection of syntaxin 1A (R31) (Lang et al., 2001), syntaxin 4 (Cat. No. 110042, Synaptic Systems, Göttingen) were used as primary antibody. For the detection of GFP-SNAP-25 constructs mouse monoclonal anti-GFP antibodies (clone 3E6, Molecular Probes, Invitrogen) were used as primary antibody. As secondary antibodies, goat anti-rabbit-Cy3 (Dianova, Hamburg, Germany) and Atto-647N labelled sheep or goat anti-mouse (provided by dept. of Nanobiophotonics, MPIBPC, Göttingen) were used.

#### **2.3.4. Recombinant syntaxin 1A binding using BHK plasma membrane sheets**

BHK cells were transfected with GFP labelled SNAP-25 or SNAP-25 mutant constructs and allowed to grow for 24-36 hours before subjecting them to sonication in ice cold sonication buffer (120 mM potassium glutamate, 20 mM potassium acetate, 20 mM HEPES pH 7.2 and 10 mM EGTA). The plasma membrane sheets were incubated with 4  $\mu$ M recombinant syntaxin 1A (1-262 + 263Cys) (a kind gift from Dr. Olga Vites, Dept. Neurobiology, Max-Planck Institute for Biophysical Chemistry, Göttingen) in K-Glu buffer containing 3% BSA and 2 mM DTT at 37°C in a humid chamber for about 10 minutes. Then membrane sheets were briefly washed in K-Glu buffer at RT for 30-40 seconds and fixed in 4% PFA in PBS, followed by immunostaining (as described in section 2.3.3), using HPC-1 (Barnstable et al., 1985) as primary antibody and goat-anti-mouse Cy3 (Dianova, Hamburg, Germany) as secondary antibody.

#### **2.3.5. Fluorescence microscopic imaging of plasma membrane sheets**

The glass-coverslips with immunostained membrane sheets were mounted in a microscopy chamber filled with PBS containing 1-(4-trimethyl-ammoniumphenyl)-6-phenyl-1,3,5-hexatriene *p*-toluenesulfonate (TMA-DPH) (Molecular Probes, Oregon, USA) for the visualization of phospholipid-membranes. For conventional, diffraction limited fluorescence microscopy an inverted Zeiss Axiovert 100 TV fluorescence

microscope with a 100x 1.4 numerical aperture plan apochromat oil objective (Zeiss, Göttingen, Germany) was used. Illumination was provided by a XBO 75 xenon lamp. For imaging, a back-illuminated charge-coupled device camera (Princeton Instruments, Princeton, NJ) with a magnifying lens (2.5x Optovar, Zeiss) was used to avoid spatial undersampling by large pixels. The focal position was controlled using a low voltage piezo translator device and a linear variable transformer displacement sensor/controller (Physik Instrumente, Waldbronn, Germany). Appropriate filter sets were used for TMA-DPH (excitation bandpass (BP) 360/50, beamsplitter (BS) 400–420, and emission longpass (LP 420), GFP (excitation BP 480/40, BS LP 505, and emission BP 527/30), Cy3 (excitation BP 525/30, BS LP 550, and emission BP 575/30). Image acquisition was performed with Metamorph 5.01 (Universal Imaging, West Chester, PA). Membrane sheets were selected and then imaged in the TMA-DPH channel documenting the integrity of the membrane sheets. Then the images were acquired in the one or two of the channels as per the staining of the samples.

For the recombinant syntaxin 1 binding studies on BHK membrane sheets expressing various SNAP-25 constructs, the sheets were quickly screened for GFP expression and when found, images were acquired in the TMA-DPH channel with an exposure time of 0.5 s, documenting the integrity of the membrane sheets. Then the image was acquired in the GFP channel with an exposure time of one second, to quantify the expression levels of GFP-SNAP-25 or SNAP-25 constructs. Then the third image was taken in the Cy3 channel for quantifying bound syntaxin 1A with an exposure time of one second.

For the experiments in figures 41 and 42 D, a Olympus IX81 fluorescence microscope with a 60x 1.49 NA Apochromat objective with a 1.6x magnifying lens (Olympus, Tokyo, Japan) and an EMCCD camera (ImagEM C9100-13, 512 × 512-chip, 16 × 16 μm pixel size; Hamamatsu Photonics, Hamamatsu, Japan) with a 2x magnifying lens was used. For detection of TMA-DPH and Cy3, the triple band fluorescence filter set U-M3DAFIC3/HC (Olympus) in combination with a 150 W Xenon-lamp integrated into the MT20-I-fluorescence illumination system (Olympus) was used.

### **2.3.6. Fluorescence microscopy - Image analysis**

The images were analyzed using Metamorph imaging version 4.0. A region of interest (ROI) was randomly placed in the TMA-DPH channel and average fluorescence intensity and background values were quantified in the respective channels and the data

was exported into Microsoft excel sheets. Then the data was processed using Sigmaplot 9.0 (Systat software, Inc.) by subtracting the background intensity and calculating a mean of fluorescence intensity of several sheets. The mean values from from three independent experiments were averaged and plotted as vertical bar graphs. For each experiment and condition 10-40 membrane sheets were analyzed. For the 'recombinant syntaxin 1 binding on BHK cell membrane sheets' experiments 15-25 sheets were analyzed for each condition. The green fluorescent intensity values (GFP-SNAP-25 construct expression level) were plotted versus cy3 fluorescence (Cy3- bound syntaxin) values.

For the experiments in figures 41 and 42 C/D, images were analyzed using Image J (NIH, USA). A region of interest (ROI) was randomly placed in the TMA-DPH channel and mean fluorescence intensity, and background values were quantified in the respective channels. The area and x, y co-ordinates of the ROI were also recorded. The mean fluorescence and the background intensity values were exported and processed using Origin Pro 8G (OriginLab Corporation, Northampton, MA), by subtracting the background intensity and calculating a mean of fluorescence intensity of several sheets. The mean values from from three independent experiments were averaged and plotted as vertical bar graphs in Sigma Plot 10.0 (Systat software, Inc.).

## **2.4. FRAP (Flourescence Recovery After Photobleaching) experiments on live cells**

### **2.4.1. Sample preparation**

Transfected PC12 or BHK cells expressing the corresponding constructs were taken for microscopic imaging 20-60 hours later and mounted in a chamber filled with Ringer solution (130 mM NaCl, 4 mM KCl, 1 mM CaCl<sub>2</sub>, 1 mM MgCl<sub>2</sub>, 48 mM D(+)Glucose, 10 mM HEPES, pH 7.4) at RT.

### **2.4.2. Confocal Microscopy for FRAP**

An inverted confocal laser scanning microscope (TCS-SP5; Leica Microsystems, Mannheim, Germany) equipped with a 63x 1.4NA (numerical aperture) plan apochromat oil objective was used. Pixel size was adjusted to 68.6 nm x 68.6 nm and scanning was performed at 700 to 1000 Hz. For GFP excitation, a 488 nm line (laser power 2%, for bleaching 75% was used) of an Argon ion laser was used and the



emission was collected at 500-600 nm (with 1 Airy disc pinhole size). When CFP-syntaxin constructs were expressed, CFP-fluorescence of the corresponding basal plasma membrane was recorded before the start of the FRAP experiment on GFP-SNAP-25 constructs, using for excitation the 458 nm line of the Argon ion laser (laser power of 25%) and the emission was collected between 461-480 nm. For FRAP experiments, the FRAP-wizard routine from the Leica Application Suite-Advanced Fluorescence (LAS-AF) (Version 1.6.3 Build 1163; Leica Microsystems, Mannheim) was applied. In brief, recordings started by 10-15 frames taken at maximal speed (approximately, 2 frames per second at 1000Hz or 2 frames per 1.5 seconds at 700Hz). Then a 3  $\mu\text{m}$  x 3  $\mu\text{m}$  region of interest (ROI) was bleached twice using the 'zoom in' option and 20-30 frames were recorded at maximum speed followed by 40 frames at a rate of 1 frame per 3 seconds. Finally, 10 frames were recorded at maximum speed (not shown in the Figure 11 B). After the recording, 2 different ROIs with 3  $\mu\text{m}$  x 3  $\mu\text{m}$  were placed – one for the background signal outside the cell surface another for a non-bleached region inside the cell surface. In addition, another ROI covering for the entire cell surface was placed. The image with all the ROIs along with all the images in the FRAP series were saved and also the corresponding signal intensities of the ROIs at different time points were exported as excel files.

#### **2.4.3. FRAP data analysis**

For data analysis the programs SigmaPlot 9.0 (Systat software, Inc.) and Origin 7.5 SR1 (OriginLab Corporation, Northampton, MA) were used. The intensity values saved as excel files were imported into Sigma plot worksheets and processed using user-defined arithmetic functions. First, signals in the ROI were background corrected and the pre-bleach value was determined by averaging the 10-15 frames recorded before bleaching. Then values of the recovery trace were normalized to the averaged pre-bleach value. Experiments exhibiting a strong z drift, as detected by a 20% decrease or 5% increases in fluorescence intensity in an unbleached control region, were excluded from the analysis.

For one experiment and condition either average of several or individual traces were fitted using Origin software applying a hyperbola function ( $t_{1/2}$  = half-time of recovery,  $a$  = offset and  $b$  = amplitude of recovery) (Ficz et al., 2005):

$$x(t) = a + b \times t / (t_{1/2} + t)$$

Maximal recovery and half times of recovery thus were obtained from the fitting and were used for the subsequent data plots in Sigma plot. The usage of the obtained values from the fitting will be described in the results section accordingly. When co-overexpressed with syntaxin 1-CFP/ syntaxin 4-CFP, a slope value was calculated for each cell by subtracting first from its half time of recovery, the mean half time of recovery value of all measured cells (including 3-6 cells) from the same experiment that overexpressed the corresponding SNAP-25 construct but had no detectable signal for syntaxin-CFP (the mean value indicates the background mobility without additional syntaxin). Then, the background corrected half time of recovery was divided by the CFP-expression level. For each condition, individual slope values (from 3-10 cells) from one experiment were averaged. The mean values from three independent experiments were calculated and plotted as mean  $\pm$  SEM.

## **2.5. STED-(Stimulated Emission Depletion) Microscopy**

### **2.5.1. STED Sample preparation**

#### **2.5.1.1. Sample preparation for SNAP-25 cluster morphology and colocalisation studies**

GFP tagged SNAP-25 or SN25-0<sub>L</sub>0 was expressed in PC12 cells and 24-36 hours later membrane sheets were prepared by subjecting the cells to sonication in ice cold sonication buffer (120 mM potassium glutamate, 20 mM potassium acetate, 20 mM HEPES pH 7.2 and 10 mM EGTA) as described above in the section 2.3.1. For experiments shown in Figure 35 and 37, prior to fixation membrane sheets were incubated in a humid chamber for 15 min at 37°C in K-Glu buffer + 3% BSA with or without 10  $\mu$ M synaptobrevin 2 (AA 1-96) (a kind gift from Dr.Olga Vites, Dept. of Neurobiology, Max-Planck Institute for Biophysical Chemistry, Göttingen) and then

briefly washed in K-Glu buffer for 30 - 40 s at RT.

Immunostaining of the plasma membrane sheets was carried out as described in section 2.3.3. As primary antibodies (1:200 in PBS + 3% BSA), polyclonal rabbit antibodies for syntaxin 1 (R31) (Lang et al., 2001) and syntaxin 4 (Cat. No. 110042, Synaptic Systems, Göttingen) and a mouse monoclonal anti-GFP antibody (clone 3E6, Molecular Probes, Invitrogen) for the GFP-tagged SNAP-25 or SN25-0<sub>L</sub>0 were used. As secondary antibodies (1:400 in PBS+3%BSA), goat anti-rabbit-Cy3 (Dianova, Hamburg, Germany) and Atto-647N labelled sheep or goat anti-mouse (provided by Dept. of Nanobiophotonics, Max-Planck Institute for Biophysical Chemistry, Göttingen, Germany) were used. After immunostaining samples were incubated for about 30 min at RT with 40 nm green fluorescent beads (F-8795, Molecular Probes, Invitrogen) that were adsorbed to the glass cover-slips and used as a reference for focusing to the plane of the plasma membrane sheets. The samples were embedded in Mowiol (6 g Glycerol (AR No. 4094, Merck, Darmstadt, Germany), 2.4 g Mowiol 4-88 -Hoechst, Frankfurt, Germany, 6 ml water, 12 ml 200 mM Tris, pH 7.2 buffer) (provided by Dept. of Nanobiophotonics, Max-Planck Institute for Biophysical Chemistry, Göttingen, Germany) and imaged.

#### **2.5.1.2. Sample preparation for Syntaxin 1 cluster morphology after cholesterol depletion**

For the experiments in figure 39 A, PC12 were plated onto 25-mm polylysine-coated glass coverslips and were allowed to grow for about 36-40 hours. The plated cells were then incubated with or without 10 mM M $\beta$ CD - methyl- $\beta$ -cyclodextrin (C4555-1G, Sigma Aldrich, Germany) in DMEM for 15 minutes at 37°C. The cells thus treated were sonicated using a 100 ms ultrasound-pulse in ice-cold sonication buffer (120 mM potassium glutamate, 20 mM potassium acetate, 10 mM EGTA and 20mM HEPES pH 7.2).

For the experiments in figure 39 B, PC12 were plated onto 25-mm polylysine-coated glass coverslips and were allowed to grow for about 36-40 hours. The plated cells were then sonicated using a 100 ms ultrasound-pulse in ice-cold sonication-buffer (120 mM potassium glutamate, 20 mM potassium acetate, 10 mM EGTA and 20 mM HEPES pH 7.2) to obtain plasma membrane sheets and incubated with or without 15 mM M $\beta$ CD -

methyl- $\beta$ -cyclodextrin (C4555-1G, Sigma Aldrich, Germany) in sonication buffer for 30 minutes at 37°C. Then the sheets were briefly washed in sonication buffer at RT.

The membrane sheets from both the experiments in Figure 39 A and B were then fixed in 4% PFA in PBS for about an hour. Then the PFA was quenched using 50 mM NH<sub>4</sub>Cl in PBS for about 20 minutes and immunostained for endogenous syntaxin 1A using mouse monoclonal HPC-1 as primary antibody (diluted 1:200) and Atto-647N-labelled sheep anti-mouse (provided by Dept. of Nanobiophotonics, Max-Planck Institute for Biophysical Chemistry, Göttingen, Germany) as secondary antibody (diluted 1:400). The samples were embedded in Mowiol (6 g Glycerol (AR No. 4094, Merck, Darmstadt, Germany), 2.4 g Mowiol 4-88 -Hoechst, Frankfurt, Germany, 6 ml water, 12 ml 200 mM Tris, pH 7.2 buffer) (provided by Dept. of Nanobiophotonics, Max-Planck Institute for Biophysical Chemistry, Göttingen, Germany) and imaging was performed using STED microscopy.

### **2.5.2. STED microscopic imaging**

Microscopic imaging was carried out using a TCS STED (Stimulated Emission Depletion) superresolution fluorescence microscope from Leica Microsystems GmbH (Mannheim, Germany) equipped with a 1.4 NA 100x objective (Leica Microsystems GmbH, Mannheim, Germany). For experiments investigating SNAP-25 cluster morphology (section 3.5), plasma membrane sheets with expressed GFP SNAP-25 constructs were selected and focussed using as reference the glass adsorbed green fluorescent beads. Multichannel confocal images were then obtained simultaneously at confocal resolution (at 100Hz scan speed) for Cy3 (syntaxin immunostaining), GFP (GFP-SNAP-25) and Atto-647N (staining for GFP) followed by imaging Atto-647N applying STED resolution (at 10Hz scan speed). For experiments investigating syntaxin cluster morphology after cholesterol depletion (section 3.5.5) plasma membrane sheets were focussed and images were taken for Atto-647N (syntaxin1 immunostaining) in confocal (at 100Hz scan speed) followed by STED mode (at 10 Hz scan speed). Pixel size was either 21.6 nm (for figures 30 and 31) or 10.1 nm (for figures 33, 35, 37 and 39). STED excitation was performed with a 635 nm diode laser, and depletion was achieved via a Spectra-Physics MaiTai tunable laser at 750 nm. Emission was collected at 645-720 nm for the Atto647N and at 551-602 nm (for figures 30 and 31) or 562-632

nm (for figures 33, 35 and 37) for Cy3 and at 498-540 nm (for figures 30 and 31) or 511-540 nm (for figures 33, 35 and 37) for GFP. Confocal imaging was performed using PMTs (photo-multiplier tubes) and an Avalanche PhotoDiode was used for STED image acquisition. The system resolution limit was approximately 70–90 nm, measured by analysis of 20 nm crimson-fluorescent beads (F-8782, Molecular Probes, Invitrogen) (personal communication with Dr. Silvio Rizzoli).

### **2.5.3. STED image analysis for SNAP-25 cluster morphology and co-localisation studies**

Image analysis was performed using self-written routines in Matlab (The Mathworks, Inc), provided by Dr. Silvio Rizzoli. Briefly, the Cy3 and STED resolved channel were aligned using the alignment of the Atto-647N STED image to the Atto-647N confocal image as reference. For alignment of these images (Atto-647N STED and Atto-647N confocal) we used a routine in Matlab and alignment was manually verified and corrected if necessary. Regions of interest (ranging from 2 to 41  $\mu\text{m}^2$ ; on average around 10  $\mu\text{m}^2$ ) on the membrane sheets were manually selected and the Pearson's correlation coefficient (see also (Sieber et al., 2006)) was determined between the Cy3 (syntaxin1) and STED resolved (staining for GFP) images. For the STED images (in figure 30) an autocorrelation analysis was applied using a routine based on the corr2 function of Matlab. For each experiment more than 6 membrane sheets were analyzed and the values were averaged and plotted as means  $\pm$  SEM using Sigmaplot 10.0.

## **2.6. Depolarisation of Bovine Chromaffin cells, immunostaining and confocal microscopy**

### **2.6.1. Sample preparation - Stimulation and immunostaining of bovine chromaffin cells**

The primary culture of bovine chromaffin cells was kindly prepared by Ina Hertford of dept. of Membrane Biophysics, MPIBPC, Göttingen, Germany, as described previously (Nagy et al., 2002). After 3-4 days, the coverslips with cells were dipped in high or low potassium buffer (low potassium: 130 mM NaCl, 4 mM KCl, 10 mM HEPES, 1 mM  $\text{MgCl}_2$ , 5 mM  $\text{CaCl}_2$ , 44 mM glucose, pH 7.4; high potassium: 50 mM NaCl, 80 mM

KCl, 10 mM HEPES, 1 mM MgCl<sub>2</sub>, 5 mM CaCl<sub>2</sub>, 44 mM glucose, pH 7.4) for 30 s at 37°C.

Cells were then fixed in paraformaldehyde in PBS for one hour. Afterwards they were washed for 20 min using PBS supplemented with 50 mM NH<sub>4</sub>Cl and additionally twice for 10 min each with PBS. The cells were permeabilized using for 5 min PBS + 0.2% Triton-X 100, followed by a treatment for 10 min with the same buffer supplemented with BSA (PBS + Triton-X-100 + 3% BSA). Permeabilized cells were incubated for 1 hr with the primary antibodies (diluted 1:200 in PBS + Triton-X-100 + 3% BSA). After three washing steps for 10 min each (in PBS + Triton-X-100 + 3% BSA) cells were incubated for 1 hr with the secondary antibody (diluted 1:200 in PBS + Triton-X-100 + 3% BSA). The samples were then washed in PBS three times ten minutes each. Then the samples were embedded in Mowiol (6 g Glycerol (AR No. 4094, Merck, Darmstadt, Germany), 2.4 g Mowiol 4-88 -Hoechst, Frankfurt, Germany, 6 ml water, 12 ml 200mM Tris, pH 7.2 buffer) (provided by Dept. of Nanobiophotonics, Max-Planck Institute for Biophysical Chemistry, Göttingen, Germany) which contained DAPI (Molecular probes, Invitrogen) at a dilution of 1:1000 to counterstain nuclear DNA in chromaffin cells.

### **2.6.2. Confocal microscopic imaging**

For confocal microscopy an Olympus FV1000 laser scanning microscope with the following settings was used: objective: PLAPON 60x NA 1.4; DAPI was excited by the 405 nm laser line and emission was collected between 425 -475 nm; Cy3 was excited at 543 nm and emission was collected between 555 - 655 nm; Frame size was 512 x 512 pixels, pixel size 207 nm and sampling speed was 80.0 µs/pixel. To avoid preferential selection of brightly stained cells during imaging, a region with chromaffin cells that was centred was selected in the transmission mode. Using the live mode in the transmission setting, the equatorial layer of the cell was focussed. Then images were recorded in the brightfield and the fluorescence channels.

**2.6.3. Analysis of confocal images of bovine chromaffin cells**

Images were analyzed using Image J. In order to avoid preferential selection of very bright or dim immunostainings, cells were chosen randomly in the brightfield channel for analysis. Then, in fluorescence Cy3 channel a linescan of 5 pixel width was placed along the edges of the cell in a circular fashion so as to record the average fluorescence intensity along the plasma membrane. The mean background fluorescence intensity outside of the cell was subtracted from the intensity recording. Values were averaged for 19-34 cells and the average obtained for fluorescence under high potassium condition was normalized to the average value obtained for low potassium treatment. Values from three independent experiments were averaged and plotted as means  $\pm$  SEM using Sigmaplot 10.0.

---

### 3. Results

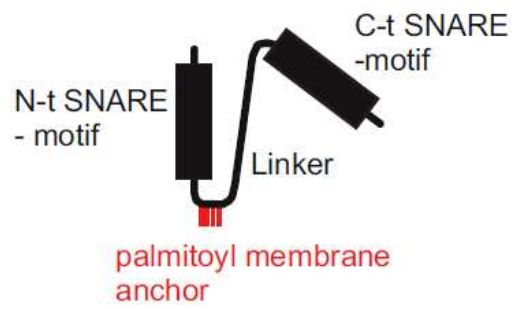
#### 3.1. Generation of GFP-SNAP-25 plasmid DNA constructs

As mentioned in the introduction and aims, one of the plasma membrane neuronal SNARE proteins, SNAP-25, is known to specifically interact with syntaxin 1 and form a heterodimer complex that is likely an initial intermediate in the pathway of SNARE complex assembly. In order to characterize the dynamics of SNARE heterodimer complex formation in their native environment, FRAP (Flourescence Recovery After Photobleaching) on live neuroendocrine (PC12) cells and plasma membrane sheet assays were employed. To begin with, several mutant constructs of SNAP-25 (with a monomeric GFP tagged at the N-terminus) involving a series of SNARE motif deletions were generated in order to disrupt the complex formation with syntaxin 1 (see Figure 9 A-E).

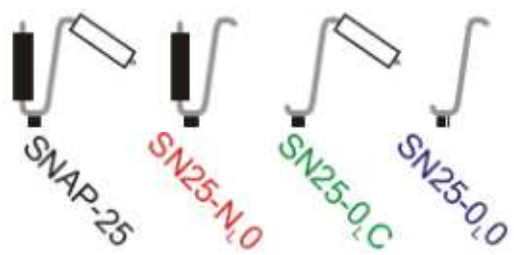
SNAP-25 has a short N-terminus followed by a N-terminal SNARE motif which connects to C-terminal SNARE motif via a linker region (see Figure 9 A). SNAP-25 is membrane anchored through palmitoylation of its cysteine residues at the linker region. In the first series of mutant constructs, either one or both the SNARE motifs were deleted (see Figure 9 B). In the second series, the mutant constructs had either the same SNARE motif on either side of the linker or the N-terminal SNARE motif at the C-terminal position (see Figure 9 C). In the third series, the N-terminal SNARE motif residues participating in the layers of interaction of the SNARE complex helical bundle were deleted in a progressive manner (see Figure 9 D). In the last series, the N-terminal SNARE motif had either proline substitutions at various residues in order to break the SNARE motif helical continuity or glycine to aspartate substitution at residue 43 (G43D), which is known to weaken the interaction with syntaxin 1 (Fasshauer et al., 1997b) (see Figure 9 E).



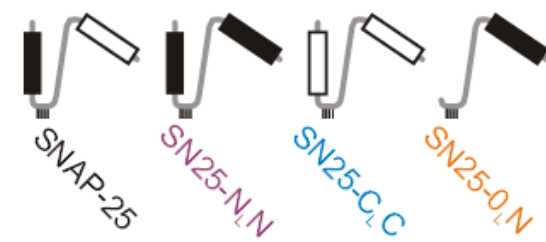
A)



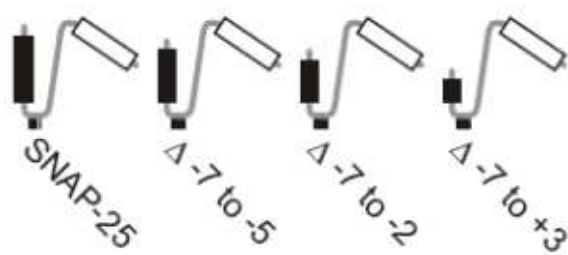
B)



C)



D)



E)



**Figure 9. Domain structure of GFP-SNAP-25 constructs**

A) SNAP-25 consists of N-t and C-t (terminal) SNARE motifs connected by a linker region which

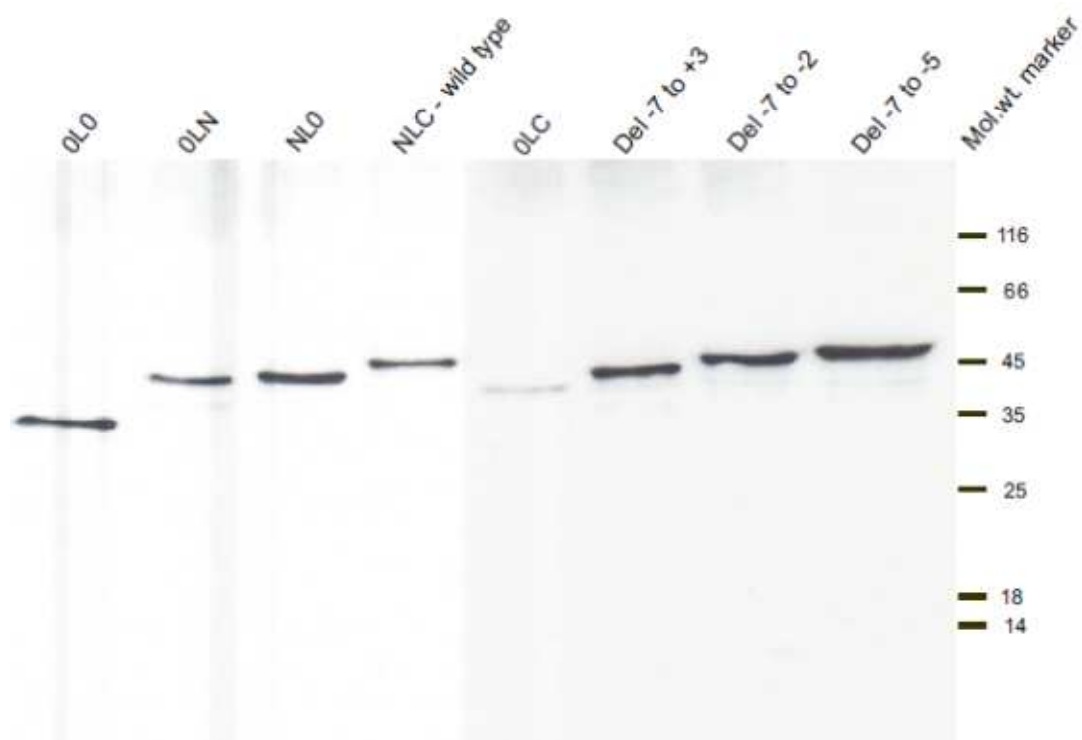
---

has four palmitoylated cysteine residues for membrane anchoring. **B)** SNAP-25 constructs with one of the two SNARE motifs or both deleted. **C)** SNAP-25 constructs with positional swapping of the SNARE motifs. **D)** SNAP-25 constructs with progressive deletion of the residues at the N-terminal SNARE motif. **E)** SNAP-25 constructs with proline (at various residues) and aspartate (G43D) substitutions at the N-terminal SNARE motif. (Please see the text in section 3.1 for details).

### **3.2. Biochemical analysis of GFP-SNAP-25 expression in PC12 cells**

To check if the GFP-SNAP-25 constructs were properly expressed in PC12 cells, immunoblots from freshly lysed transfected PC12 cells were performed. PC12 cells were transfected with the indicated GFP-SNAP-25 constructs using electroporation and grown in 75 cm<sup>2</sup> flask to full confluence. After 24-36 hours, the cells were lysed in a sample buffer and a fraction of samples was subjected to SDS-PAGE and a Western blot analysis was carried out. For detection of expressed constructs, rabbit polyclonal anti-GFP antibody (cat. No. 132002, Synaptic Systems, Göttingen) as primary antibody and HRP-conjugated goat anti-rabbit antibody (BioRad Laboratories) as secondary antibody were used. The bands were detected by enhanced chemiluminescence (ECL, Perkin Elmer, Boston) on a FujiFilm LAS-1000 imaging station (Fuji Photo Film, Tokyo, Japan). As shown in Figure 10 A and B, all constructs showed only one band of the expected size, indicating their proper expression and absence of any degradation products. Please note that the varying levels of band intensities in the blots shown in Figure 10 A & B reflect either the variable transfection efficiencies or expression levels for the corresponding constructs. The procedure was carried out by Dagmar Diezmann, department of Neurobiology, MPIBPC, Göttingen.

A)



B)

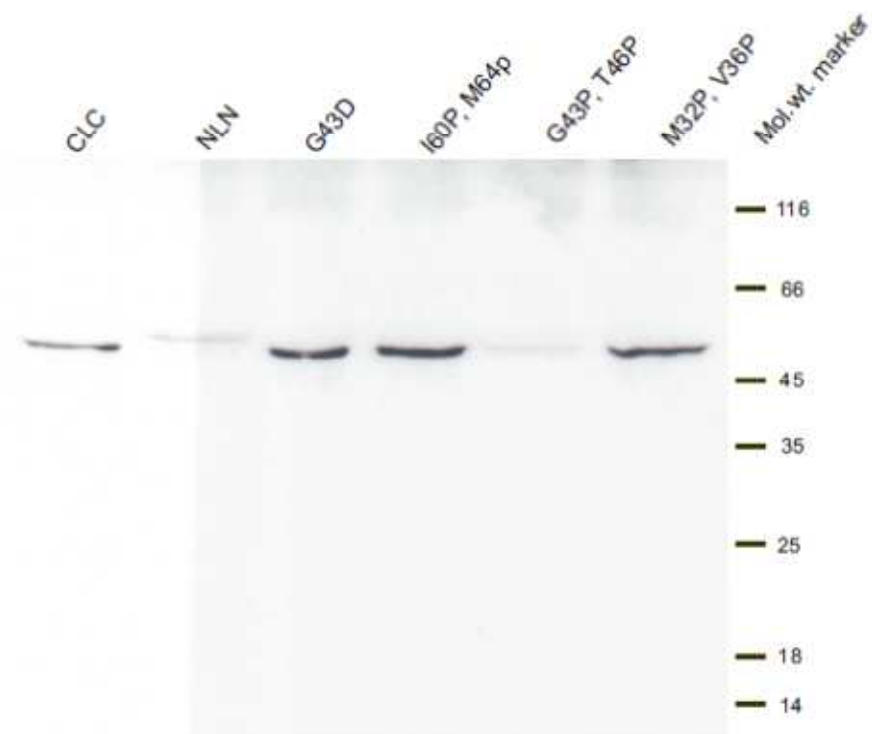


**Figure 10. Immunoblot analysis of expression of GFP-SNAP-25 and its mutants in PC12 cells.** Each of the plasmid DNA constructs was over expressed in PC12 cells through

electroporetic transfection and a day later a confluent flask of cells expressing corresponding construct was lysed and the samples were subjected to SDS-PAGE analysis and immunoblotting using anti- GFP antibody (see the text for more details). As shown in the figure panel A and B, band sizes correspond to respective sizes of the GFP-SNAP-25 constructs. Band intensity for O<sub>L</sub>C in A) and for N<sub>L</sub>N and G43P, T46P in B) was lower than the rest of the bands. This could be due to variation in transfection and/or expression efficiency. [The data was kindly provided by Dagmar Diezmann and Dr.Thorsten Lang.](#)

### 3.3. Setting up the FRAP assay

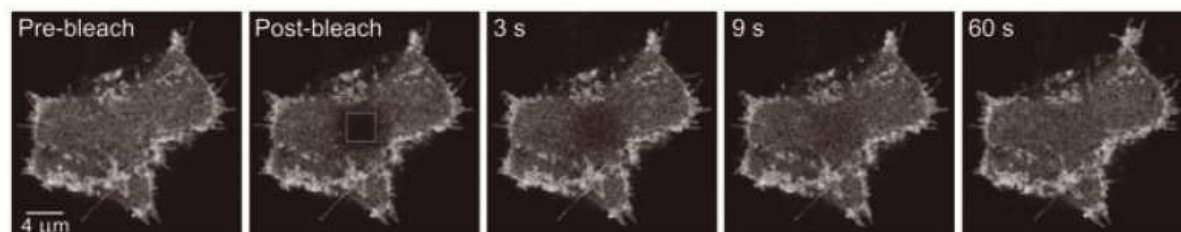
As described in the above section, introduction (and aims), the results from the various *in-vitro* and *in vivo* studies remained inconclusive on the exact nature of the sequence of the SNARE assembly in live cells. Therefore, an attempt, to design an assay based on FRAP (Fluorescence Recovery After Photobleaching) (Axelrod et al., 1976; Reits and Neefjes, 2001) was made for studying the SNARE interactions in live cells using the mobility of SNAP-25 in the membrane as readout. FRAP on live cells is a rapid and non-invasive technique to study protein mobility in the native environment. This mobility depends on the diffusion of the free protein but should be slowed when the protein interacts with slower diffusing molecules or trapped in a membrane compartment. The interacting partner syntaxin 1 has a TMR and is organized in clusters (Sieber et al., 2006). Therefore interactions of SNAP-25 with syntaxin 1 should slow down SNAP-25 mobility and mobility of SNAP-25 should reflect, atleast in part, its interaction with syntaxin.

In our FRAP studies, SNAP-25 was fused to monomeric variant of GFP which rendered it green fluorescent. This construct was transfected into neuroendocrine PC12 cells and FRAP experiments were performed approximately a day later. Using Leica TCS SP5 confocal set up the cells were selected for their SNAP-25 expression (too bright or too dim cells were excluded) and the basal plasma membrane was brought into focus. Initially, pre-bleach frames were taken with maximal speed before bleaching twice a 3µm x 3µm squared region followed by several post bleach frames to monitor the fluorescence recovery over a time period (see Figure 11 A). The data obtained was processed and fitted as described in Materials and Methods. As shown in Figure 11 A and B, SNAP-25 diffused into the bleached region within seconds achieving 70-80 % recovery. A construct lacking the N-terminal SNARE motif showed increased mobility

(see Figure 11 B, green trace) indicating the involvement of the N-terminal SNARE motif (Q<sub>b</sub>) in restriction of the SNAP-25 mobility.

A)

SNAP-25-GFP



B)

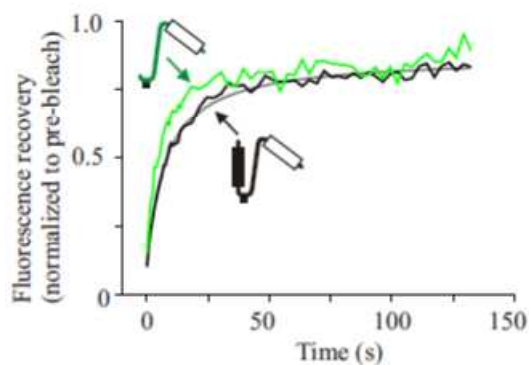


**Figure 11. FRAP micrographs and recovery traces**

**A)** Confocal micrographs monitoring the basal plasma membrane of a PC12 cell expressing GFP-labeled SNAP-25. FRAP was monitored in a squared region (indicated by a box in the second image) after bleaching. **B)** Recovery traces from A (black trace) and another cell expressing a SNAP-25 construct lacking the N-terminal SNARE-motif (SN25-0<sub>LC</sub>; green trace). Traces have been background corrected and normalized to an averaged pre-bleach value (for details see Materials and Methods). For the SNAP25 trace, a fitted hyperbola function (gray trace) is shown from which half-time and maximal recovery was determined. [Figures taken from Halemani et al., \(2010\).](#)

### 3.4. Studying the Q-SNARE interactions through FRAP and membrane sheet binding studies

The mobility pattern and recovery rate obtained from FRAP studies should indirectly reflect the strength of the interactions of the SNAP-25 with its partners and serve as a

readout for the dynamics of the SNAP-25 SNARE motif interactions to help model the structure of a putative syntaxin 1 - SNAP-25 (Q<sub>a</sub>Q<sub>b</sub>) complex. As shown in Figure 11 B, the Q<sub>b</sub> SNARE motif could be involved in this interaction. To study this in further detail, FRAP assays were performed on live PC12 cells testing more constructs and with co-overexpressed syntaxin 1-CFP. In addition, a membrane sheet assay was employed that allows for studying SNARE interactions with one partner being in its native environment. Thus the two approaches complement each other enabling the studies on the Q-SNARE interactions in their native environment.

### 3.4.1. Structure and dynamics of Q-SNARE-interactions - a Q<sub>a</sub>Q<sub>b</sub> SNARE complex formation as revealed by FRAP studies

#### 3.4.1.1. N-terminal SNARE motif is required for complex formation

The mobility of the protein and therefore its half time of recovery in FRAP studies, depends on its free diffusion rate which changes upon its interactions with molecules that diffuse slower or are immobile. SNAP-25 being a lipid anchored protein via its palmitoyl side chains diffuses faster than its Q-SNARE partner, syntaxin 1, which is TMR anchored and diffuses slower owing to its self clustering mechanism (Sieber et al., 2007).

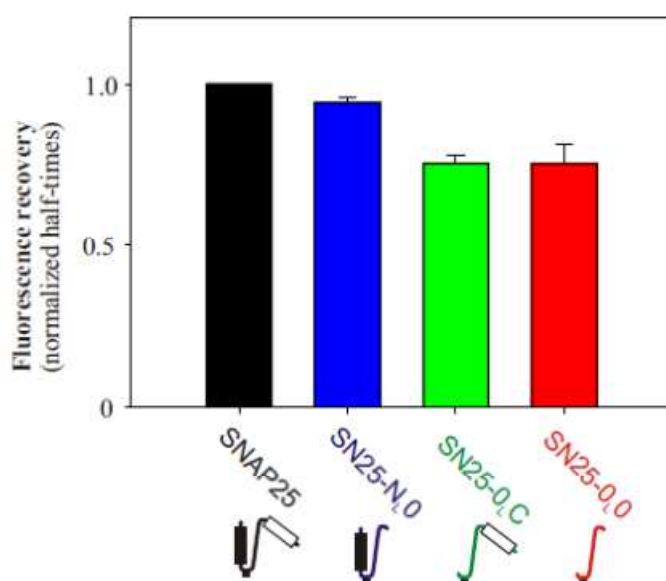


**Figure 12. Restriction of SNAP-25 mobility involves its N-terminal SNARE-motif.**

SNAP-25 mobility was compared to constructs lacking either one or both SNARE-motifs (SN25-

---

N<sub>L</sub>0, SN25-0<sub>L</sub>C and SN25-0<sub>L</sub>0). Each recovery trace from each cell was analyzed to obtain half time of recovery and for each experiment, the average half time of recovery from several cells was normalised to the value obtained for wild type SNAP-25. The mean half time of recovery from 3 independent experiments was plotted as vertical bar graph. Values are means  $\pm$  SEM (n = 3 experiments and analyzing 4-7 cells for each experiment). [Figure taken from Halemani et al., \(2010\).](#)

The FRAP studies on SNAP-25 and its SNARE motif deletion constructs – either one or both of its SNARE motifs deleted, showed that the mobility of SNAP-25 constructs with the N-terminal SNARE motif intact (SN25-N<sub>L</sub>C, SN25-N<sub>L</sub>0) is slightly slower than the ones without (SN25-0<sub>L</sub>C, SN25-0<sub>L</sub>0). Deletion of only the C-terminal SNARE motif – SN25-N<sub>L</sub>0, did result in recovery rates as close as for wild type – SN25-N<sub>L</sub>C, but deletion of the N-terminal SNARE motif - SN25-0<sub>L</sub>C, slightly decreased the recovery rate as much as SN25-0<sub>L</sub>0 with both SNARE motifs deleted (see Figure 12). Hence, the N-terminal SNARE motif is responsible for slower mobility of SNAP-25 in the plane of the membrane most likely due to its engagement in protein-protein interactions. This could be homomeric or heteromeric interactions. Although, homomeric oligomerisation of SNAP-25 might result in its cluster formation similar to syntaxins, heteromeric interactions involving syntaxin 1 are well known and very likely to be responsible for the observed mobility phenotype of SNAP-25. Hence it was decided to investigate SNAP-25 mobility in the presence of increased syntaxin 1 concentrations.

#### **3.4.1.2. Co-overexpressed syntaxin 1 decreases SNAP-25 mobility manifold**

To investigate if the observed SNAP-25 mobility phenotype is due to syntaxin 1 interactions, syntaxin 1-CFP and GFP- SNAP-25/SNAP-25 constructs were co-overexpressed in PC12 cells and FRAP experiments performed (see Figure 13).

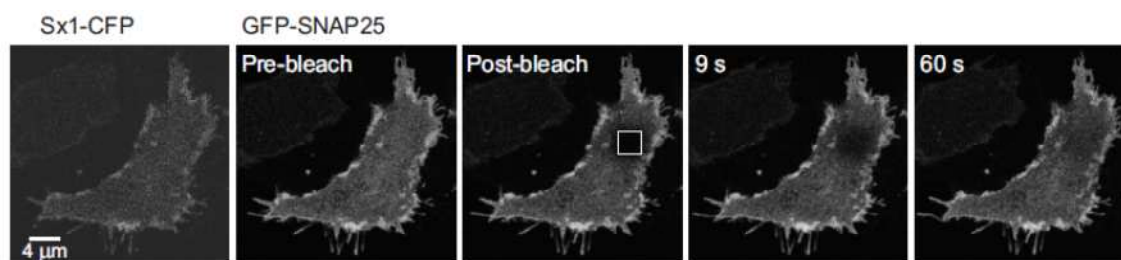


**Figure 13. Confocal micrographs monitoring the basal plasma membrane of a PC12 cell expressing GFP-labelled SNAP-25 and syntaxin 1-CFP.** An image was taken in the CFP channel to record the intensity levels of expressed Syx1-CFP. Then, in the GFP channel, GFP-SNAP-25 was recorded and a squared region was bleached. Fluorescence recovery was monitored over a time period and the recovery traces were used for the subsequent analysis. [Figure taken from Halemani et al., \(2010\).](#)

The cells co-expressing both syntaxin 1 and SNAP-25 were selected in the CFP and GFP channels respectively and then recorded the syntaxin 1 levels at the basal plasma membrane in the CFP channel before proceeding with the FRAP on GFP-SNAP-25. It was made sure that no cross talk exists between the GFP and CFP channels while setting a good spectral separation between the two emissions using Leica SP5's very efficient spectral detection system (see Materials and Methods for details). Moreover, very bright GFP-SNAP-25 cells and very low syntaxin 1-CFP expressing cells were avoided by omitting the ones from the analysis which showed CFP levels less than 1.0 (after background fluorescence subtraction). From the same samples, FRAP experiment was carried out on the cells expressing GFP-SNAP-25 but no syntaxin 1-CFP as an internal control for the experiment. FRAP analysis yielded half times of recovery for individual cells expressing SNAP-25 or the SNAP-25 constructs and the values were plotted against their respective syntaxin 1-CFP levels. It should be noted here that in addition to the overexpressed syntaxin 1-CFP, the cells also have endogenous syntaxin available. The plot for SNAP-25 constructs with one or both SNARE motifs deleted is shown in Figure 14. Each spot in the figure shown represents one cell and a linear fitting of all the spots from one construct shows the relation of the half time of recovery to syntaxin 1-CFP expression. It is evident that mobility of SNAP-25 got progressively reduced with increasing concentrations of syntaxin 1-CFP and as well as for the mutant construct, SN25-N<sub>L</sub>0. The construct without both SNARE motifs, SN25-0<sub>L</sub>0, did not exhibit any



mobility changes with increasing syntaxin 1-CFP concentrations. Similarly  $0_{LC}$ , did not exhibit any consistent mobility changes (see Figure 14). Please note that the noise in the measurement might be in part caused by the varying degree of endogenous syntaxin levels.

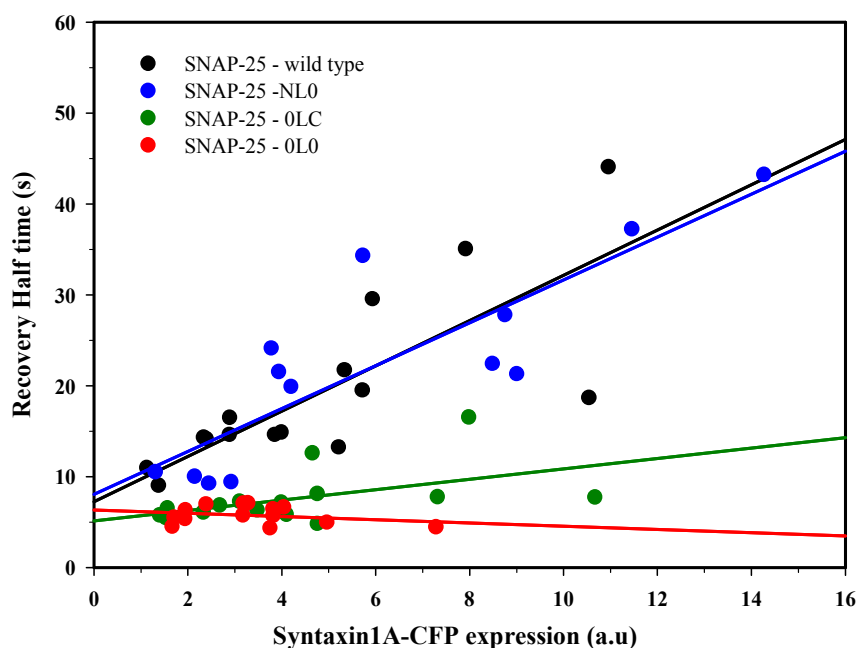


**Figure 14.** Half times of recovery as a function of syntaxin 1-CFP levels shown for SNAP-25, SN25- $N_{L0}$ , SN25- $0_{LC}$  and SN25- $0_{L0}$ . From individual cells for each condition half times of recovery were plotted versus syntaxin 1-CFP expression level and the data was fitted with a linear regression line indicated in the respective colours.

The half times of recovery were analyzed for cells expressing only SNAP-25 or SNAP-25 constructs without syntaxin 1- CFP expression. The FRAP traces from several such cells from each construct were averaged and hyperbola fitted to obtain background half time of recovery for each experiment. Then a so called ‘slope value’ was calculated for each cell (expressing both SNAP-25 and syntaxin 1 by subtracting from its half time of recovery the respective background half time of recovery and dividing the resulting value with the respective syntaxin 1-CFP overexpression level. Slope values were averaged for one experiment and then a mean of three experiments calculated and plotted as shown in Figure 15.

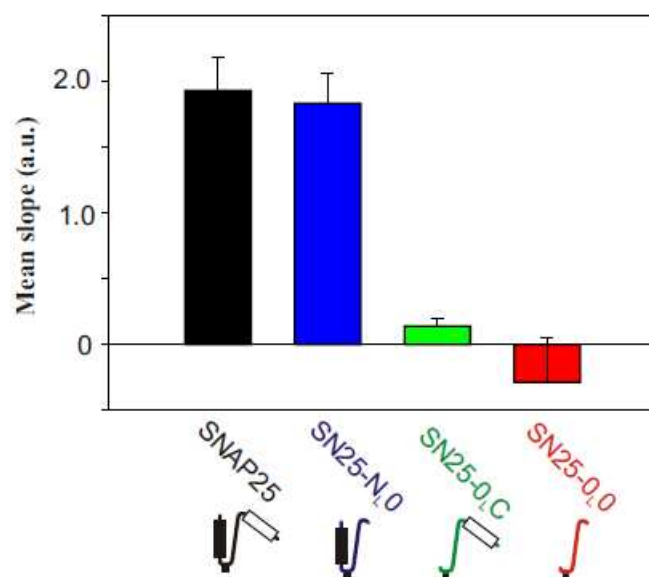


**Figure 15. Restriction of SNAP-25 mobility involves its N-terminal SNARE-motif and syntaxin.** SNAP-25 mobility was compared to constructs lacking either one or both SNARE-motifs (SN25-N<sub>L</sub>0, SN25-0<sub>L</sub>C and SN25-0<sub>L</sub>0). For each cell in each condition shown in Figure 14, a slope value was determined as described in 'FRAP data analysis - Materials and Methods section'. Slope values were averaged for one experiment and then a mean of three experiments calculated. Values are means  $\pm$  SEM ( $n = 3$  experiments). [Figure taken from \(Halemani et al., 2010\).](#)

The slope plot reiterates that the SNAP-25 mobility is restricted as a function of syntaxin 1 expression in the cell only if the N-terminal SNARE motif of SNAP-25 is intact. In these conditions, the C-terminal SNARE motif doesn't seem to have any significant role in the mobility of SNAP-25 as SNAP-25 is as fast as SN25-N<sub>L</sub>0. SN25-0<sub>L</sub>0, having no SNARE motifs is unable to interact with syntaxin 1 and therefore represents 'freely diffusing SNAP-25' with a recovery half time of 5.3 s as determined from the FRAP data (the mean recovery half times from SN25-0<sub>L</sub>0 overexpressing cells that had no signal in the CFP-channel, i.e, cells with no syntaxin overexpression, as calculated from a total of 6 independent experiments shown in Figures 12 and 15). Any interaction between 'freely diffusing SNAP-25' and freely diffusing syntaxin 1 with recovery half time in the range of 10-15 s (for syntaxin construct having only the transmembrane region as determined by Sieber et al., (2007), using live cell FRAP approach) should slow down SNAP-25 two to three fold. But, the data shown in figure 14 indicate that the interaction with syntaxin 1 decreases SNAP-25 mobility up to eight

fold suggesting that the slowed mobility via the N-terminal SNARE motif is due to interaction with immobile syntaxin 1 clusters.

Having been encouraged by the results, it was decided to investigate the mechanism of interaction of the N-terminal SNARE motif in detail. Is the N-terminal SNARE motif dependent SNAP-25 mobility position specific? Would there be a similar effect on SNAP-25 mobility if the N-terminal SNARE motif is at the C-terminus or does the C-terminal SNARE motif exert restricted mobility on SNAP-25 if it is positioned at the N-terminus? To put it in other words - does the position of the SNARE motifs (N and C terminal) which dictates their steric orientation and molecular flexibility either by being close to or away from palmitoyl anchor, encode the specificity for the SNAP-25 mobility phenotype?

#### **3.4.1.3. Position of the N-terminal SNARE motif is important for efficient syntaxin interaction**

To be able to understand the position specific importance of the SNARE motifs, SNAP-25 constructs were designed which contained N-terminal or C-terminal motifs at either termini (SN25-N<sub>L</sub>N and SN25-C<sub>L</sub>C) or the N-terminal SNARE motif at the C-terminus only (SN25-0<sub>L</sub>N). PC12 cells were transfected with SNAP-25 and the new constructs SN25-N<sub>L</sub>N, SN25-C<sub>L</sub>C and SN25-0<sub>L</sub>N along with syntaxin 1-CFP and the FRAP experiment was performed approximately a day later. The recovery rates for all the tested constructs were plotted as a function of syntaxin 1-CFP expression levels (see Figure 16 and for slope value analysis of the same data see Figure 17). As shown earlier, the SNAP-25 mobility got progressively slowed down in the presence of increasing levels of syntaxin 1-CFP. Likewise, mobility of the construct SN25-N<sub>L</sub>N, with an additional N-terminal SNARE motif at the C-terminus, shows linear correlation with syntaxin 1-CFP expression levels albeit with a more robust response than its wild type counterpart. Although SN25-N<sub>L</sub>N is slower than SNAP-25, the slowdown is not two fold to suggest that not each of the two N-terminal SNARE motifs interacts as efficient as N-terminal SNARE motif alone. To support this, the SN25-0<sub>L</sub>N construct – with only the N-terminal SNARE motif at the C-terminus was tested. But it doesn't seem to slowdown SNAP-25 with increasing syntaxin 1 concentration as efficient as SN25-N<sub>L</sub>0 (compare Figures 14 and 15). Taking together, one tends to see that the N-terminal

SNARE motif at the C-terminus doesn't provide efficient contribution towards slowing down the SNAP-25 mobility. SN25-C<sub>L</sub>C, with C-terminal SNARE motif at both termini, does not slow down with increasing syntaxin 1 concentration showing that positioning of the C-terminal SNARE motif at the N-terminus does not enforce its interaction with syntaxin 1.

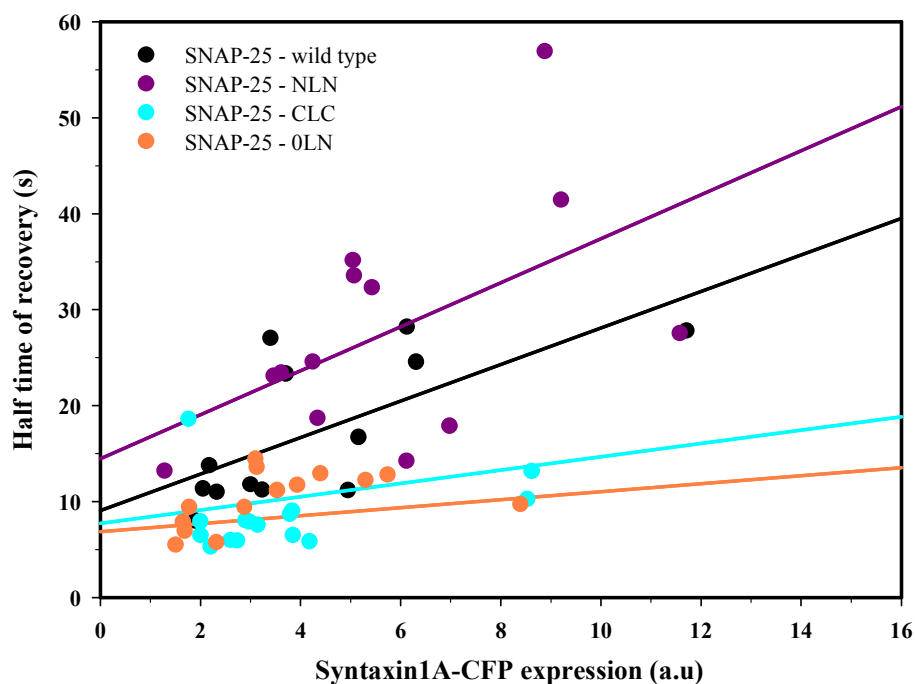


**Figure 16.** Half times of recovery as a function of syntaxin1-CFP levels shown for SNAP-25, SN25-N<sub>L</sub>N, SN25-C<sub>L</sub>C and SN25-0<sub>L</sub>N. From individual cells from each condition half times of recovery were plotted versus syntaxin 1-CFP expression levels and the data was fitted with a linear regression line indicated in the respective colours.

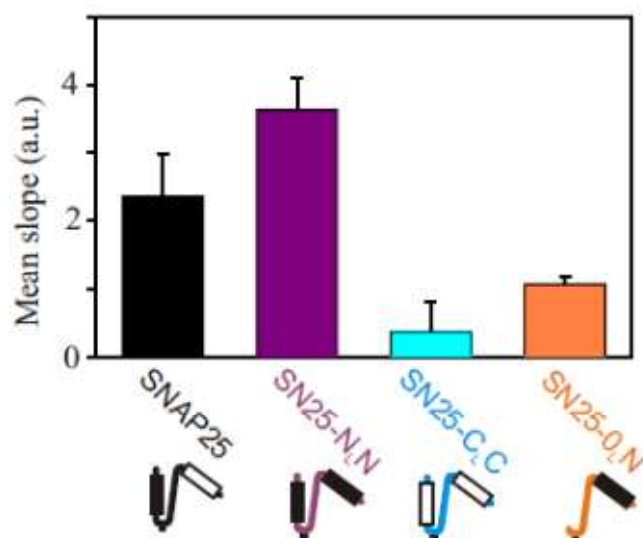


**Figure 17. Positional specificity of the N-terminus of SNAP-25 for its interaction with syntaxin.** SNAP-25 mobility was compared to constructs SN25-N<sub>1</sub>N, SN25-C<sub>1</sub>C and SN25-O<sub>1</sub>N. For each cell in each condition shown in Figure 16, a slope value was determined as described in 'FRAP data analysis - Materials and Methods section'. Slope values were averaged for one experiment and then a mean of three experiments calculated. Values are means  $\pm$  SEM (n = 3 experiments). [Figure Taken from Halemani et al., \(2010\).](#)

#### **3.4.1.4. Most of the N-terminal SNARE motif is required for SNAP-25 mobility restriction**

Having discovered the positional significance of the N-terminal SNARE motif which imparts specific steric orientation and a defined molecular flexibility for the SNAP-25 interaction with syntaxin 1, it was decided to investigate the extent of interaction along the axis of the SNARE motif. That is, what are the critical residues within the SNAP-25 SNARE motif? As shown in figure 18, there are 16 residues along the SNARE motif numbered from -7 to +8 that would participate in corresponding layers of interaction within a neuronal SNARE core complex involving syntaxin 1 and synaptobrevin 2. The residues participating in these layers would probably be also required for Q-SNARE complex formation. In order to test this hypothesis, a series of constructs were designed with progressive deletion of these residues and co-overexpressed the constructs in PC12 cells along with syntaxin 1.

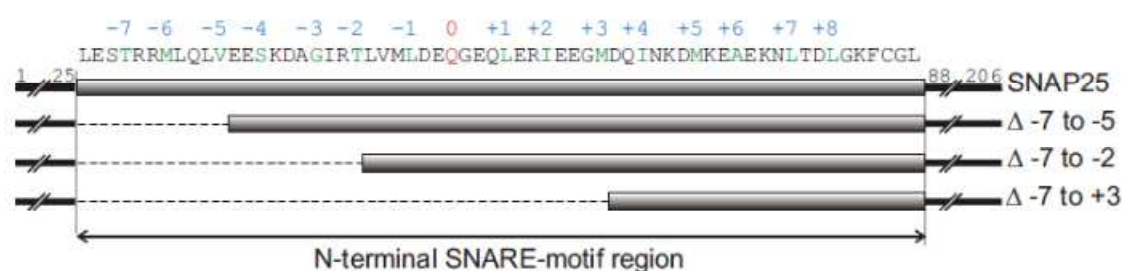


**Figure 18. Illustration of N-terminal SNARE motif amino acid deletion constructs.**

The amino acid sequence of the N-terminal SNARE-motif is depicted. The numbers -7 to +8 refer to amino acids (highlighted in green and red) forming layers of interaction in the SNARE-complex. Bars indicate the remaining part of the N-terminal SNARE-motif of the construct. Figure taken from Halemani et al., (2010).

As shown before, half time of recovery values from the FRAP data analysis were plotted against syntaxin 1-CFP over expression levels as shown in Figure 19 (also see Figure 20 for the slope value analysis). Mobility of wild type SNAP-25 slows down as a function of syntaxin 1-CFP expression levels. But deletion of the first three interacting residues is sufficient enough to make SNAP-25 diffuse freely. As expected, any subsequent deletions of the residues, from layer -7 to -2 or from -7 to +3 also resulted in free mobility of SNAP-25 without any regard to syntaxin 1 concentrations. The data suggest that the N-terminal amino acids are significantly involved in the interaction with syntaxin 1 as in line with the observation that the deletion of amino acids 1-38 in SNAP-25 inhibits SNARE complex formation (Fasshauer and Margittai, 2004).

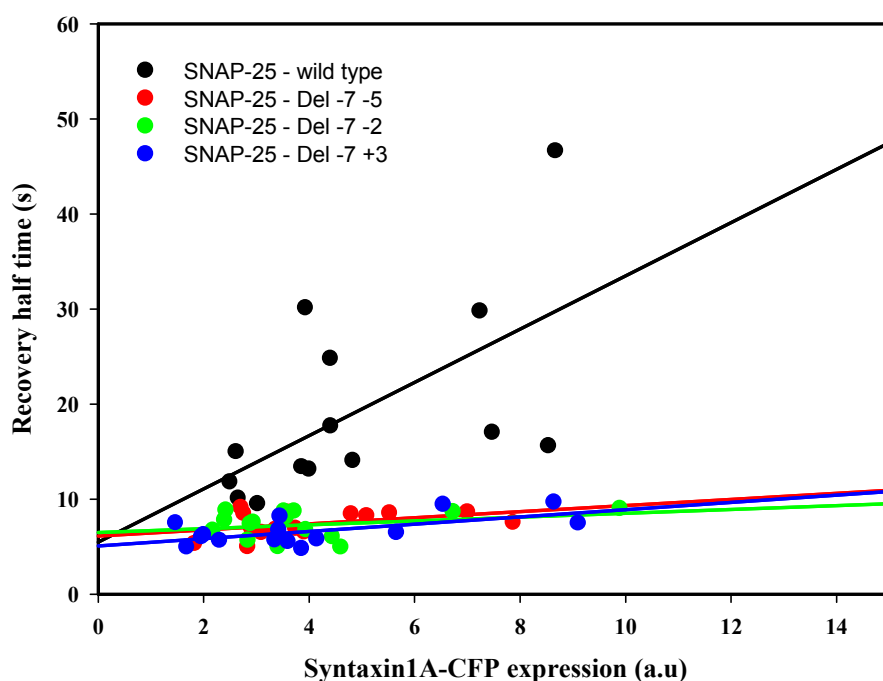


**Figure 19.** Half times of recovery as a function of syntaxin1-CFP levels shown for SNAP-25 and deletion constructs, including deletions from residues -7 to -5, -7 to -2 and from -7 to +3. From individual cells, from each condition half times of recovery were plotted versus syntaxin 1-CFP expression levels and the data was fitted with a linear regression line indicated in the respective colours. (Del = deletion).

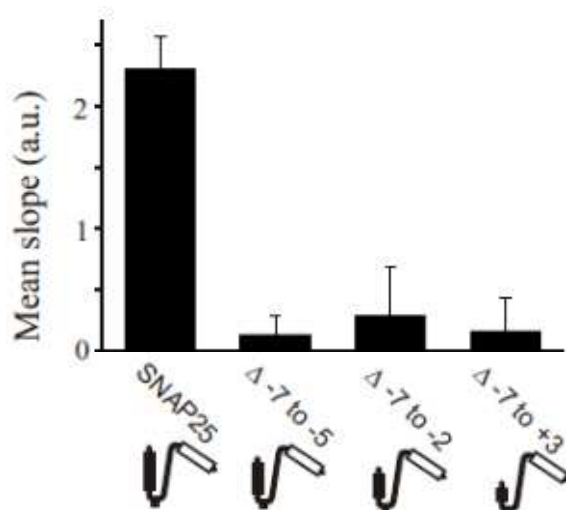


**Figure 20.** SNAP-25 interaction with syntaxin 1 requires N-terminal amino acids.

SNAP-25 mobility was compared to a series of constructs with progressive amino acid deletions (see Figure 18). For each cell in each condition shown in figure 19, a slope value was determined as described in 'FRAP data analysis - Materials and Methods section'. Slope values were averaged for one experiment and then a mean of three experiments calculated. Values are

---

means  $\pm$  SEM (n = 3 experiments). ( $\Delta$  = deletion).

#### **3.4.1.5. Alpha helical conformation of the N-terminal SNARE motif is required for SNAP-25 mobility restriction**

The SNARE motif of syntaxin 1 and the N-terminal SNARE motif of SNAP-25 assume alpha helical conformation when present in binary or ternary complex (Zhong et al., 1997). In order to test if the complex observed in our studies also adapts an alpha helical conformation, a series of SNAP-25 constructs were designed with proline substitutions to break the alpha helix at various positions along the N-terminal SNARE motif. Proline either twists or breaks a helix or both because having no amide hydrogen it cannot donate an amide hydrogen bond and also because its side chain interferes sterically with the backbone of the preceding turn - inside a helix, this forces a bend of about 30° in the helix axis (von Heijne, 1991). Hence constructs were designed with proline substitutions of the amino acids involved in layer formation - M32P-V36P at the N-terminal end and I60P-M64P at the C-terminal end of the N-terminal SNARE motif (see Figure 21). In addition, another construct, SN25-G43D was designed and tested. Glycine at either position 43 (in SNAP-25) or corresponding position (in other SNAP-25 homologues), is known to be highly conserved among the members of Q<sub>b</sub>/Q<sub>c</sub> SNARE family (Fasshauer et al., 1997b). SN25-G43D is incapable of forming *in-vitro* SNARE complexes (Fasshauer et al., 1997b) because the mutation Gly to Asp disrupts packing through steric and electrostatic forces as the glycine at residue 43 accommodates the bulky phenylalanine in syntaxin 1 at residue 216 in the hydrophobic core of the SNARE four-helix bundle (Fasshauer et al., 1998). Also, the analogous Gly to Asp mutation in the yeast SNAP-25 homologue – Sec9p (Brennwald et al., 1994) and G50E in the *Drosophila* SNAP-25 homologue (Rao et al., 2001) results in temperature sensitive mutants. However, it was demonstrated that *in-vivo* complexes are still possible (An and Almers, 2004).



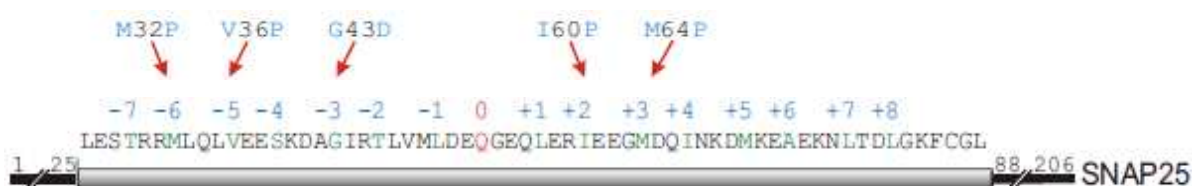


**Figure. 21. Illustration of amino acid substitution constructs.**

The amino acid sequence of the N-terminal SNARE-motif is depicted. The numbers -7 to +8 refer to amino acids (highlighted in green and red) forming layers of interaction in the ternary SNARE-complex. Red arrows point to amino acids with substitutions. [Figure taken from Halemani et al., \(2010\).](#)

The constructs were tested with syntaxin 1-CFP co-overexpression in PC12 cells. Mobility of SNAP-25, once again progressively slows down with increasing concentration of syntaxin 1 expression. The constructs M32P-V36P and I60P-M64P do not show significant change in their mobility pattern with regard to increasing syntaxin 1-CFP concentration. However, it is interesting to note that mobility of G43D moderately slows down with increasing syntaxin 1-CFP concentration and was less than the wild type but more than the proline mutants (see Figure 22 and for mean values from slope analysis see Figure 23) indicating that its syntaxin 1 interaction seems to be weaker compared to SNAP-25 as has been suggested by An and Almers, (2004).

The data suggests that the helix breaking SNAP-25 proline mutants prevent  $Q_aQ_b$  complex formation *in vivo* and therefore that the N-terminal SNARE motif of SNAP-25 assumes an alpha helical conformation along most part of its length upon formation of the  $Q_aQ_b$  complex.

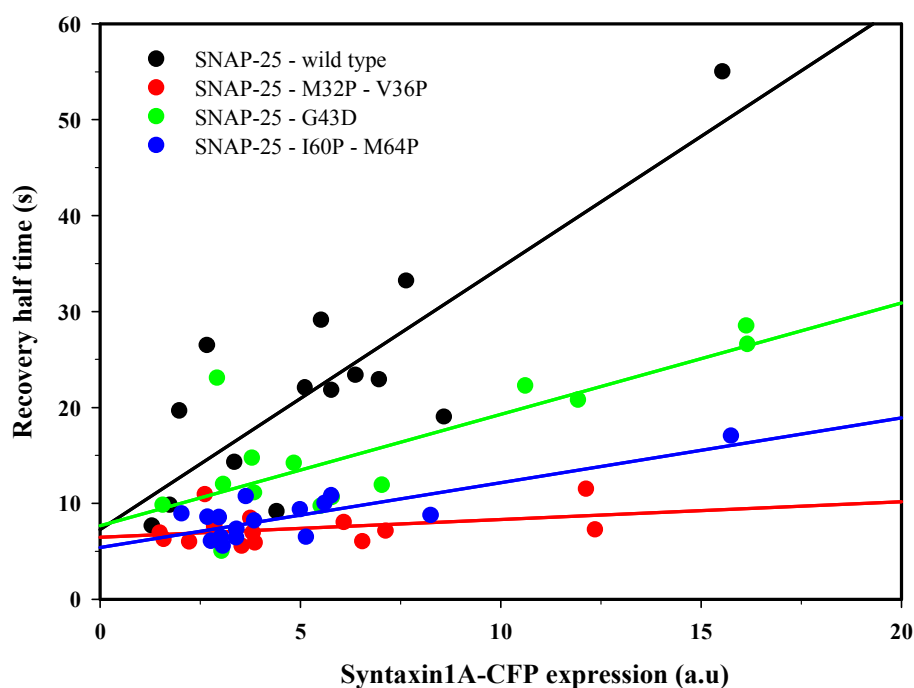


**Figure 22.** Half times of recovery as a function of syntaxin 1-CFP levels shown for SNAP-25 and the AA substitution constructs – M32P-V36P, I60P-M64P and G43D. From individual cells from each condition half times of recovery were plotted versus syntaxin 1-CFP expression level and the data was fitted with a linear regression line indicated in respective colours.

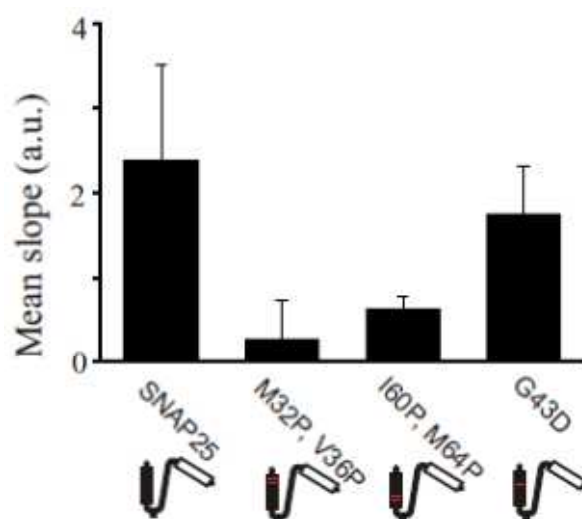


**Figure 23.** Effect of amino acid substitutions in the N-terminal SNARE motif on the SNAP-25 / syntaxin 1 interactions. SNAP-25 mobility was compared to a series of constructs with different AA substitutions (see Figure 21). For each cell in each condition shown in figure 22, slope values were determined as described in 'FRAP data analysis - Materials and Methods section'. Slope values were averaged for one experiment and then a mean of three experiments

---

calculated. Values are means  $\pm$  SEM (n = 3 experiments). [Figure taken from Halemani et al., \(2010\).](#)

#### **3.4.1.6. Correlation of expression levels of GFP-SNAP-25/syntaxin 1-CFP and maximal recovery and half time**

A recent study has shown that the density of proteins within the plasma membrane significantly reduces the rates of diffusion for the observed proteins (Frick et al., 2007). Therefore, it is possible that the FRAP experiments in the present study are subjected to similar effect since the co-overexpression of GFP-SNAP-25 and syntaxin 1-CFP in PC12 cells would increase the density of proteins within the plasma membrane and thereby influence the mobility of the constructs under study. Hence, for GFP-SNAP-25, the half-time recovery and maximal recovery values from several FRAP experiments were pooled and plotted as a function of GFP-SNAP-25 expression levels. Similarly, maximal recovery values for GFP-SNAP-25, SN25-G43D and SN25-N<sub>L</sub>0 were pooled and plotted as a function of syntaxin 1-CFP expression levels.

The data shows that the values varied largely between individual cells but no correlation between GFP-SNAP25 expression levels and half-times of recovery or maximal recovery was observed (see Figure 24 A). Syntaxin 1-CFP did not affect maximal recovery of SNAP25, SN25-G43D and SN25-N<sub>L</sub>0 at low and medium syntaxin 1-CFP expression levels (see Figure 24 B). However, at increased expression levels, syntaxin 1-CFP tends to decrease the maximal recovery of SNAP-25 but not of SN25-N<sub>L</sub>0 and SN25-G43D. This could indicate that for this effect, the C-terminal SNARE motif of SNAP-25 is needed in addition to the N-terminal SNARE-motif and that at artificially very high syntaxin 1: SNAP-25 ratios SNAP-25 is driven into complexes different from a simple two helix Q<sub>a</sub>Q<sub>b</sub> complex.

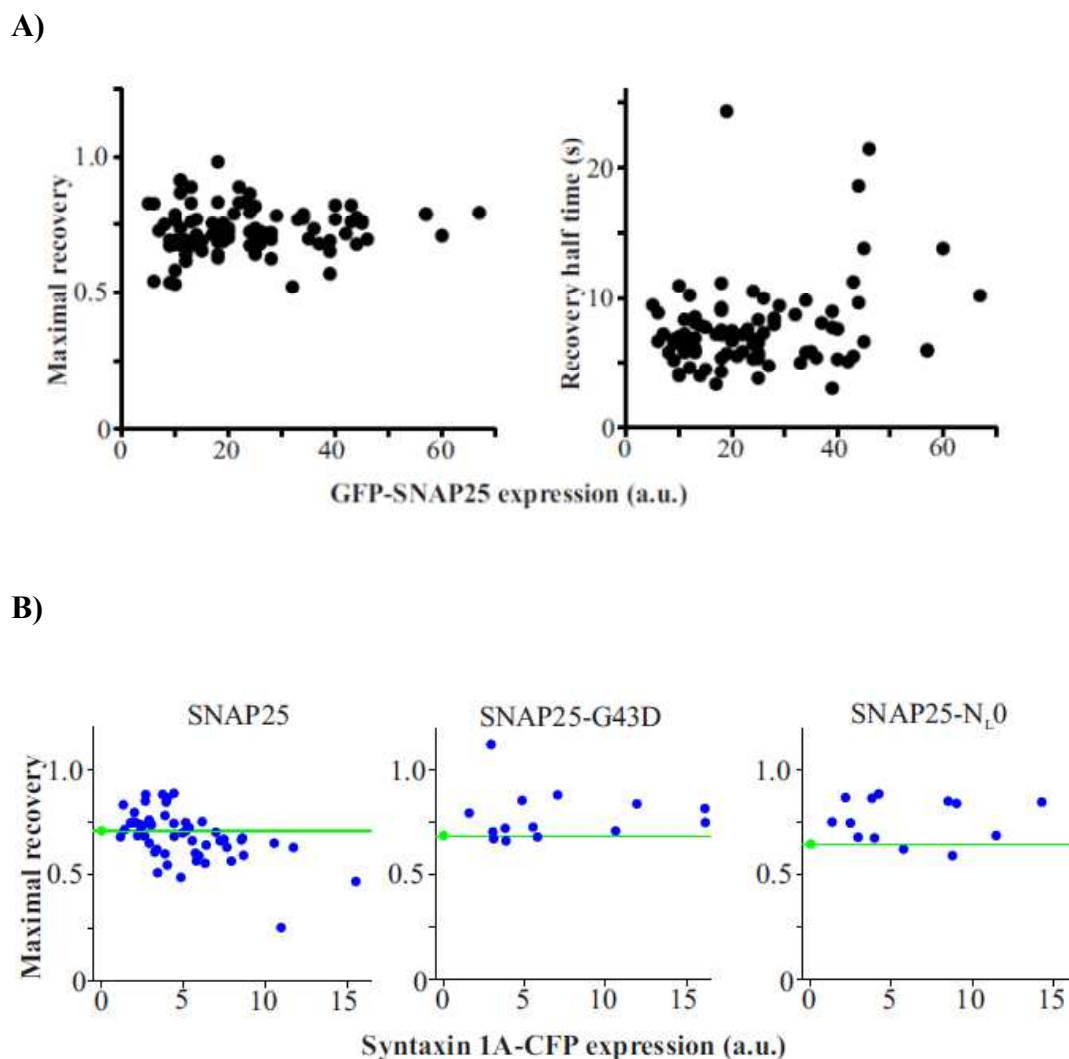


**Figure 24. Correlation between expression levels and maximal recovery or half time of recovery.** (A) The GFP-SNAP-25 expression level in individual cells was plotted against maximal recovery (left) or half time of recovery (right). (Only cells without syntaxin 1-CFP co-expression are included). The analysis shows that both maximal recovery and half time of recovery are independent from GFP-SNAP-25 overexpression levels. (B) The syntaxin 1-CFP expression level in individual cells was plotted against maximal recovery (blue dots) of GFP-SNAP-25 or GFP-SNAP-25 constructs (from left to right: GFP-SNAP-25, SN25-G43D and SN25-N<sub>L</sub>0). Green dots indicate average maximal recovery values obtained from cells showing no syntaxin1-CFP expression (see also green reference line). [Figure taken from Halemani et al., \(2010\).](#)

#### **3.4.1.7. Restricted SNAP-25 mobility through non-cognate SNARE interactions using syntaxin 4 as an example**

*In vitro*, SNARE proteins are known to be promiscuous in their interactions (Fasshauer et al., 1999). Therefore, in the present study, it was investigated if this is true *in vivo* as well and if a non-cognate  $Q_a$  SNARE could slow down SNAP-25 mobility indicating the formation of a non-cognate  $Q_aQ_b$  complex. FRAP experiments were performed to look for the SNAP-25 mobility pattern in PC12 cells with co-overexpressed syntaxin 4. As a control, the construct SN25-0<sub>L</sub>C was used. In addition, for comparison FRAP experiments were performed on cells co overexpressing syntaxin 1-CFP.

The half time of recovery values from the three independent FRAP experiments from PC12 cells were pooled and plotted as shown in Figure 25. As the data shows SNAP-25 mobility gradually slows down with increasing syntaxin 4-CFP or syntaxin 1-CFP concentration, though less efficiently for syntaxin 4 than syntaxin 1. Mobility of SN25-0<sub>L</sub>C remains unchanged with increasing levels of both syntaxin 1 and syntaxin 4 overexpression. The same is depicted as bar plots using the mean slope value analysis. The data indicate that like *in vitro*, SNAP-25 forms non-cognate SNARE complexes *in vivo*, although less efficiently than the cognate ones.

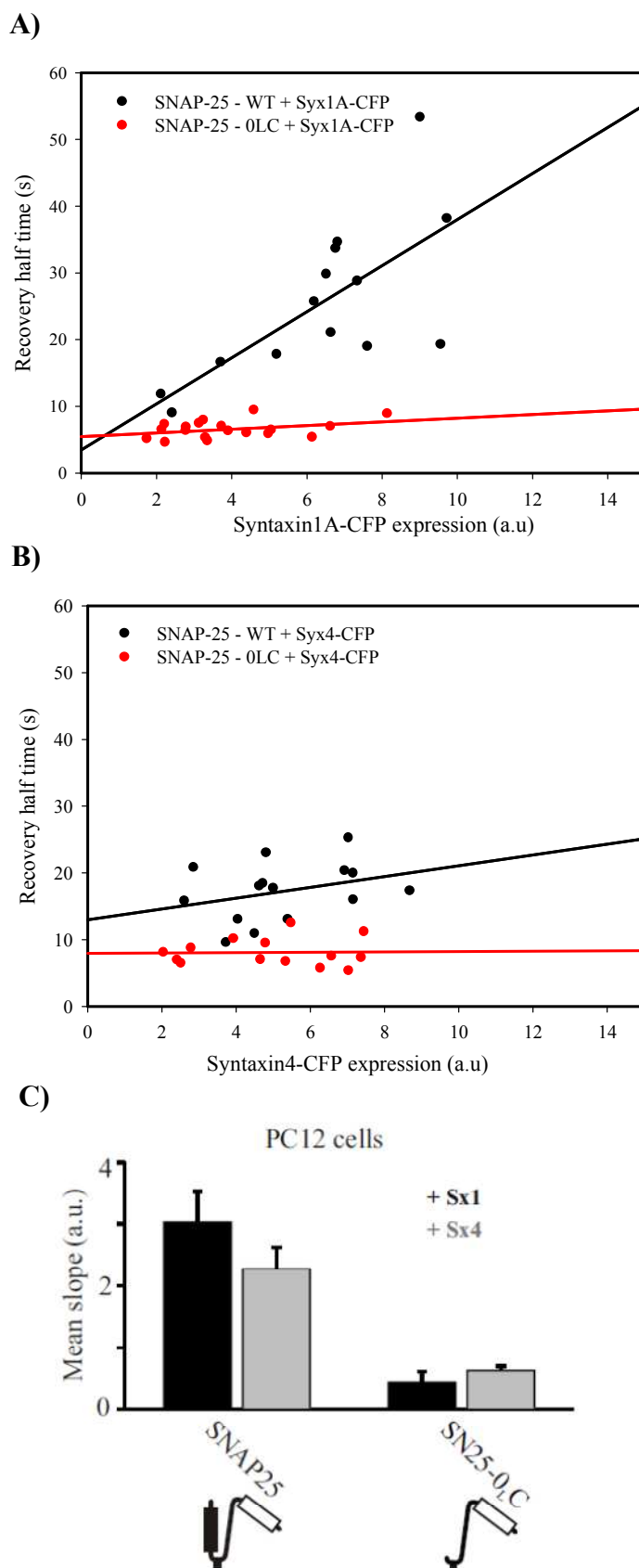


**Figure 25. SNAP-25 interacts with the non-cognate Q<sub>a</sub>-SNARE syntaxin 4 in PC12 cells.**  
 The dependence of recovery times of SNAP-25 or SN25-0<sub>LC</sub> on **A)** syntaxin 1-CFP or **B)**

syntaxin 4-CFP expression levels. From individual cells half times of recovery were plotted versus syntaxin 1-CFP or syntaxin 4-CFP expression levels. **C)** Mean slope plots obtained from A and B show that SNAP-25 interacts with syntaxin 4 though less efficiently than syntaxin 1 while SN25-0<sub>L</sub>C cannot interact with either of the two. Values are means  $\pm$  SEM (n = 3 experiments).

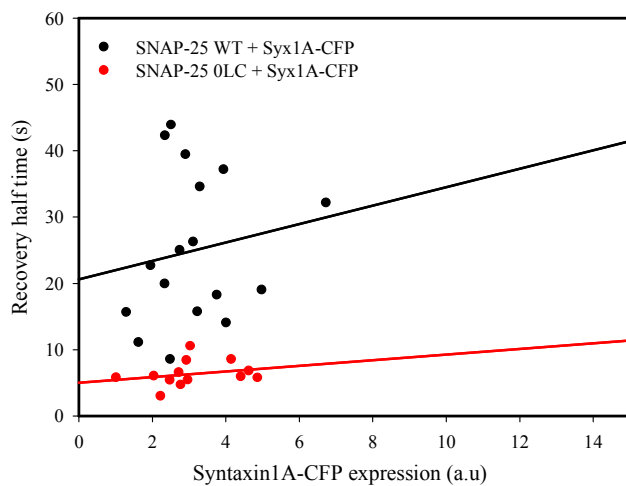
#### **3.4.1.8. The restricted SNAP-25 mobility through syntaxin 1 interactions does not require any neuronal co-factors**

The FRAP experiments so far were done using PC12 cells which are neuro-endocrine cells and the extent of variation in the SNAP-25 mobilitydirect was interpreted in terms of the extent of interaction syntaxin 1. However, the interaction of these neuronal SNAREs could be neuronal cell specific phenotype and potentially involve in addition other neuronal co-factors. Hence a set of FRAP experiments were performed for SNAP-25 mobility in non-neuronal BHK (Baby Hamster Kidney) fibroblast cells co-overexpressing GFP-SNAP-25 and syntaxin 1-CFP or syntaxin 4-CFP to look if other factors are involved. Again, SNAP-25 mobility gradually slows down with increasing syntaxin 1-CFP and syntaxin 4-CFP expression levels (see Figure 26 A & B) but the mobility of SN25-0<sub>L</sub>C remains unchanged for both syntaxin 1 and syntaxin 4 expression levels. The same data is depicted as bar plots using the values from mean slope analysis (see Figure 26 C).

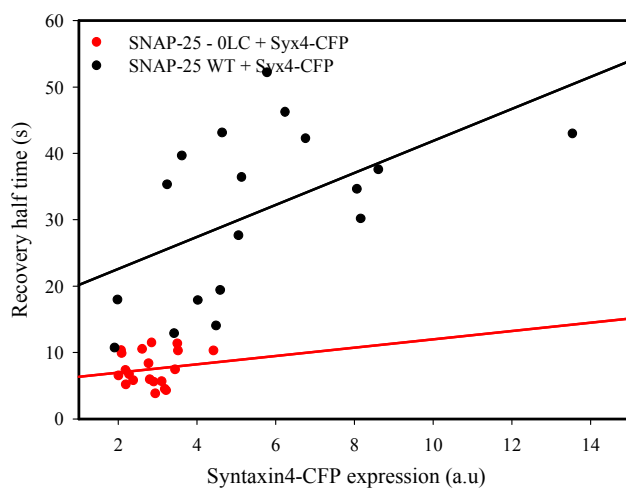
Interestingly, recovery times of SNAP-25 in BHK cells are even longer than in PC12 cells for the same level of syntaxin expression. This could possibly be explained by high levels of endogenous SNAP-25 getting into complex formation with co-overexpressed syntaxin 1 in PC12 cells and therefore less syntaxin 1 would be left for the overexpressed SNAP-25 for complex formation leading to proportionally higher amounts of free SNAP-25 than in BHK cells. Whereas in BHK cells, owing to their lack of endogenous SNAP-25, co-overexpressed syntaxin is all available for overexpressed SNAP-25 for complex formation and thus longer recovery times are observed than in PC12 cells for similar levels of syntaxin expression. Also, recovery times for SNAP-25 in BHK cells do not show a consistently linear response to syntaxin 1 concentrations resulting in variable half times of recovery at similar levels of syntaxin 1 overexpression. This might be due to lesser stability of formed Q<sub>a</sub>Q<sub>b</sub> SNARE complex in these cells. However, the data clearly suggest that the formation of cognate or non-

cognate  $Q_aQ_b$  complex does not require any neuronal co-factors.

A)



B)



C)

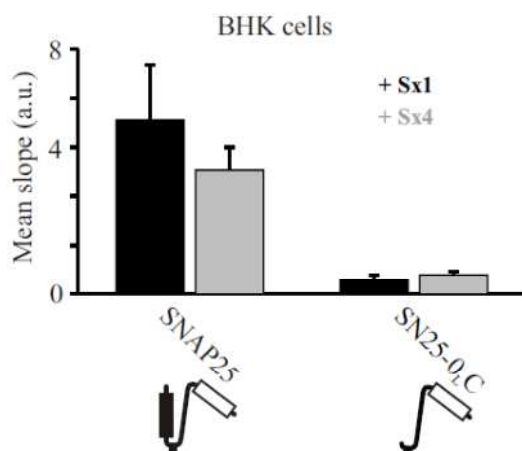


**Figure 26. SNAP-25 - syntaxin interactions require no neuronal co-factors.**

Dependence of recovery times of SNAP-25 or SN25-0<sub>LC</sub> on **A)** syntaxin 1-CFP or **B)** syntaxin 4-



---

CFP expression levels in fibroblast BHK cells. From individual cells half times of recovery were plotted versus syntaxin 1-CFP or syntaxin 4-CFP expression levels. **C)** Mean slope plots obtained from A and B show that SNAP-25 interacts with both syntaxin 1 and syntaxin 4 while SN25-0<sub>L</sub>C cannot interact with either of the two. Values are means  $\pm$  SEM (n = 3 experiments).

### **3.4.2. Syntaxin1 - SNAP-25 interactions studied in native plasma membrane sheets**

As shown from FRAP studies, efficient interaction of the N-terminal SNARE motif with syntaxin 1 in live cells is position specific which mechanistically could be due to either a need for the parallel orientation of the two interacting SNARE motifs (brought about by TMR and palmitoyl membrane anchor) or diminished reactivity at the C-terminal position. In order to address which of the two possibilities operate, a biochemical binding assay using native plasma membrane sheets from BHK cells was employed. BHK cells are fibroblasts lacking endogenous syntaxin 1 and SNAP-25 and were chosen for the present studies so as to obtain a clean background upon which binding of soluble recombinant syntaxin 1 to respective overexpressed GFP-SNAP-25 / SNAP-25 constructs can be studied.

BHK cells overexpressing GFP- SNAP-25 or SNAP-25 constructs were subjected to a brief ultrasound pulse disrupting the upper parts of the cells and leaving behind basal plasma membranes attached to the glass coverslip. Membrane sheets were reacted with soluble recombinant syntaxin 1A (lacking the TMR) and bound syntaxin 1 was quantified by immunofluorescence (see section 2.3 of Materials and Methods section for more details). Using this assay, it could be clarified if diminished reactivity of the C-terminal SNARE motif of SNAP-25 (Q<sub>c</sub>) with syntaxin 1 in live cells as observed from the FRAP data, is due to requirement for the parallel orientation of the two. As in this binding assay, the exogenous recombinant syntaxin is soluble and should be able to approach the C-terminal SNARE motif (Q<sub>c</sub>) of the expressed SN25-0<sub>L</sub>C or SN25-C<sub>L</sub>C, in a similar manner and should possibly bind to form Q<sub>a</sub>Q<sub>c</sub> complex. Similarly, if the interaction of syntaxin (Q<sub>a</sub>) with SNAP-25 is N-terminal SNARE motif (Q<sub>b</sub>) specific only, the position of the Q<sub>b</sub> domain around the linker region of SNAP-25 should be irrelevant and therefore, the soluble syntaxin should possibly bind to the expressed SN25-0<sub>L</sub>N.

### 3.4.2.1. Soluble syntaxin 1 readily reacts with the N-terminal SNARE motif of SNAP-25

In a first series of experiments, it was tested if binding of exogenous recombinant syntaxin 1 to plasma membrane sheets from BHK cells overexpressing GFP-SNAP-25 or the constructs SN25-N<sub>L</sub>0, SN25-0<sub>L</sub>C and SN25-0<sub>L</sub>0 depends on the presence or absence of the N-terminal SNARE motif, in support of the FRAP data. As shown in Figure 28, the amount of bound syntaxin 1 was proportionate to the expression levels (shown as GFP fluorescence levels) of wild type SNAP-25 (see also Figures 27). Although, the amount of bound syntaxin 1 was also proportionate to the SN25-N<sub>L</sub>0 expression levels, the binding seems to be less efficient and not quite reflecting the FRAP data (see Figures 14 and 15). However, the observed, approximately 2 fold difference is most likely due to the difference in the dynamics of Q-SNARE complex formation *in vivo* and *in vitro*. Here, in the binding assays (as also in other *in vitro* assays) the availability of syntaxin 1 for the expressed SNAP-25 is unlimited so that SNAP-25 forms probably (Q<sub>a</sub>)<sub>2</sub>Q<sub>b</sub>Q<sub>c</sub> complexes, explaining why it binds 2 fold more syntaxin 1 than SN25-N<sub>L</sub>0 which can form only Q<sub>a</sub>Q<sub>b</sub> complexes. In FRAP assays where live cells were used, the SNAP-25 to syntaxin ratio was very high and therefore limited syntaxin availability could only allow the formation of a Q<sub>a</sub>Q<sub>b</sub> complex but not a (Q<sub>a</sub>)<sub>2</sub>Q<sub>b</sub>Q<sub>c</sub> complex with SNAP-25, and therefore SNAP-25 and SN25-N<sub>L</sub>0 show a similar recovery rate. On the other hand, consistent with the FRAP data, SN25-0<sub>L</sub>C and SN25-0<sub>L</sub>0 failed to bind any syntaxin.

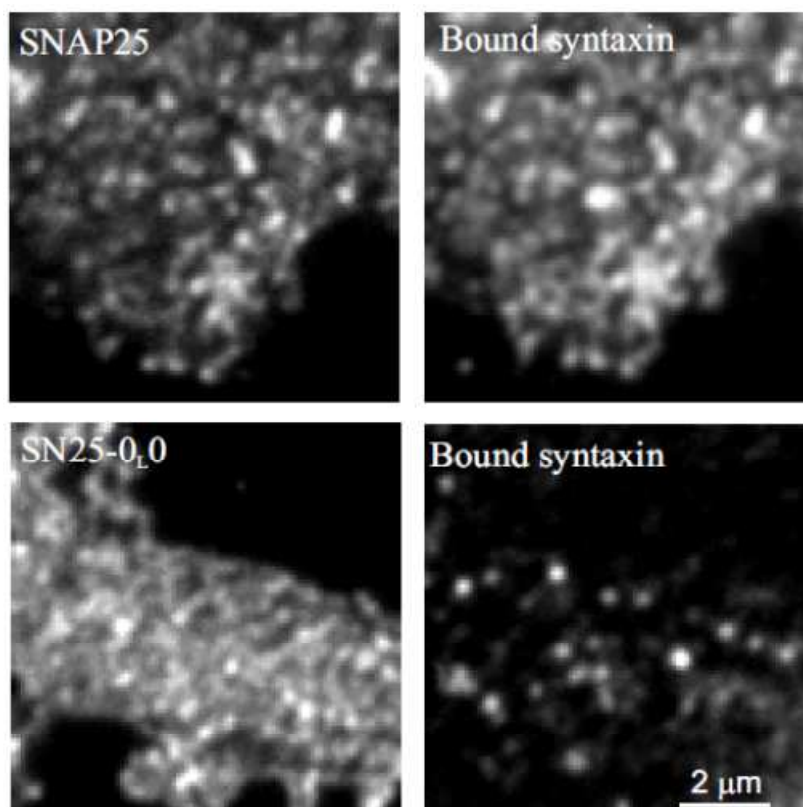


**Figure 27. Representative images showing binding of soluble syntaxin 1 to membrane sheets expressing either SNAP-25 or SN25-0<sub>L0</sub>.** A plasma membrane sheet from a fibroblast BHK cell expressing GFP-SNAP-25 (upper panels) efficiently binds soluble syntaxin 1 but a membrane sheet expressing SN25-0<sub>L0</sub> hardly binds any syntaxin 1 (lower panels). Left panels, GFP-fluorescence; right panels, immunostaining for bound syntaxin 1. [Figure taken from Halemani et al., \(2010\).](#)

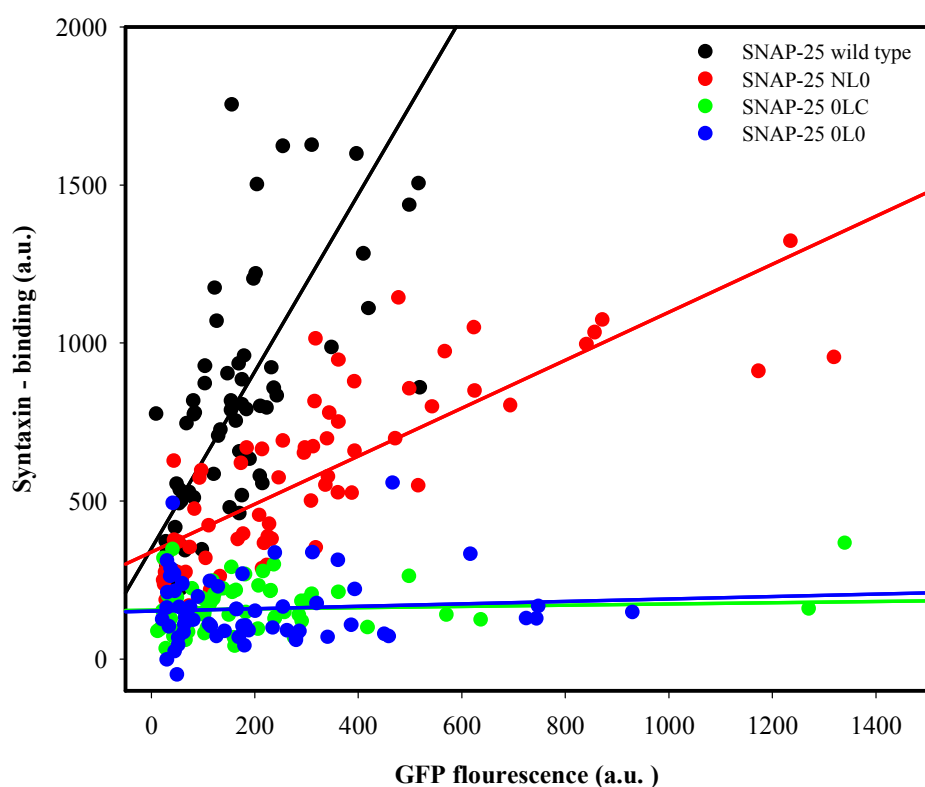


**Figure 28. Soluble syntaxin 1 readily reacts with the N-terminal SNARE motif of SNAP-25.** Each spot represents a membrane sheet from a BHK cell expressing the GFP-SNAP-25 or SN25-N<sub>L</sub>0, SN25-0<sub>L</sub>C and SN25-0<sub>L</sub>0 incubated with soluble syntaxin 1. The expression level of the respective construct was quantified in the GFP channel and the syntaxin binding, which was visualised by immunostaining in the cy3 channel. GFP expression level was plotted versus bound syntaxin. For each condition data was obtained from three experiments and pooled for analysis. Fitting of a linear regression line reveals the relative syntaxin binding capacity of the corresponding constructs.

### 3.4.2.2. Soluble syntaxin 1 binds the N-terminal SNARE motif efficiently only when it is at the N-terminus of SNAP-25

In the next set of experiments, it was tested if the position of the N-terminal SNARE motif is important for efficient interactions with syntaxin 1. As shown in Figure 29, plasma membrane sheets from BHK cells expressing GFP-SNAP-25 and or SN25-N<sub>L</sub>N, SN25-0<sub>L</sub>N and SN25-C<sub>L</sub>C bound exogenous recombinant syntaxin 1 depending on the presence or absence of the N-terminal SNARE motif at the N-terminus. The amount of bound syntaxin 1 was proportionate to the expression levels (shown as GFP fluorescence levels) of wild type SNAP-25 and SN25-N<sub>L</sub>N. Amount of syntaxin bound

to SN25-N<sub>L</sub>N was as good as SNAP-25, probably due to the formation of (Q<sub>a</sub>)<sub>2</sub>(Q<sub>b</sub>)<sub>2</sub> complex in the presence of excess syntaxin. On other hand, SN25-0<sub>L</sub>N and SN25-C<sub>L</sub>C bound little, if any, although the N-terminal SNARE motif of SN25-0<sub>L</sub>N is, in principle, flexible enough to react with soluble syntaxin 1. In summary, the binding assay shows that the parallel orientation of the two SNARE motifs is not required for efficient Q-SNARE complex formation but rather the position of the N-terminal SNARE motif within the SNAP-25 molecule has an influence on the reactivity of the SNARE motif.

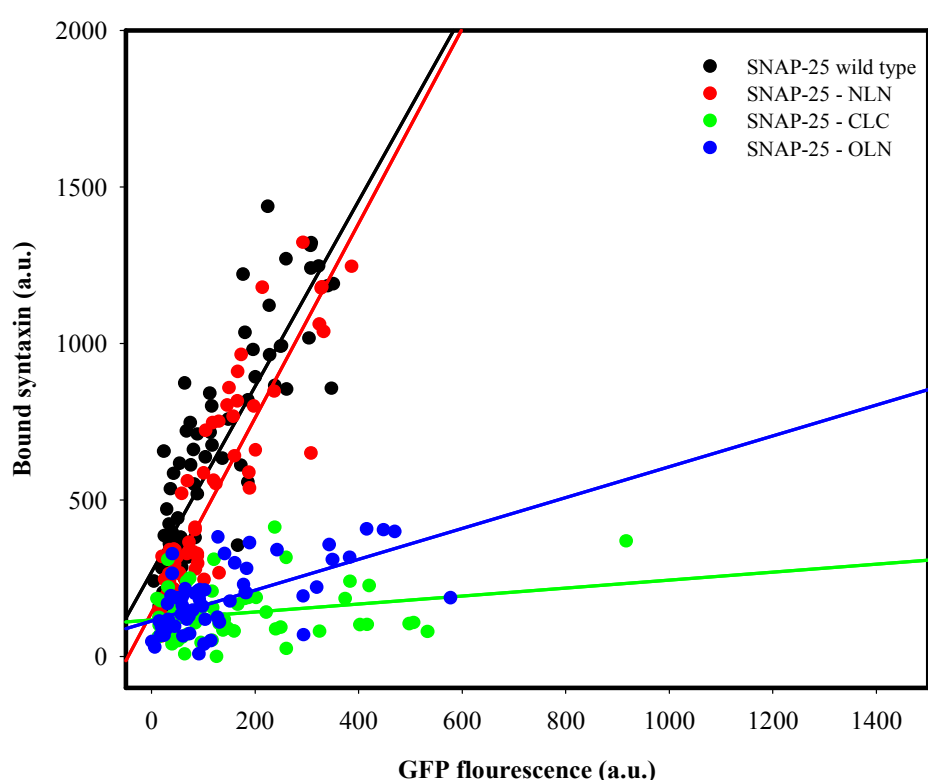


**Figure 29. Enhanced reactivity mediated by the N-terminal position does not require parallel oriented syntaxin.** Membrane sheets from BHK cells expressing GFP-labelled SNAP25, SN25-N<sub>L</sub>N, SN25-0<sub>L</sub>N or SN25-C<sub>L</sub>C were analyzed after incubation with soluble syntaxin 1. The expression level of the respective construct was quantified in the GFP channel and the syntaxin binding, which was visualised by immunostaining in the cy3 channel. Each spot represents a membrane sheet for which GFP-expression level was plotted versus bound syntaxin. For each condition data was obtained from three experiments and pooled for analysis. Fitting of a linear regression line reveals the relative syntaxin binding capacity of the corresponding constructs.

### **3.5. Nanoscale organization of SNAP-25 and syntaxin 1 in the plasma membrane**

As discussed in the introduction, the Q-SNAREs SNAP-25 and syntaxin 1 are organized as clusters on the plasma membrane of PC12 cells that overlap partially (Lang et al., 2001). Syntaxin clustering is mediated by specific homo-oligomerization involving the SNARE motifs (Sieber et al., 2006). Mechanism of SNAP-25 clustering is not studied in detail although it is thought that SNAP-25 through its palmitoyl membrane anchors is targeted to lipid rafts in the plasma membrane (Salaun et al., 2005b). Therefore, in the present study it was investigated if similar protein-protein interactions would mediate clustering as for syntaxin. For resolving the SNAP-25 clusters, nanoscale STED (Stimulated Emission Depletion) microscopy (Willig, 2006) which overcomes the diffraction barrier and offers unprecedented nano-scale resolution for imaging the cellular ultra structures, has been applied.

All the studies so far on SNAP-25 clusters and their correlation to syntaxin 1 clusters were derived from diffraction limited light microscopy imaging. This diffraction limited resolution approach was not sufficient enough to further dissect the apparent physical overlap of the two clusters (Lang et al., 2001; Nagy et al., 2005) or in other words, it could not be differentiated if signals overlap concentrically or if the overlap is caused by clusters that are very close to each other. Hence, the STED microscopy was employed to further resolve the physical overlap between the SNAP-25 and syntaxin 1 clusters.

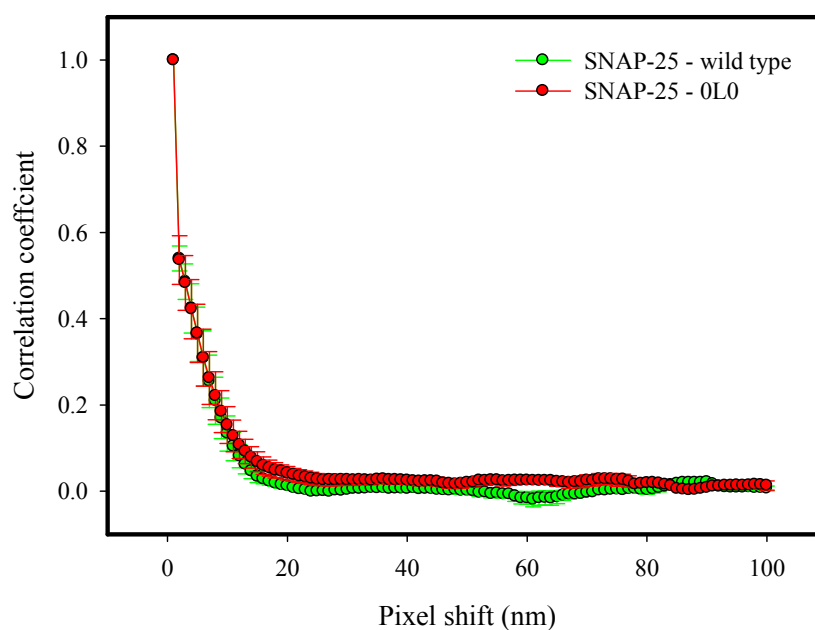
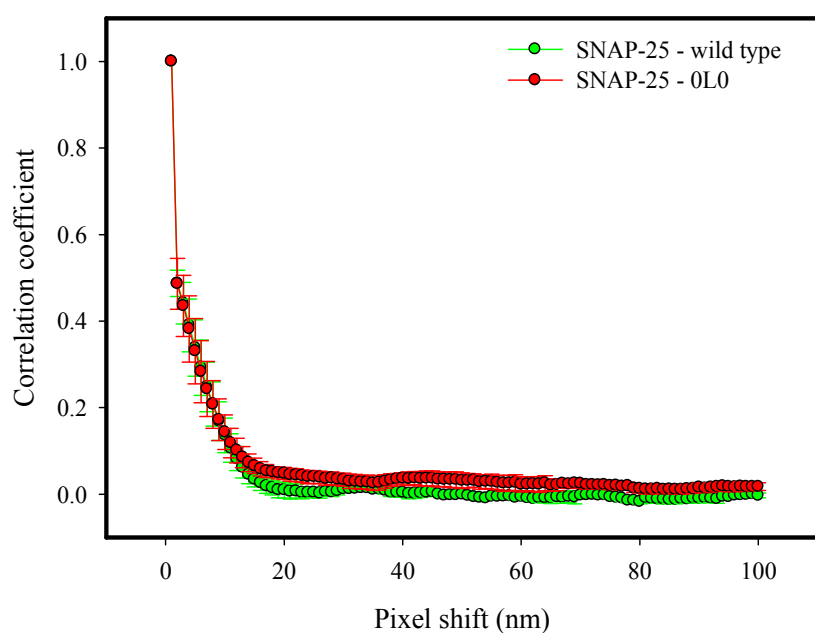
#### **3.5.1. SNAP-25 cluster morphology is independent of its SNARE motifs**

To begin with, it was tested if the SNARE motifs are essential for SNAP-25 cluster formation. Plasma membrane sheets from PC12 cells over-expressing GFP tagged SNAP-25 and SN25-0<sub>L</sub>0 were immunostained for GFP using Atto-647N antibody in order to visualise the clusters in the STED channel which is not sensitive for GFP (and the samples were also co-immunostained for syntaxin 1 and visualised using cy3 in the confocal channel – see section 3.5.2). Please refer section 2.5 of Materials and Methods for the details on sample preparation and imaging procedure.

In order to characterize the cluster sizes of SNAP-25 and SN25-0<sub>L</sub>0 relative to each other an auto-correlation analysis was used which analyzes the correlation of an image with itself. Each STED image from SNAP-25 and SN25-0<sub>L</sub>0 (see Figure 31 for representative images) were aligned with itself and an autocorrelation analysis was

performed within a region of interest (ROI) by progressively shifting the aligned images pixel-by-pixel either vertically or horizontally. With each pixel shift, the correlation values were calculated. According to the object size, the correlation value drops. The correlation value is plotted against the pixel shift and the steepness of the drop of the signal indicates the mean object size. Three independent experiments were performed and several membrane sheets were imaged for each condition in each experiment. The images were analyzed using MatLab routines (written by Dr. Silvio Rizzoli). An average of the values from each experiment was taken and the mean  $\pm$  SEM for three experiments was plotted (see Figure 30).

The correlation versus pixel shift followed a characteristic decay curve and curves for the two constructs were identical for both the constructs. Hence, no difference in the signal distribution between SNAP-25 and SN25-0<sub>L</sub>0 could be detected at this level. The data indicates that the cluster size for the two constructs lies within similar range and hence we conclude that the SNARE motifs are not involved in cluster formation and determination of their size.

**A) Plot for Correlation versus Horizontal pixel shift****B) Plot for Correlation versus vertical pixel shift**

**Figure 30. SNAP-25 or SN25-0<sub>L</sub>0 signal distribution characterized by autocorrelation analysis.** The drop of correlation against pixel shift reflects the mean object sizes in the image. No difference in the mean object size between SNAP-25 and SN25-0<sub>L</sub>0 could be detected. **A)** Correlation versus horizontal pixel shift. **B)** Correlation versus vertical pixel shift. Values are means  $\pm$  SEM ( $n = 3$  experiments, for each experiment 8-24 membrane sheets were analyzed for SNAP-25 and 11-18 membrane sheets for SN25-0<sub>L</sub>0).

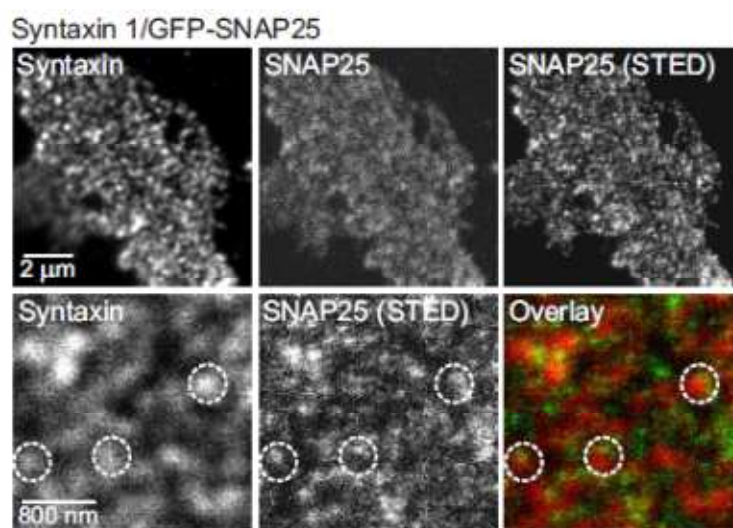


### 3.5.2. SNAP-25 and syntaxin 1 form distinct but close clusters

Next it was investigated if the reported microscopic overlap of SNAP-25 and syntaxin 1 clusters can further be resolved. As briefly mentioned in the previous section, plasma membrane sheets from PC12 cells over-expressing GFP tagged SNAP-25 and SN25-0<sub>L</sub>0 were co-immunostained for GFP (Atto-647N) and endogenous syntaxin1 (Cy3). The fixed samples were first imaged for GFP and Atto-647N (SNAP-25 or SN25-0<sub>L</sub>0) and Cy3 (syntaxin1) in the confocal channels simultaneously followed by recording in the STED channel for Atto-647N (SNAP-25 and SN25-0<sub>L</sub>0). Three independent experiments were performed and several membrane sheets were imaged for each condition in each experiment. The images were analyzed using MatLab routines (written by Dr. Silvio Rizzoli). An average of the values from each experiment was taken and the mean  $\pm$  SEM for three experiments was plotted (see Figure 32).

The images show that SNAP-25 clusters or SN25-0<sub>L</sub>0 clusters are frequently found close to syntaxin 1 clusters but do not overlap concentrically (see Figure 31 A & B). To further clarify the images were analyzed for cross-correlation between syntaxin 1 (confocal mode) and SNAP-25 / SN25-0<sub>L</sub>0 clusters (in STED mode), resulting in a correlation coefficient of 0.2 (see Figure 32). Although syntaxin 1 clusters cannot be completely resolved with confocal microscopy, we can safely conclude that the majority of the SNAP-25 and syntaxin 1 signals are very close to each other but do not arise from the same structure (Figure 31 A & B). This relatively high degree of similarity in the absence of concentric signals is caused by close but physically non overlapping clusters from which the blurred signals arise, overlapping at their borders.

A)



B)

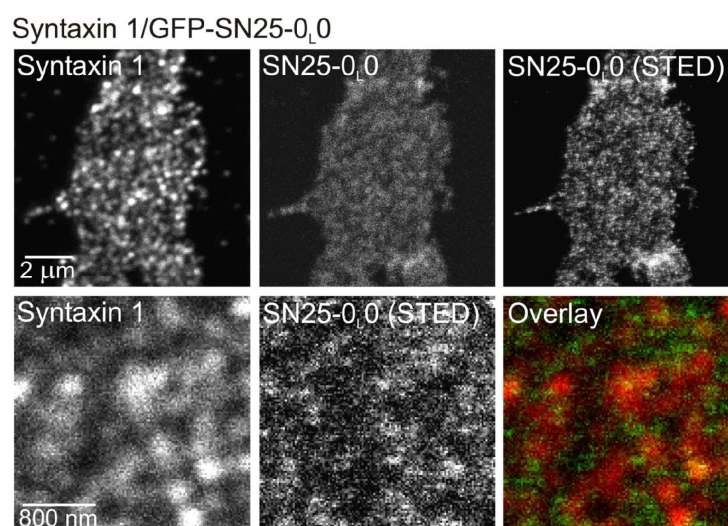


**Figure 31. Representative images of co-localisation studies between SNAP-25/SN25-0<sub>L</sub>0 and syntaxin 1 clusters.** Native plasma membrane sheets from PC12 cells overexpressing A) GFP - SNAP-25 or (B) GFP-SN25-0<sub>L</sub>0 were immunostained for GFP and endogenous syntaxin 1. **A)** In the top panel (from left to right), confocal image of syntaxin 1, confocal and STED resolved images of SNAP-25 are shown. The bottom panel (from left to right) shows the magnified views from syntaxin 1 and STED-resolved SNAP-25 and the overlay of two images. Circles placed at identical pixel locations show that the SNAP-25 and syntaxin 1 clusters are placed within a distance of only a few hundred nanometers. **B)** In the top panel (from left to right), confocal image of syntaxin 1, confocal and STED resolved images of SN25-0<sub>L</sub>0 are shown. The bottom panel (from left to right) shows the magnified views from syntaxin 1 and STED-resolved SNAP-25 and overlay of the two images. [Figure taken from Halemani et al., \(2010\).](#)

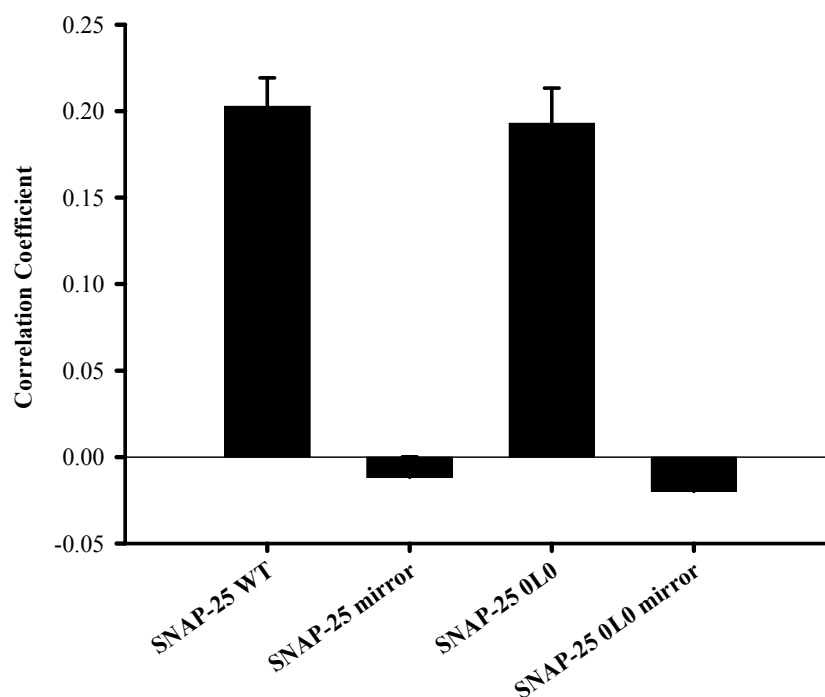


**Figure 32. Co-localisation analysis of syntaxin 1 and STED-resolved SNAP-25 and SN25-0<sub>L</sub>0 images.** Images as shown in Figure 31 were analyzed and the correlation between syntaxin 1 and SNAP-25 / SN25-0<sub>L</sub>0 was quantified by calculating the Pearson-correlation coefficient. The correlation between syntaxin 1 and SN25-0<sub>L</sub>0 provides a reference value for the overlap in the absence of any SNARE–SNARE interactions. SN25-0<sub>L</sub>0 overlapped with syntaxin 1 equally well as SNAP-25 indicating that the proximity of SNAP-25 and syntaxin 1 clusters is independent of SNAP-25 SNARE motifs and does not reflect a pool of SNARE complexes. For each condition, mirrored images were also analyzed as control. Values are means ± SEM (n = 3 experiments, for each experiment 8-24 membrane sheets were analyzed for SNAP-25 and 11-18 membrane sheets for SN25-0<sub>L</sub>0).

### 3.5.3. SNAP-25 and syntaxin 4 clusters are more distant than the SNAP-25 and syntaxin 1 clusters

If the observed proximity of SNAP-25 clusters to syntaxin 1 clusters is independent of its SNARE motifs despite their involvement in the interaction of the two proteins then could it also be the same for SNAP-25 and syntaxin 4 clusters? Syntaxin 4 clusters are separate from syntaxin 1 clusters (Sieber et al., 2006) and unlike for syntaxin 1, its interaction with SNAP-25 is promiscuous. Therefore, it was investigated if the cognate pairing converts into physical proximity.

---

Plasma membrane sheets from PC12 cells over-expressing GFP tagged SNAP-25 and SN25-0<sub>L</sub>0 were co-immunostained for GFP (Atto-647N) and endogenous syntaxin 4 (Cy3). The fixed samples were first imaged for GFP and Atto-647N (SNAP-25 or SN25-0<sub>L</sub>0) and Cy3 (syntaxin 4) in confocal channels simultaneously followed by imaging in the STED channel for Atto-647N (SNAP-25 and SN25-0<sub>L</sub>0). Three independent experiments were performed and several membrane sheets were imaged for each condition in each experiment. The images were analyzed using MatLab routines (written by Dr. Silvio Rizzoli). An average of the values from each experiment was taken and the mean  $\pm$  SEM for three experiments was plotted (see Figure 34).

The images (see Figure 33 A & B) were analyzed for correlation between syntaxin 4 (confocal mode) and SNAP-25 / SN25-0<sub>L</sub>0 clusters (in STED mode). A correlation coefficient of around 0.08 (see Figure 34) was found, suggesting that SNAP-25 clusters are more distant from syntaxin 4 clusters than from syntaxin 1 clusters (a correlation coefficient of around 0.2). In addition, since no significant difference was found in the correlation values between syntaxin 4 and SNAP-25 / SN-0<sub>L</sub>0 clusters, the proximity of the SNAP-25 and syntaxin 4 clusters is independent of SNAP-25 SNARE motifs (see Figure 34). Thus, the data show that SNAP-25 clusters are closer to syntaxin 1 than to syntaxin 4 probably either owing to the slightly increased specificity of the interaction with syntaxin 1 or because additional factors are involved in the regulation of a process that brings cognate SNAREs in clusters close to each other (see also Figure 25 for interaction efficiency of SNAP-25 and syntaxin 4 in PC12 cells).

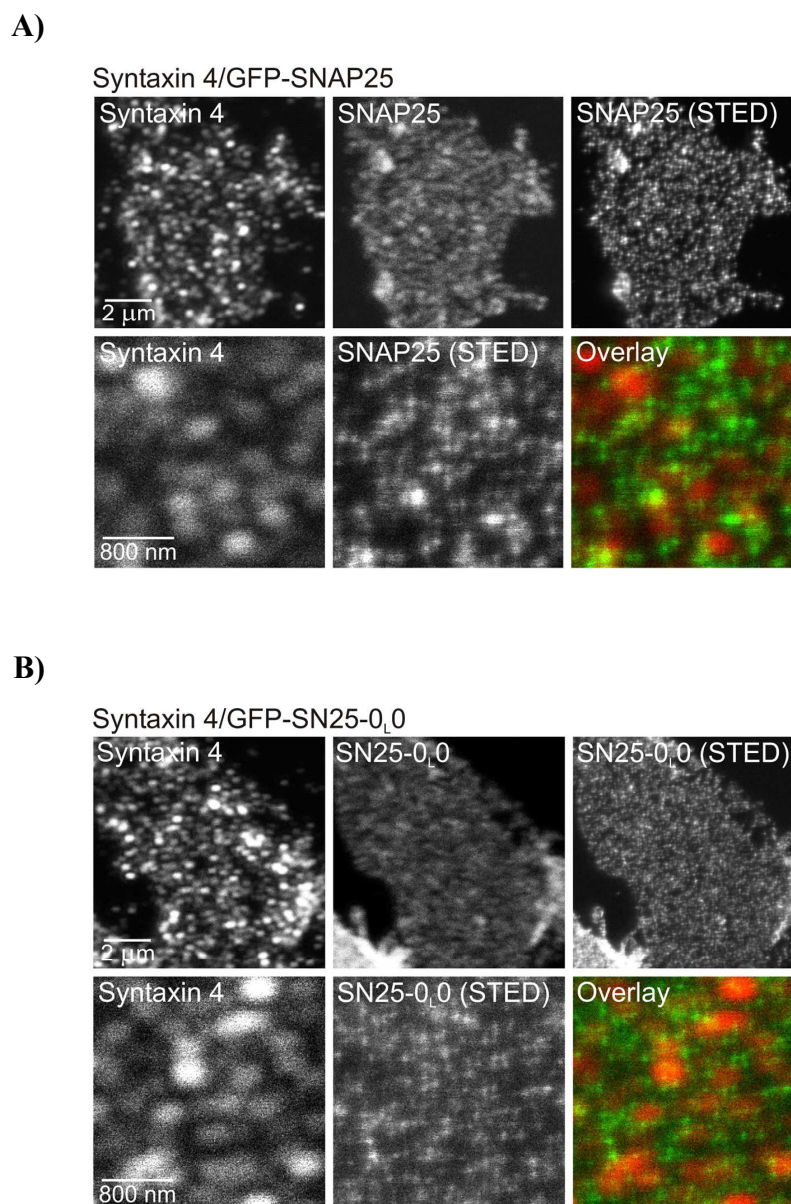


**Figure 33. Representative images of co-localisation studies of SNAP-25/SN25-0<sub>L</sub>0 and syntaxin 4 clusters.** Native plasma membrane sheets from PC12 cells overexpressing **A)** GFP - SNAP-25 or **(B)** GFP-SN25-0<sub>L</sub>0 were immunostained for GFP and endogenous syntaxin 4. **A)** In the top panel (from left to right), confocal image of syntaxin 4, confocal and STED resolved images of SNAP-25 are shown. The bottom panel (from left to right) shows the magnified views from syntaxin4 and STED-resolved SNAP-25 and the overlay of the two images. **B)** In the top panel (from left to right), confocal image of syntaxin 4, confocal and STED resolved images of SN25-0<sub>L</sub>0 are shown. The bottom panel (from left to right) shows the magnified views from syntaxin 4 and STED-resolved SNAP-25 and overlay of the two images. [Figure taken from Halemani et al., \(2010\).](#)

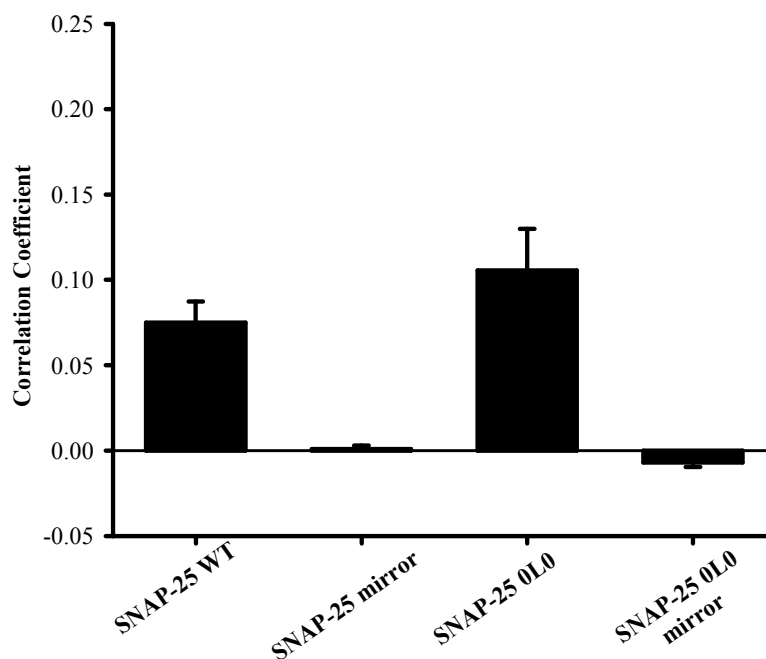


**Figure 34. Co-localisation analysis of syntaxin 4 and STED-resolved SNAP-25 and SN25-0<sub>L0</sub> images.** Correlation between the two channels was quantified by calculating the Pearson-correlation coefficient. correlation between syntaxin 4 and SN25-0<sub>L0</sub> provides a reference value for the overlap in the absence of any SNARE–SNARE interactions. As there is no significant difference in the correlation values between SNAP-25/SN-0<sub>L0</sub> and syntaxin 4, the proximity of SNAP-25 and syntaxin 4 clusters is independent of SNAP-25 SNARE motifs. For each condition, mirrored images were also analyzed as control. Values are means  $\pm$  SEM ( $n = 3$  experiments, for each experiment 6-11 membrane sheets were analyzed for SNAP-25 and 6-16 membrane sheets for SN25-0<sub>L0</sub>).

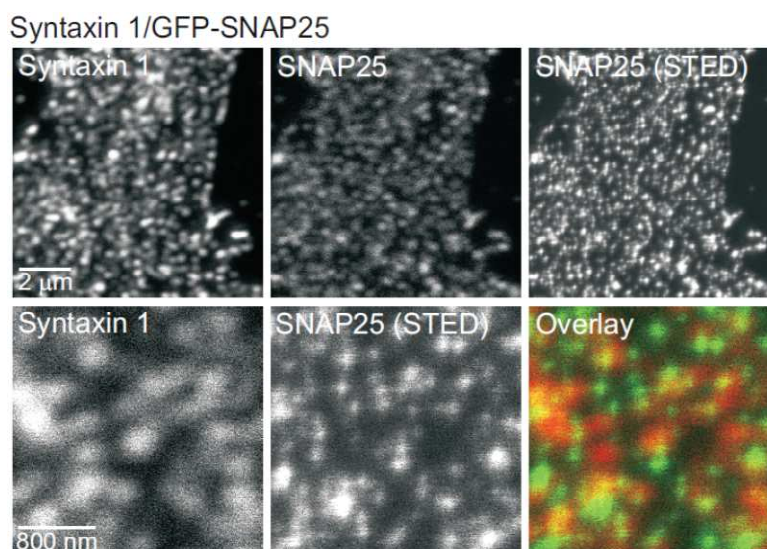
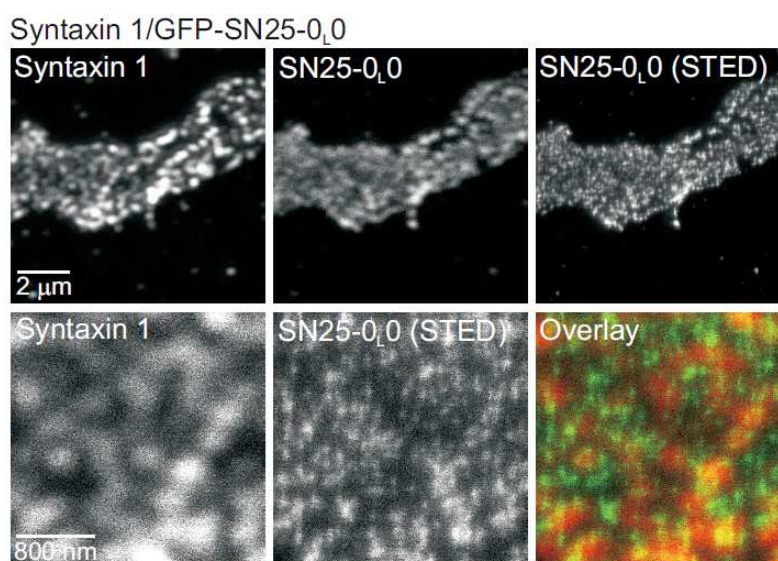
### 3.5.4. Overlap between SNAP-25 and syntaxin 1 upon SNARE complex formation

Endogenous SNAREs in plasma membrane sheets have been shown to be segregated but still active to form binary (SNAP25-syntaxin) and ternary SNARE (SNAP-25-syntaxin-synaptobrevin) complexes with exogenously added syntaxin and synaptobrevin (Lang et al., 2002). Therefore, it was tested if incubation of freshly prepared membrane sheets with recombinant synaptobrevin (by driving the endogenous SNAP-25 and syntaxin 1 into ternary *cis*-SNARE complexes) would increase the colocalization of SNAP-25 and syntaxin 1 clusters.

Membrane sheets from PC12 cells overexpressing either GFP-SNAP-25 or SN25-0<sub>L0</sub> were incubated with or without 10  $\mu$ M synaptobrevin 2 for 15 min at 37°C and co-immunostained for GFP (Atto-647N) and endogenous syntaxin 1 (Cy3) (see Figures 35

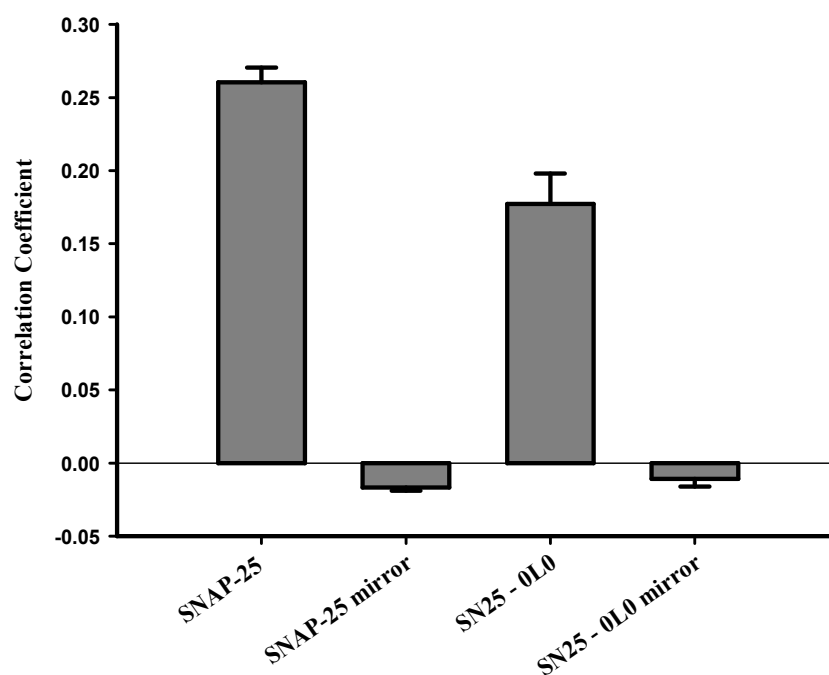
A & B and Figures 37 A & B). The fixed samples were first imaged for GFP and Atto-647N (SNAP-25 or SN25-0<sub>L</sub>0) and Cy3 (syntaxin 1) in the confocal channels simultaneously followed by imaging in the STED channel for Atto-647N (SNAP-25 and SN25-0<sub>L</sub>0). The images were analyzed for correlation between syntaxin 1 (confocal mode) and SNAP-25 / SN25-0<sub>L</sub>0 clusters (in STED mode). For the ease of presentation, the data is split into two parts, showing the results as ‘controls - incubation without synaptobrevin 2’ (see Figures 35 and 36) and ‘incubation with synaptobrevin 2’ (see Figures 37 and 38). Three independent experiments were performed and several membrane sheets were imaged for each condition in each experiment. The images were analyzed using MatLab routines (written by Dr. Silvio Rizzoli).

The data shows that the colocalisation of SNAP-25 and syntaxin 1 slightly increases upon incubation of the plasma membrane sheets without any synaptobrevin 2 (see Figure 36 and compare it to Figure 32 for correlation analysis without any incubation). This could be due to promotion of binary and ternary SNARE complex formation in the plasma membrane sheets, shown to take place under these conditions (Lang et al., 2002).

**A) Incubation without synaptobrevin 2 - GFP - SNAP-25****B) Incubation without synaptobrevin 2 - GFP - SN25-0<sub>L</sub>0**

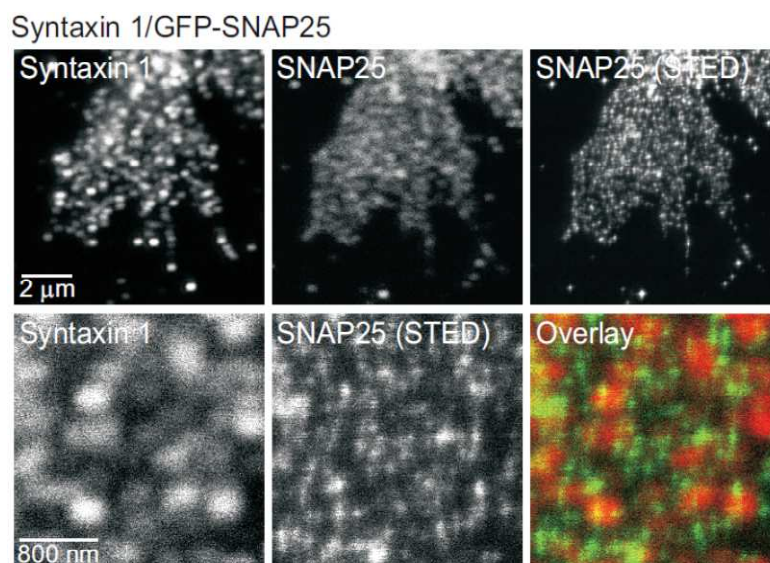
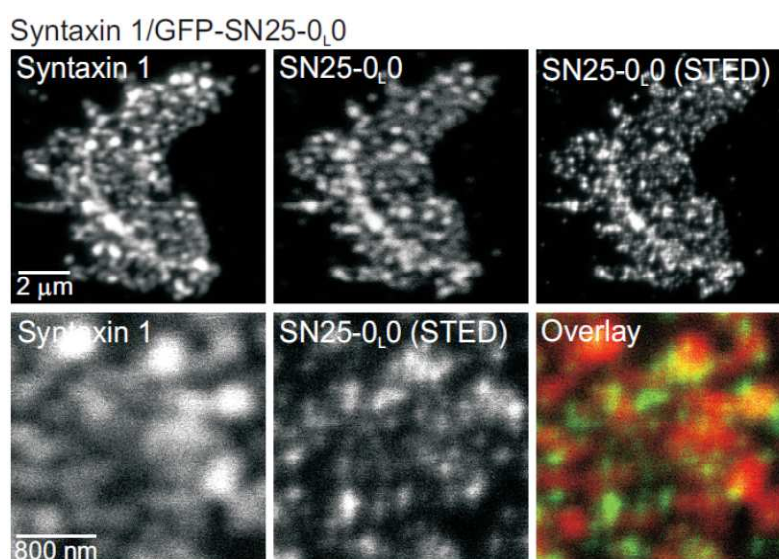
**Figure 35. Overlap between syntaxin 1 and SNAP-25/SN25-0<sub>L</sub>0 upon incubation without synaptobrevin 2.** Native plasma membrane sheets from PC12 cells expressing either GFP-SNAP25 (**A**) or SN25-0<sub>L</sub>0 (**B**) were incubated for 15 min at 37°C in the absence of synaptobrevin 2 and immunostained for syntaxin 1 and GFP as described in the text. The overviews (upper panels) and magnified views (lower panels) show immunostainings for syntaxin 1 and GFP-SNAP-25 (**A**) or for syntaxin 1 and SN25-0<sub>L</sub>0 (**B**). Magnified views from confocal image for syntaxin 1 and STED image for GFP-SNAP-25 (**A**) or GFP-SN25-0<sub>L</sub>0 (**B**) were overlaid to show the extent of overlap between the two clusters. [Figures taken from Halemani et al., \(2010\).](#)





**Figure 36. Quantification of the overlap between syntaxin 1 and SNAP-25/SN25-0<sub>L</sub>0 upon incubation without synaptobrevin 2.** Native plasma membrane sheets from PC12 cells expressing either GFP-SNAP25 were incubated for 15 min at 37°C in the absence of synaptobrevin 2 and immunostained for syntaxin 1 and GFP as described in the text. Pearson-correlation coefficients between syntaxin 1 and the STED-resolved GFP-SNAP-25/SN25-0<sub>L</sub>0 images were calculated. The correlation between syntaxin 1 and SN25-0<sub>L</sub>0 provides a reference value for the overlap in the absence of any SNARE-SNARE interactions. Upon incubation of the membrane sheets, we find that the colocalisation of syntaxin 1 and SNAP-25 slightly increases with respect to SN25-0<sub>L</sub>0 indicating that the SNAP-25 interaction with syntaxin 1 promotes the proximity between the clusters (compare with Figure 32 - colocalisation analysis without incubation). For each condition, mirrored images were analyzed as a control. For each experiment 9-12 membrane sheets were analyzed for SNAP-25 and 7-9 membrane sheets for SN25-0<sub>L</sub>0. Values are means ± SEM (n = 3 experiments).

When the effect of incubation of plasma membrane sheets in the presence of 10μM recombinant synaptobrevin 2 (see Figure 37 A and B) was studied, the correlation analysis revealed no difference from the control incubation (see Figures 37 and 38). Addition of exogenous synaptobrevin does not seem to have any additional effect over the ability of endogenous synaptobrevin, on the amount of SNARE complex formation and hence the proximity of SNAP-25 and syntaxin 1 clusters remains unchanged. Therefore, it is possible that the binary complexes are closer to clusters than the ternary complexes.

**A) Incubation with synaptobrevin 2 - GFP-SNAP-25****B) Incubation with synaptobrevin 2 - GFP-SN25-0<sub>L</sub>0**

**Figure 37. Overlap between syntaxin 1 and SNAP-25/SN25-0<sub>L</sub>0 upon incubation with synaptobrevin 2.** Native plasma membrane sheets from PC12 cells expressing either GFP-SNAP-25 (A) or SN25-0<sub>L</sub>0 (B), were incubated for 15 min at 37°C in the presence of 10  $\mu\text{M}$  recombinant synaptobrevin2 and immunostained for syntaxin 1 and GFP (A and B) as described in the text. The overviews (upper panels) and magnified views (lower panels) show immunostainings for syntaxin 1 and GFP-SNAP-25 (A) or for syntaxin 1 and SN25-0<sub>L</sub>0 (B). Magnified views from confocal image for syntaxin 1 and the STED resolved images for GFP-SNAP-25 (A) or SN25-0<sub>L</sub>0 (B) were overlaid to show the extent of overlap between the two clusters. [Figures taken from Halemani et al., \(2010\).](#)

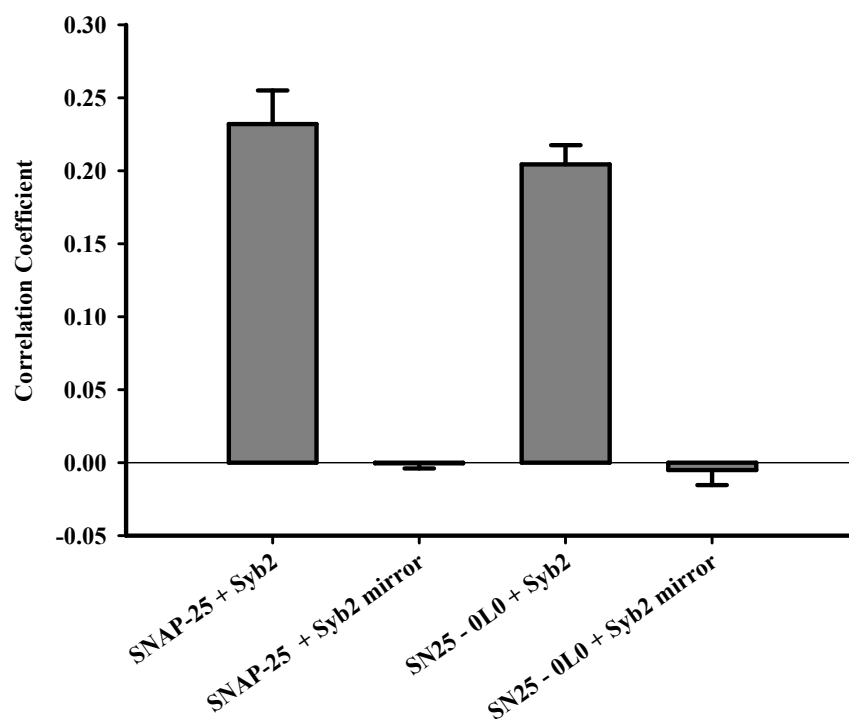


**Figure 38. Quantification of the overlap between syntaxin 1 and SNAP-25/SN25-0<sub>L</sub>0 upon incubation with synaptobrevin 2.** Native plasma membrane sheets from PC12 cells expressing either GFP-SNAP-25 or SN25-0<sub>L</sub>0 were incubated for 15 min at 37°C in the presence of 10 μM recombinant synaptobrevin 2 and immunostained for syntaxin 1 and GFP as described in the text. Pearson-correlation coefficients between syntaxin 1 and the STED-resolved SNAP-25 / SN25-0<sub>L</sub>0 images were calculated. The correlation between syntaxin 1 and SN25-0<sub>L</sub>0 provides a reference value for the overlap in the absence of any SNARE-SNARE interactions (see the text for details). For each condition, mirrored images were analyzed as a control. For each experiment, 7-11 membrane sheets were analyzed for SNAP-25 and 7-9 membrane sheets for SN25-0<sub>L</sub>0. Values are means ± SEM (n = 3 experiments).

### 3.5.5. Effect of cholesterol depletion on syntaxin 1 cluster morphology

It has been shown that the syntaxin clustering on the plasma membrane is mediated by homo oligomerisation through its SNARE motifs (Sieber et al., 2006) and clusters disintegrate when treated with cholesterol depleting agents such as M $\beta$ CD (methyl- $\beta$ -cyclodextrin) (Lang et al., 2001). Although it's not clear to what extent each of the two factors – homo oligomerisation through SNARE motifs and cholesterol effect, contribute to the regulation of syntaxin clustering, both seem to be important. However, recently, our research collaborator, Dr. Rory Duncan and his colleagues (from University of Edinburgh, UK) found out that mild cholesterol depletion in the cells can induce a change in the proportion of Q-SNARE binary intermediates adopting a certain conformation (Rickman et al., 2010). In order to check if this observation relates to a change in the distribution of syntaxin clusters, cholesterol depletion (under mild conditions) experiments were performed and syntaxin 1 cluster morphology studied using super-resolution STED microscopy.

The data shows that the treatment of PC12 cells with 10 mM M $\beta$ CD for 15 min (at 37°C) resulting in ~25% reduction in plasma membrane cholesterol (Rickman et al., 2010), did not result in any obvious change in the morphology of syntaxin 1 clustering as revealed by super resolution STED microscopy (see Figure 39 A). This finding suggests that syntaxin 1 molecules are mainly held together by homo oligomeric interactions.

As a control for the effectiveness of cholesterol depletion with M $\beta$ CD, plasma membrane sheets from PC12 cells were treated with 15 mM M $\beta$ CD for 30 min (at 37°C) – a treatment that depletes ~ 40% of the cholesterol from cells (Lang et al., 2001) and depletes probably even more cholesterol when directly applied to membrane sheets. The data shows that the disruption of syntaxin clusters resulting in the uniform distribution of syntaxin 1 molecules (see Figure 39 B) which is in line with previous findings applying similar conditions (Lang et al., 2001).

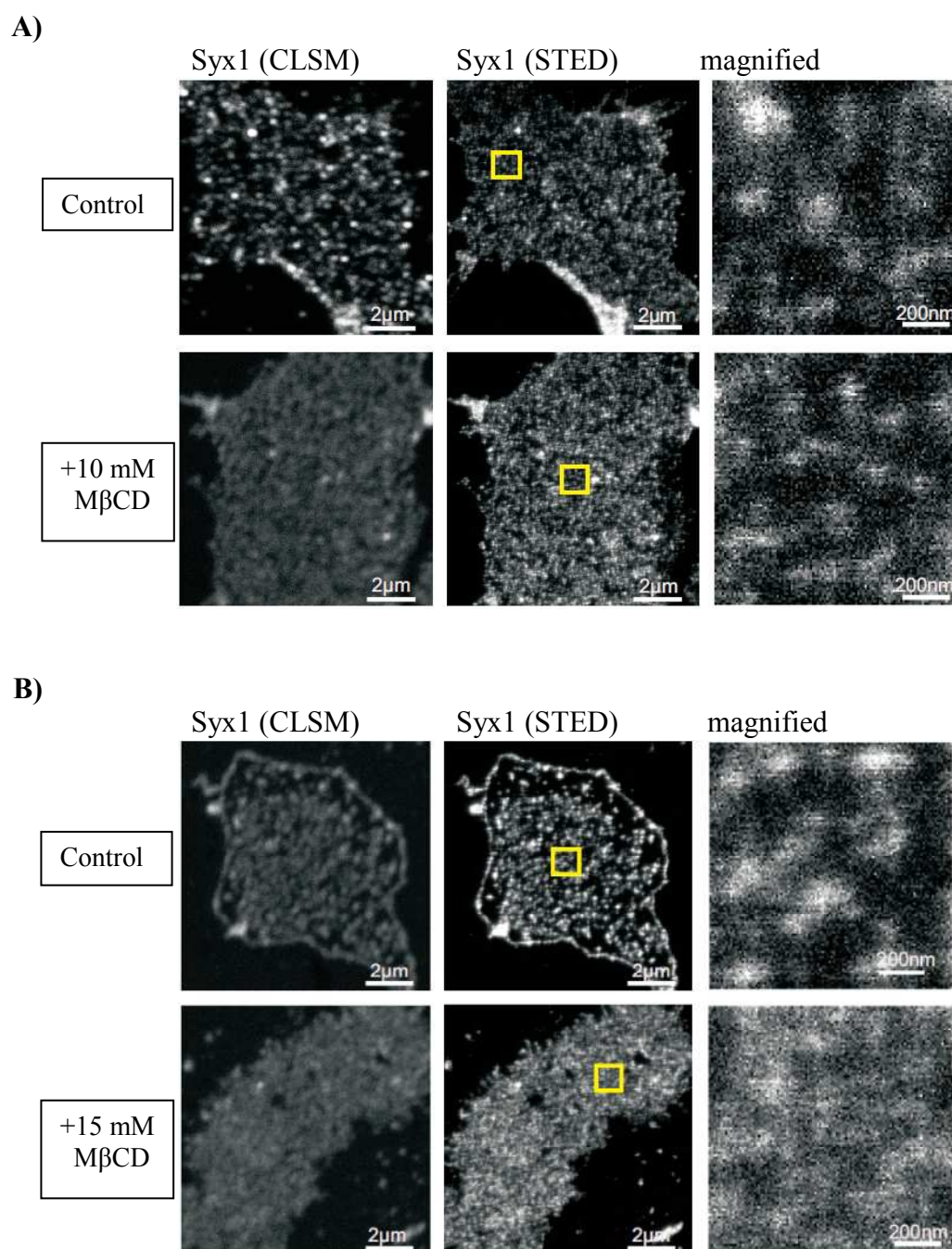


**Figure 39. Effect of cholesterol depletion on syntaxin 1 cluster morphology.**

**A)** PC12 cells were incubated in the absence (upper panel) or presence of 10 mM MβCD (lower panel) for 15 minutes at 37°C and sonicated to obtain plasma membrane sheets. Confocal and STED images of immunostained sheets reveal that the mild cholesterol depletion does not affect the integrity of syntaxin 1 cluster morphology. **B)** Plasma membrane sheets from PC12 cells were incubated in the absence (upper panel) or presence of 15 mM MβCD (lower panel) for 30 minutes at 37°C and immunostained for syntaxin 1. Confocal and STED images of immunostained sheets reveal that the cholesterol depletion leads to dispersion of syntaxin 1 clusters (lower panel) in contrast to control conditions (upper panel).

### 3.6. Ca<sup>2+</sup> induced remodelling of membrane proteins

The differential interactions between the membrane components - proteins and lipids, create lateral heterogeneities in the membrane (van Meer et al., 2008). The lipid-lipid, lipid-protein and protein-protein interactions segregate membrane components into submicron sized membrane domains. The inherent asymmetry of the plasma membrane lipid bilayer, particularly with the inner cytoplasmic leaflet carrying a large proportion of negatively charged membrane lipids like PS and PI (phosphatidylserine and phosphatidylinositol), creates a net negative surface potential (Devaux and Morris, 2004; Mulgrew-Nesbitt et al., 2006). This promotes non-specific electrostatic interactions between the membrane and positively charged membrane proteins facilitating their membrane recruitment and organization (McLaughlin and Murray, 2005; Mulgrew-Nesbitt et al., 2006). A local increase in the levels of divalent cation calcium, can modulate the membrane association of the proteins through electrostatic interactions (Hurley and Misra, 2000; McLaughlin and Murray, 2005; Mulgrew-Nesbitt et al., 2006). Therefore, it seems that the calcium has a major influence on the recruitment of membrane proteins and possibly also on the lateral organization.

The intracellular Ca<sup>2+</sup>-concentration in the cytosol of unstimulated cells is normally low, between 50-200 nM (Carafoli, 1987) but is transiently up-regulated many fold during a multitude of signalling events (Rizzuto and Pozzan, 2006). For instance, a transient rise in intracellular calcium concentration ranging from several micromolar to several hundred micromolar near to the mouth of Ca<sup>2+</sup>- channels (Bollmann and Sakmann, 2005; Heidelberger et al., 1994) presumably results in local exertion of strong electrostatic effects. In order to test if mimicking such condition would effect membrane protein organization, Felipe Zilly - then a student under the supervision of Dr. Thorsten Lang (then at the dept. Neurobiology, MPIBPC, Göttingen) - performed some initial experiments. The effect of increased Ca<sup>2+</sup> on the organization of a structurally diverse set of membrane proteins was studied using plasma membrane sheets from PC12 cells. The membrane proteins selected for the study included: synaptophysin (with multiple transmembrane domains), munc18 (peripherally associated membrane protein), SNAP-23 and SNAP-25 (membrane associated via palmitoyl-anchors), transferrin receptor and syntaxin 1 (each containing a single span transmembrane domain but with different topology) (see Figure 40 B). PC12 cells were treated with a Ca<sup>2+</sup> carrier, ionomycin, in the absence or presence of calcium and subjected to sonication to obtain plasma

membrane sheets. The analysis of the immunostaining intensities of the membrane proteins revealed a significant reduction in the staining intensities of the proteins studied as well as enhanced clustered appearance of the signals (Figures 40 A & B) (Zilly et al., 2011).

Therefore, the effect observed was studied with more experiments where calcium levels were delivered by using carefully buffered calcium solutions or induced by depolarization. In addition, it was tested how other divalent cations, such as  $Mg^{2+}$ , would influence the organization of membrane proteins.

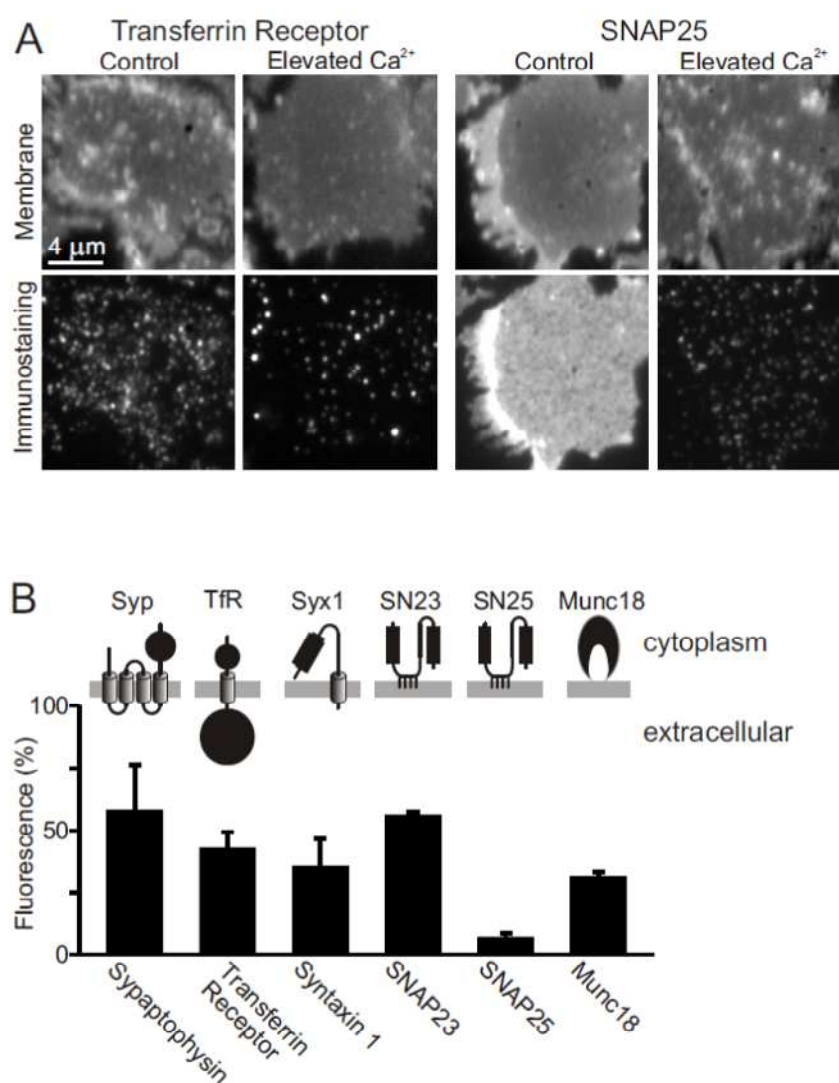


**Figure. 40. An increase in intracellular calcium diminishes membrane protein immunostaining intensities.** PC12 cells were treated for 5 min with 20  $\mu m$  ionomycin in the absence or presence of extracellular free calcium, followed by the generation of membrane sheets and immunostaining for a variety of structurally diverse membrane proteins. (A) Upper

---

panels, TMA-DPH staining for the visualization of phospholipid membranes, indicating location and integrity of the basal plasma membranes; lower panels, immunostaining for transferrin receptor (left) or SNAP-25 (right). **(B)** Immunostaining intensities after calcium incubation were normalized to no calcium condition and expressed as percentage. For each condition, 31-78 membrane sheets were analyzed for one experiment. Values are means  $\pm$  SEM (n = 3 independent experiments). [Figure taken from Zilly et al., 2011.](#)

### **3.6.1. Influence of $Mg^{2+}$ ions and the incubation process on the organization of membrane proteins**

Like calcium, magnesium ion is also an essential intracellular divalent cation (Permyakov and Kretsinger, 2009). Therefore, the influence of  $Mg^{2+}$  on the organization of membrane proteins was investigated. Moreover, in order to check for any effect of the incubation of plasma membrane sheets on the organization of membrane proteins, the following experiments were performed. Plasma membrane sheets from PC12 cells were incubated for 5 minutes at 37°C, fixed and immunostained for the membrane proteins as mentioned earlier. As shown in Figure 41, there seems to be no significant effect of 5 minutes incubation on the immunostaining intensities of the membrane proteins studied apart from SNAP23 which upon incubation, for unknown reasons, becomes less accessible for immunostaining. Similarly, incubations with 2mM  $Mg^{2+}$  also had no clear effect (except for the unusual effect observed for transferrin receptor) on the immunostaining pattern for the membrane proteins studied.



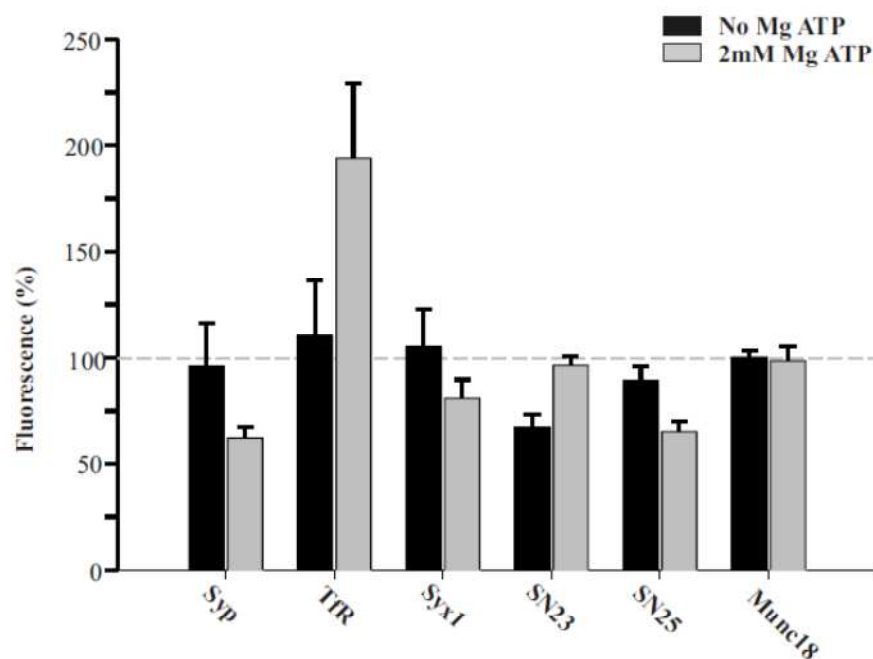


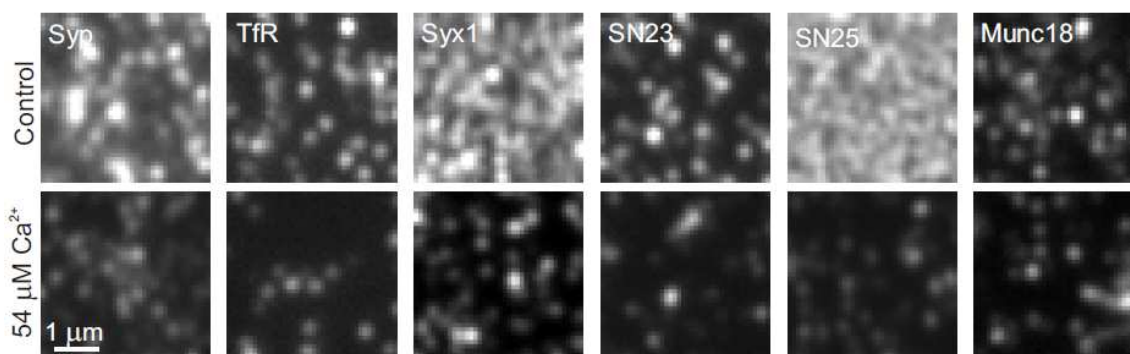
**Figure 41. Influence of the incubation process and  $Mg^{2+}$  ions on the membrane protein immunostaining intensities.** Plasma membrane sheets from PC12 cells were either directly fixed or treated for 5 min without any divalent ions or with 2 mM  $MgCl_2$  and 2 mM ATP and immunostained for membrane proteins as indicated. Quantified immunofluorescence intensities were normalized to the values obtained from directly fixed membrane sheets. Black bars - incubations in the absence of any ions and grey bars – incubation with 2mM MgATP. Values are means  $\pm$  SEM (n = 3-4 experiments and 14-40 sheets for each experiment).

### 3.6.2. Direct modulation of membrane protein organization by $Ca^{2+}$

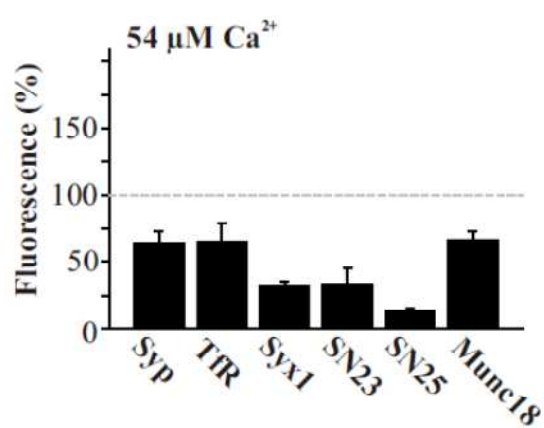
Following the calcium induced effect described in the above section (Figure 40) a detailed study of the same was taken up using carefully buffered calcium solutions applied to native plasma membrane sheets. As shown in Figure 42 A and B, addition of 54  $\mu M$   $Ca^{2+}$  in the presence of MgATP resulted in similar changes in membrane protein staining patterns as shown in figure 40. Intriguingly, the effect was brought about at 850 nM  $Ca^{2+}$  and even without MgATP (Figure 42 C) indicating that  $Ca^{2+}$  alone is responsible for the phenomenon that occurs well within the physiological range of calcium concentrations. As expected, basal levels of  $Ca^{2+}$  seemed to have no effect (Figure 42 D). Through sequence analysis of the proteins investigated it was discovered that the magnitude of the effect correlates positively with the abundance of negatively

charged side chains (Zilly et al., 2011). In addition, as the plasma membrane sheets do not have any cellular components for secondary effects such as membrane trafficking, actin remodelling or protease action, the data suggests that the calcium induced organization of the membrane proteins is likely due to an electrostatic interaction with the negatively charged phospholipid bilayer and the negatively charged membrane protein and not through some cell signaling cascade.

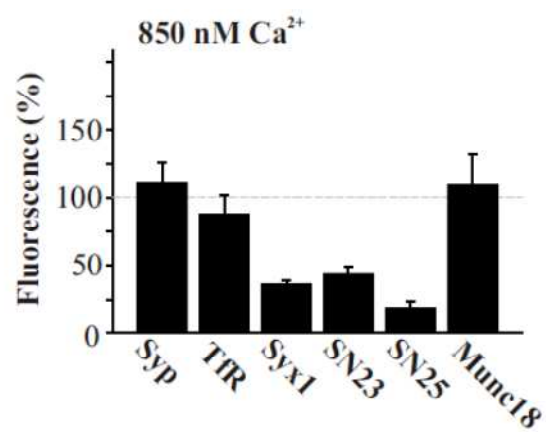
A)



B)



C)



D)

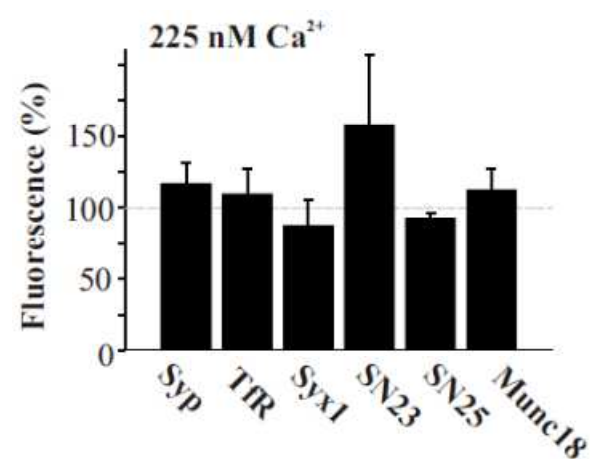


**Figure 42. Effect of calcium on plasma membrane proteins**

(A-D) Freshly prepared plasma membrane sheets were incubated in the presence (A and B) or absence (C and D) of MgATP for 10 min at  $37^\circ\text{C}$  with specified  $\text{Ca}^{2+}$  concentration and immunostained for various membrane proteins mentioned. (A) Upper panels show magnified

---

views from immunostained membrane sheets with no calcium and lower panels show sheets with 54  $\mu\text{M}$   $\text{Ca}^{2+}$ . **(B-D)** The immunostaining intensities for the membrane proteins were quantified and normalized to no calcium conditions - after 54  $\mu\text{M}$  (B), 850 nM (C) or 225 nM (D)  $\text{Ca}^{2+}$ . For each condition, 42-106 (for 54  $\mu\text{M}$  free  $\text{Ca}^{2+}$ ) and 18-32 (for 800 nM free  $\text{Ca}^{2+}$ ) and 20-53 (for 225 nM free  $\text{Ca}^{2+}$ ) membrane sheets were analyzed for one experiment. Values are means  $\pm$  SEM (n = 3-5 independent experiments). [Figure modified from Zilly et al., 2011.](#)

### **3.6.3. Calcium induced remodelling of membrane proteins under physiological conditions**

To test whether the observed phenomenon can be replicated under physiological conditions, primary neuroendocrine cells (bovine chromaffin cells) were stimulated by high potassium which depolarizes the cells and opens up voltage-gated calcium-channels, generating a transient rise in intracellular calcium. As shown in Figures 43 and 44, the immunostaining intensity at the equatorial plane of the cells was recorded and analyzed. Amongst all, SNAP-25 exhibits an appreciable decrease in plasmalemmal immunostaining. However, the effect was either mild or moderate for other proteins probably due to short duration (30 s) of the treatment.

Hence, membrane protein remodelling occurs under physiological condition of a transient rise in intracellular calcium concentration. Though the strong effects are seen for SNAP-25 only (see Figure 44), the data demonstrate that the calcium entry through ion channels can mediate remodelling of membrane proteins.

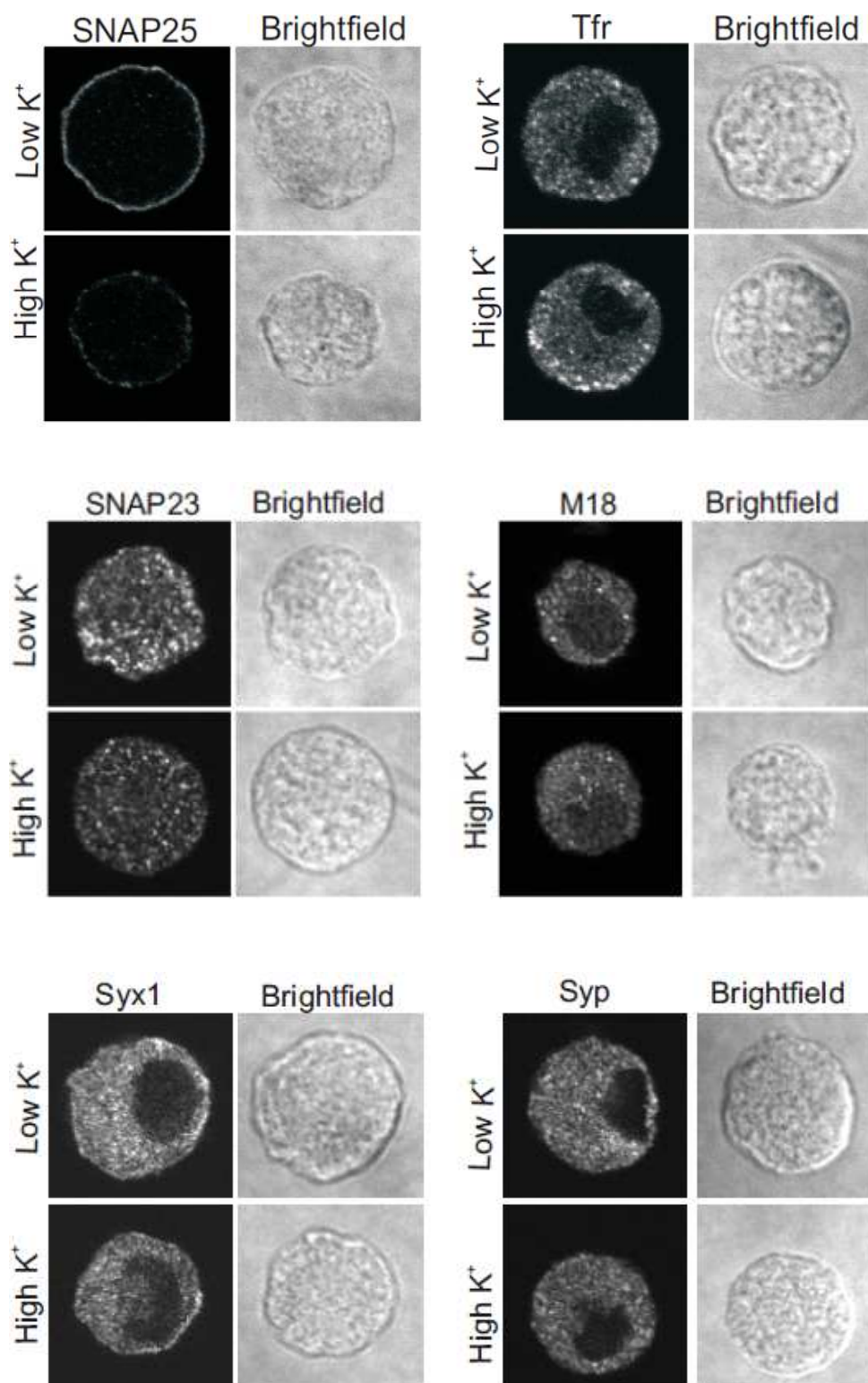


**Figure 43. Confocal micrographs from bovine chromaffin cells stimulated by depolarisation with high potassium.** Bovine chromaffin cells were treated with low or high potassium at 37°C for 30 s, fixed and immunostained for the membrane proteins as mentioned. Confocal micrographs from the equatorial plane in the immunofluorescence (left) and in the brightfield (right) channels are shown.

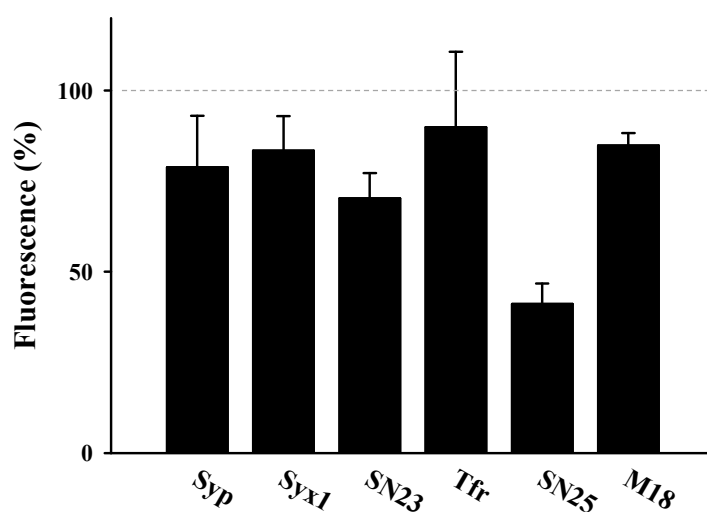


**Figure 44. Quantification of depolarisation induced decrease in the membrane protein immunostaining.** Bovine chromaffin cells were treated with low or high potassium at 37°C for 30 s, fixed and immunostained for the membrane proteins as mentioned. Quantification of the plasmalemmal immunofluorescence was analyzed by linescans placed on the periphery of the cells. Immunointensity value for the the high potassium condition were normalised to the low potassium value. Values are means  $\pm$  SEM (n = 3-4 independent experiments and 19-34 cells in each experiment were analyzed).

---

## 4. Discussion

### 4.1. SNARE protein organization on the plasma membrane

The plasma membrane exhibits a lateral heterogeneity in its architecture. Constituent proteins and lipids are subjected to regulation by lipids rafts, protein clusters and actin cytoskeleton barrier. The protein clusters are nanoscale dynamic structures and provide platforms for diverse cellular activities like signaling and secretion. For instance, syntaxin is concentrated in clusters that define docking and fusion sites for secretory granules (Lang et al., 2001). Syntaxin clustering on the plasma membrane is mediated by specific homo-oligomerization involving its SNARE motifs (Sieber et al., 2006) and the cluster integrity is maintained by the associated plasma membrane cholesterol (Lang et al., 2001). However, mild cholesterol depletion treatment does not result in any visible change in syntaxin 1 cluster morphology (see Figure 39 A) indicating that the self association through SNARE motifs is likely to play a prominent role in syntaxin1 clustering. Plasma membrane SNAP-25 is membrane associated with its palmitoyl anchors and is suggested to associate with the lipid rafts (Salaun et al., 2005b) but the exact mechanism of its clustering is not studied in detail. Therefore, in this study, it was investigated if similar protein-protein interactions mediate SNAP-25 clustering.

Superresolution STED microscopic imaging of the SNAP-25 clusters and auto correlation analysis on the clusters (see Figure 30) revealed that the SN25-0<sub>L</sub>0 cluster size does not significantly differ from wild type SNAP-25 meaning that the SNARE motifs are not involved in SNAP-25 homophilic clustering. In agreement with this, SN25-0<sub>L</sub>0, unable to interact with syntaxin 1 (see Figure 2, Appendix), should have been many fold faster in its mobility if it would be free and not clustered (see Figure 15). Therefore the question remains as how does SNAP-25 cluster? The partial association of SNAP-25 with lipid rafts through its palmitoyl anchors at the linker region could be an explanation (Salaun et al., 2005b) and the differential affinities of SNAP-25 and SNAP-23 (2.5 fold higher than SNAP-25) owing to the presence of an extra cysteine on the SNAP-23 cysteine rich linker region is intriguing (Salaun et al., 2005a). Interestingly, the differential affinity for lipid rafts contributes to the functional difference between the isoforms in supporting exocytosis – SNAP-25 being more potent than SNAP-23 (Salaun et al., 2005a). Therefore, one can safely conclude that the SNAP-25 clustering through association of its palmitoyl anchors with the lipid rafts

renders its SNARE motifs freely available for SNARE motif interactions with syntaxin. In contrast, syntaxin clustering results in masking of its SNARE motifs and as a result inhibition of SNARE motif interactions with SNAP-25. This view is further supported by the observation that the binding of exogenously added recombinant syntaxin 1 to the reactive SNAP-25 on native plasma membranes is efficient unlike for exogenously added SNAP-25 that does not bind efficiently to endogenous syntaxin (Lang et al., 2002). This is because endogenous syntaxin has its SNARE motif used up for its clustering thereby relatively increasing the availability of endogenous SNAP-25 for complex formation with exogenously added syntaxin. Whereas, endogenous clustered SNAP-25 has its SNARE motif free for complex formation with all the available endogenous syntaxin leaving no free reactive syntaxin for the recombinant SNAP-25 (Lang et al., 2002).

It has been previously reported that syntaxin 1 and SNAP-25 clusters partially overlap (Lang et al., 2001). But the estimates on the extent of overlap suffered from diffraction limited resolution of conventional microscopy. Using super resolution STED microscopy it could be shown that the two cluster types are very close but clearly separated (see Figures 31 & 32). The SNAP-25 SNARE motif neither mediates SNAP-25 clustering nor places SNAP-25 clusters very close to syntaxin 1 clusters. This suggests that the spatial proximity between the two cluster types is possibly mediated by a preference for same lipid phases. Nevertheless, a proportion of freely moving SNAP-25 clusters might specifically interact with less mobile syntaxin 1 clusters resulting in an overlap of the two clusters. This is reflected in the more pronounced overlap of SNAP-25 clusters with syntaxin 1 clusters (with a correlation coefficient of 0.2) than with the syntaxin 4 clusters (with a correlation coefficient of 0.08) (compare Figure 32 and 34 and see also Figure 1 from Appendix for differential levels of physical association of SNAP-25 with syntaxin 1 and syntaxin 4). Although there is a slight increase in the overlap of SNAP-25 and syntaxin 1 clusters with the incubation alone (see Figure 36) possibly due to increased levels of binary SNARE complex formation in agreement with the previous findings (Lang et al., 2002), the addition of synaptobrevin does not affect the proximity of the two clusters significantly (see Figure 38). This suggests that increased binary SNARE complex formation might be associated with more clusters being close to each other and *cis*-SNARE complexes may slightly move away from the original cluster sites.



#### 4.2. Calcium induced remodeling of membrane proteins

Dynamics of membrane microdomains is regulated mainly by protein-lipid and protein-protein interactions. In this study, yet another mechanism is described whereby plasma membrane remodeling is subjected to electrostatic effects of submicromolar  $\text{Ca}^{2+}$ . The data show that calcium, most likely through electrostatic mechanisms, exerts rapid remodelling of diverse membrane proteins resulting in diminished immunoreactivity which is brought about by increased clustering (see Figures 40 and 42) and epitope masking. The strength of the effect correlated well with the net negative charge on the protein studied (Zilly et al., 2011) and is independent of the structure or membrane anchorage of the protein (see Figure 40 B). The phenomenon observed is most likely due to direct action of calcium on the proteins as is evident from native plasma membrane sheets which are devoid of any cytosolic factors or proteases, actin cortex remodelling and moreover there are no specific calcium binding sites on the proteins studied. The effect is as fast as 30 s (although evident only for SNAP-25 immunostaining on chromaffin cells) (see Figures 43 & 44) which supports the idea that calcium in a physiological concentration range acts on membrane proteins through non specific electrostatic mechanisms brought about by compensating negative repulsive charges between the negatively charged phospholipid bilayer and negatively charged membrane proteins.

The observed reduced immunostaining could be due to epitope masking either by steric hindrance of the clustered protein or conformational changes in the protein. Comparison of calcium effects on the immunostaining intensity and the distribution of fluorescent protein tagged SNAP-25 and syntaxin revealed that both mechanisms of epitope masking might operate albeit to a varying degree – a major proportion of SNAP-25 seems to undergo a conformational change whereas most syntaxin seems to cluster to a higher degree (Zilly et al., 2011). In case of SNAP-25, since its epitope region is part of the SNARE motif and required for the SNARE complex formation with syntaxin and synaptobrevin (Xu et al., 1999), the functional reactivity goes down with increasing calcium concentration (Zilly et al., 2011).

Like calcium, magnesium is a divalent cat ion but available at much higher intracellular concentrations and not involved in signaling. However,  $\text{Mg}^{2+}$  is smaller and therefore has a much higher charge density requiring higher energy to remove the surrounding water molecules of  $[\text{Mg}(\text{H}_2\text{O})_6]^{2+}$  to be able to interact with negatively charged amino

acid residues or lipids. For this reason,  $Mg^{2+}$  is less efficient in mediating the electrostatic effect (see Figure 41). Although the physiological relevance of the observed calcium induced membrane protein remodelling remains obscure, it is possible that at least in the case of SNARE proteins the mechanism allows for a feedback regulation of calcium dependent neuronal exocytosis (Spafford and Zamponi, 2003).

### **4.3. Structure and dynamics of syntaxin 1 ( $Q_a$ ) and SNAP-25 ( $Q_bQ_c$ ) interactions in live cells**

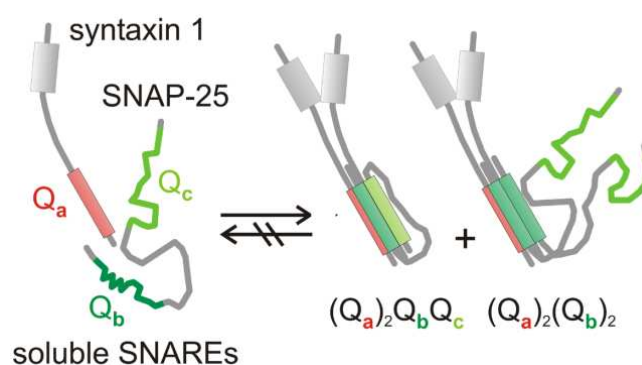
#### **4.3.1. $Q_aQ_b$ SNARE complex formation predominates in live cells**

Exocytosis at the neuronal synapse is a highly regulated sequential process. Upon the arrival of an action potential, neurotransmitter filled vesicles at the presynaptic active zone fuse with the plasma membrane within milliseconds of entry of calcium. The fusion of two membranes – from vesicles and plasma membrane, is known to be mediated by a so called ‘fusion machinery’ which in its core involves SNAREs and in addition regulatory proteins. The three SNARE proteins, one from vesicle (synaptobrevin) and other two from plasma membrane (syntaxin 1 and SNAP-25) come together to assemble in an orderly fashion to pull the two opposing membranes together for fusion. Hence, characterizing the intermediates in the SNARE complex assembly pathway that leads to fusion has been a very important aspect of understanding the release cascade and efficiency.

Over the years, studies have indicated that the putative initial SNARE intermediate complex is a  $Q_aQ_bQ_c$  (1:1, 1 syx and 1 SNAP-25) heterodimer, also called 'acceptor complex', serving to accept synaptobrevin as a binding partner. But the detailed characterization of this intermediate complex has been challenging owing to its transient nature and high propensity of the Q-SNAREs to engage into diverse four helix bundles (reviewed in (Brunger, 2005)) for example,  $(Q_a)_2Q_bQ_c$  (2:1) complex, a non-physiological dead end complex rather than a true intermediate (see Figure 45 A). But recent smFRET (single molecule FRET) imaging studies by Weninger et al., 2008 elegantly demonstrated the presence of a highly dynamic  $Q_aQ_bQ_c$  bundle – involving three helices  $Q_a$ ,  $Q_b$  and  $Q_c$  with  $Q_a$  and one of the helices of SNAP-25 either  $Q_b$  or  $Q_c$  in dissociated states. Intriguingly, the complex can be stabilized into the  $Q_aQ_bQ_c$  state

when incubated with SNARE complex regulatory proteins like munc-13, complexin, munc-18 and synaptotagmin. However, most of these *in vitro* studies do not reflect the actual situation in live cells as the SNARE proteins are incubated at artificial conditions – monomeric and unclustered, using only SNARE motifs (without other domains which might have some regulatory roles), at artificial stoichiometry and lack of membrane anchorage or proper orientation.

**A) *In vitro***



**B) *In vivo***

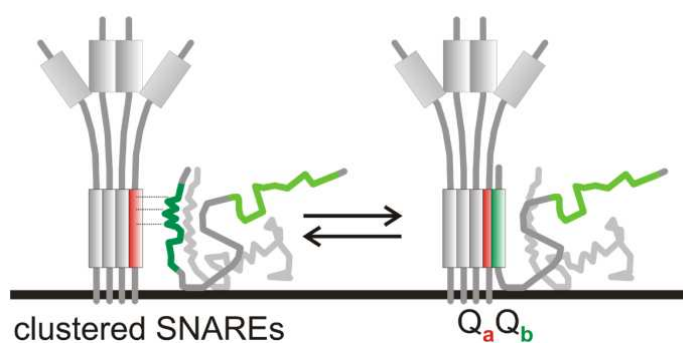


**Figure 45. Q- SNARE complexes forming *in vitro* and *in vivo*.**

**A)** In solution Q-SNAREs form stable four-helix bundles that most likely play no physiological role. **B)** In native membranes a reversible interaction of clustered syntaxin 1 and SNAP-25 yields a two-helix  $Q_aQ_b$  intermediate. [Figure taken from \(Halemani et al., 2010\).](#)

In the present studies, FRAP assays allowed for direct readout of mobility of fluorescently labelled SNAP-25 variants which was interpreted in terms of their extent of interaction with the known cognate partner syntaxin 1. Through a series of FRAP

experiments it was interpreted and supposed that the observed significant reduction in the mobility of SNAP-25 by syntaxin 1 (see Figures 14 & 15) can easily be explained by its interaction with the less mobile syntaxin clusters (see Figure 45 B) and the two proteins engage in a stable interaction forming a  $Q_aQ_b$  complex without significant contribution from the C-terminal SNARE motif of SNAP-25 (see Figures 14 & 15). Formation of this complex was linearly dependent on syntaxin 1 expression levels as reflected in the half time recovery times measured for SNAP-25 (Figure 14). The  $Q_aQ_b$  complex can also be formed by promiscuous interaction between SNAP-25 and syntaxin 4 (Figures 25 & 26). However, formation of this complex seems to be slightly less efficient or less stable compared to the complex with syntaxin 1 which was also reflected in the respective cluster overlap (see Figures 32 & 34) and co-immunoprecipitation studies (see Figure 1 from Appendix).

But for efficient complex formation, the position of the SNARE motif within SNAP-25 is important as the data from FRAP and binding experiments show that the SNAP-25  $N_L0$  is more reactive than the SNAP-25  $0_LN$  (see Figures 14-17 & Figures 28-29). Placing the N-terminal SNARE motif at the C-terminus prevents its interaction with syntaxin 1 even when the syntaxin is soluble (not membrane anchored with some specific orientation) as in the binding experiments. The significance of the positional specificity of the N-terminal SNARE motif for its efficient interaction with syntaxin 1 could only be explained by speculating that the complex becomes more stable when both the SNARE motifs are tightly associated with the membrane or that when  $Q_b$  is in the C-terminal position an inhibitory mechanism comes into play. Supporting the latter idea a recent study on yeast SNAREs proposed that the C-terminal SNARE motif of SNAP-25 homologue Sec9p is unstructured only when the complex is membrane anchored as a membrane proximal region of the SNARE complex binds to the membrane, a mechanism which competes with the SNARE complex assembly (Su et al., 2008). If this is also true for the neuronal SNARE complex, one can safely assume that the same inhibitory mechanism applies to the C-terminal SNARE motif diminishing its reactivity with syntaxin.

Though the data presented here cannot rule out the  $Q_aQ_bQ_c$  complex formation completely, it is possible that it exists in minor proportions (see Figure 2 from Appendix). However, the C-terminal motif ( $Q_c$ ) seems to be, in principle, dispensable as it is not stabilizing the observed  $Q_aQ_b$  complex. Moreover, placing the C-terminal

SNARE motif at the N-terminus ( $C_LC$  construct) does not enforce its interaction with syntaxin (see Figures 16, 17 and 29) stressing the fact that the C-terminal SNARE motif intrinsically cannot bind alone to syntaxin irrespective of its position in the SNAP-25 molecule.

Live cell FRET imaging studies by An and Almers, (2004) have indicated the formation of  $Q_aQ_b$  complex only at low syntaxin 1 concentrations and could be induced by the calcium influx. This suggested that the formation of the observed complex dependent on some other factors and possibly represented a relatively late event in the SNARE complex assembly. However, such ensemble intensity based FRET measurements are not suitable for characterizing the highly dynamic SNARE intermediate and FRET readout for such complexes was possible only in certain orientation as the observed complex would presumably lie nearly flat on the membrane. Moreover, the study did not address the  $Q_aQ_b$  complex structure in detail. Therefore the exact nature of the complex remained inconclusive.

In live cells, SNAREs are membrane anchored in a specific orientation, SNAP-25 is more abundant than syntaxin 1 (SNAP-25 being 6-7 fold more than syntaxin1 in PC12 cells) (Tucker et al., 2003) and SNAREs are clustered (Chamberlain et al., 2001; Lang et al., 2001). Therefore, in live cells, all these factors presumably prevent the formation of the non-physiological 2:1 (two syntaxin 1 and one SNAP-25) complex as in solution. Hence, in live cells, we only find the  $Q_aQ_b$  complex (see Figure 45 B) but not the  $Q_aQ_c$  complex as observed by Weninger et al., (2008) and the complex most likely represents a foremost intermediate in the SNARE assembly pathway as it forms independent of any neuronal cofactors (see Figure 26). In the later stages,  $Q_aQ_bQ_c$  complex formation could be promoted by SNARE interacting proteins - munc18, munc13, complexin and synaptotagmin as has been shown by Weninger et al., (2008).

#### **4.3.2. The $Q_aQ_b$ SNARE complex in live cells is most likely zippered all along its length**

There are 16 layers of interaction from -7 to +8 along the neuronal ternary SNARE complex involving the SNARE motifs of SNAP-25, syntaxin 1 and synaptobrevin 2. The residues participating in these layers would probably be also required for  $Q$ -SNARE complex formation. The SNARE motif of syntaxin 1 and the N-terminal

SNARE motif of SNAP-25 assumes alpha helical conformation when in binary or ternary complexes (Zhong et al., 1997). Accordingly, the SNARE motif truncations of SNAP-25 could not engage syntaxin 1 into the complex (see Figures 18-20). The data suggest that the N-terminal amino acids are significantly involved in the interaction with syntaxin 1 as in line with the observation that the deletion of amino acids 1-38 in SNAP-25 inhibits SNARE complex formation (Fasshauer and Margittai, 2004). Q<sub>a</sub>Q<sub>b</sub> complex formation is sensitive to any slight change in the alpha helical conformation of the SNARE motifs as helix breaking proline substitutions anywhere along its length resulted in faster mobility of SNAP-25 (see Figures 22 & 23). The G43D mutant, which corresponds to temperature sensitive SNAP-25 mutants in *Drosophila* (G50E) (Rao et al., 2001) and in Yeast (mutant *Sec9-4<sup>ts</sup>* with G458D) (Brennwald et al., 1994) also shows slowed down mobility (see Figures 22 & 23) indicative of it being able to form binary Q<sub>a</sub>Q<sub>b</sub> complex with syntaxin 1 as contrary to *in vitro* studies where mutant SNAP-25 form neither binary Q<sub>a</sub>Q<sub>b</sub> interactions (for *Sec9-4<sup>ts</sup>* see (Rossi et al., 1997) and for SNAP-25 G51D mutant - leech numbered, see (Fasshauer et al., 1997a)) nor a tetramer - a four helix bundle of (Q<sub>a</sub>Q<sub>b</sub>)<sub>2</sub> (Misura et al., 2001). Thus, *in vivo*, G43D mutant of SNAP-25 can form Q<sub>a</sub>Q<sub>b</sub> complex (also shown by An and Almers, (2004)) although interactions seem less robust.

Although *in vitro* studies suggest that the last few residues of the Q<sub>b</sub> (N-terminal) SNARE motif remain unstructured in binary Q-SNARE complexes (Margittai et al., 2001), a recent study of X-ray crystal structure of the neuronal SNARE complex using full length SNAREs suggest that the helical continuity goes beyond SNARE motifs involving linkers and trans membrane regions (Stein et al., 2009). We therefore, conclude that the observed Q<sub>a</sub>Q<sub>b</sub> complex in live cells is largely alpha helical and involves N-terminal to C-terminal zippering all along their SNARE motifs.

#### **4.3.3. Do syntaxin clusters represent sites of Q-SNARE complex formation?**

The syntaxin 1 clusters are thought to define sites of vesicle docking and fusion (Lang et al., 2001). The data presented so far suggest that the initial intermediate in the SNARE complex assembly, Q<sub>a</sub>Q<sub>b</sub> is more likely occur at the interface between the SNAP-25 and syntaxin 1 clusters whose spatial proximity is possibly mediated by a preference for same lipid phases but not by the SNARE-SNARE interactions. In support

of our data, recently, a FLIM FRET (Fluorescence Lifetime Imaging FRET) study using live cells on the dynamics of Q-SNARE complexes (Rickman et al., 2010) demonstrated that a proportion of Q-SNARE heterodimers on the plasma membrane exist as  $Q_aQ_b$  complexes operating under the influence of membrane lipids and is spatially segregated from the ones representing  $Q_aQ_bQ_c$  'acceptor' complexes. Cholesterol depletion resulted in decreased proportion of the observed  $Q_aQ_b$  heterodimers (Rickman et al., 2010). Thus the site of  $Q_aQ_b$  complex formation could possibly be at the interface between cholesterol enriched SNARE clusters. From here, one can only speculate that the next stage of SNARE assembly proceeds through spontaneous or protein mediated engagement of  $Q_c$  with simultaneous stabilization by munc18, serving to accept synaptobrevin from the secretory vesicle. However, the  $Q_aQ_bQ_cR$  (*cis*-SNARE) complexes that form subsequently may slightly move away from bulky syntaxin clusters.

#### **4.4. FRAP as a method to measure protein-protein interactions in live cells**

In the last few decades, measuring protein-protein interactions has become a prerequisite for understanding the structural and functional mechanisms of the cell(s). Development of sophisticated biochemical and biophysical tools to study protein dynamics has been a great endeavor and has contributed immensely to the understanding of the same. However, these tools suffer from inherent limitations mainly in the lack of native environment for the study of membrane proteins. This has been overcome in recent years by the emergence of advances in usage of genetically encoded fluorescent tags and fluorescence imaging. Techniques like FRET (Förster's Resonance Energy Transfer), FCS (Fluorescence Correlation Spectroscopy) that were normally used to study protein dynamics in solution have been successfully employed for live cell approaches. While, FCS in live cells still faces some hard technical challenges, FRET imaging in live cells has seen a tremendous usage and support (Mayor, 2007). FRET offers high spatial and temporal resolution of the protein dynamics like protein-protein interactions, conformational changes during protein folding or ligand binding. In addition, FRET can be determined in several ways of steady state and time resolved measurements (Mayor, 2007). Nevertheless, FRET imaging in live cells is not without

its shortcomings. When overexpressed, proteins in live cells need proper controls for monitoring donor and acceptor concentrations, if otherwise, might lead to false detection of FRET efficiency and thereby an erroneous interpretation. Another important caution to be exercised in FRET imaging is position and orientation of the acceptor and donor fluorophore with respect to each other as the FRET efficiency is very sensitive for these two aspects. Therefore, in live cells, FRET imaging can be performed only when one knows the proper location and orientation of the acceptor and donor fluorophores of the interacting proteins (Mayor, 2007). The FRAP approach we employed in our studies is able to overcome these limitations making it a simple assay for studying protein-protein interactions in live cells. In principle, only one interaction partner needs to be overexpressed and stoichiometry of the interacting proteins is not a major problem.

FRAP measures the ensemble average of lateral diffusion of molecules within the membrane. We have established an assay where we exploit the change in rates of lateral diffusion of protein mutants to infer their extent of ability to interact with the partner protein (s). We have demonstrated that the density of protein on the plasma membrane does not significantly affect the rates of diffusion (see Figure 24). The rates of diffusion of the protein under study (SNAP-25 wild type) correlate well with the expression levels of its partner protein (syntaxin) and therefore the mobility readout provides an indirect measure of strength of interaction of the two proteins. The assay is simple and can also be used to determine diffusion constants and the mobile fraction of the tagged proteins. The instrumentation required is also simple requiring only the confocal or TIRF (Total Internal Reflection Fluorescence) microscope set up with appropriate excitation laser lines and AOTF (Acousto-Optical Tunable Filter) (Lippincott-Schwartz et al., 2003). However, one has to take certain precautions while performing FRAP experiment - these include: 1) selecting discontinuous compartments for photobleaching might result in either lack of recovery or partial recovery, 2) optimizing the excitation laser intensity for photobleaching and acquisition to minimize possible photo damage of the cells, 3) calibrating the system to avoid fluorophore cross talk, 4) avoiding cells with too bright or too dim fluorescence intensities and 5) minimizing the ground or surrounding vibration so as not to disturb the plane of focus over the entire time period.



#### 4.5. Conclusions

The structure and composition of the plasma membrane has been a subject of intense discussion due to its immense biological significance. The organization of the membrane proteins into clusters, particularly for SNAREs – syntaxin by homo-oligomerisation and SNAP-25 possibly by lipidic interactions – evidently creates a lateral heterogeneity in the plasma membrane. Existence of yet another mechanism of plasma membrane remodeling through non-specific electrostatic interactions between membrane proteins and divalent cations, in particular calcium ions at sub-micromolar concentrations is beginning to unravel. However, the functional relevance of such a mechanism for the function of SNAREs needs to be explored in detail. It is possible that the segregation of Q-SNAREs into respective clusters through diverse mechanisms serves to regulate the formation of the intermediate SNARE complex in a spatial and temporal fashion especially in the context of neuronal exocytosis.

---

## 5. Bibliography

- Aguado, F., G. Majo, B. Ruiz-Montasell, J. Llorens, J. Marsal, and J. Blasi. 1999. Syntaxin 1A and 1B display distinct distribution patterns in the rat peripheral nervous system. *Neuroscience* 88(2):437-446.
- An, S.J., and W. Almers. 2004. Tracking SNARE complex formation in live endocrine cells. *Science* 306(5698):1042-1046.
- Antonin, W., D. Fasshauer, S. Becker, R. Jahn, and T.R. Schneider. 2002. Crystal structure of the endosomal SNARE complex reveals common structural principles of all SNAREs. *Nat Struct Biol* 9(2):107-111.
- Avery, J., D.J. Ellis, T. Lang, P. Holroyd, D. Riedel, R.M. Henderson, J.M. Edwardson, and R. Jahn. 2000. A cell-free system for regulated exocytosis in PC12 cells. *J Cell Biol* 148(2):317-324.
- Axelrod, D., P. Ravdin, D.E. Koppel, J. Schlessinger, W.W. Webb, E.L. Elson, and T.R. Podleski. 1976. Lateral motion of fluorescently labeled acetylcholine receptors in membranes of developing muscle fibers. *Proc Natl Acad Sci U S A* 73(12):4594-4598.
- Bark, I.C., K.M. Hahn, A.E. Ryabinin, and M.C. Wilson. 1995. Differential expression of SNAP-25 protein isoforms during divergent vesicle fusion events of neural development. *Proc Natl Acad Sci U S A* 92(5):1510-1514.
- Bark, I.C., and M.C. Wilson. 1994. Human cDNA clones encoding two different isoforms of the nerve terminal protein SNAP-25. *Gene* 139(2):291-292.
- Barnstable, C.J., R. Hofstein, and K. Akagawa. 1985. A marker of early amacrine cell development in rat retina. *Brain Res* 352(2):286-290.

- Baumert, M., P.R. Maycox, F. Navone, P. De Camilli, and R. Jahn. 1989. Synaptobrevin: an integral membrane protein of 18,000 daltons present in small synaptic vesicles of rat brain. *Embo J* 8(2):379-384.
- Bennett, M.K., N. Calakos, and R.H. Scheller. 1992. Syntaxin: a synaptic protein implicated in docking of synaptic vesicles at presynaptic active zones. *Science* 257(5067):255-259.
- Bethani, I., T. Lang, U. Geumann, J.J. Sieber, R. Jahn, and S.O. Rizzoli. 2007. The specificity of SNARE pairing in biological membranes is mediated by both proof-reading and spatial segregation. *Embo J* 26(17):3981-3992.
- Bethani, I., A. Werner, C. Kadian, U. Geumann, R. Jahn, and S.O. Rizzoli. 2009. Endosomal fusion upon SNARE knockdown is maintained by residual SNARE activity and enhanced docking. *Traffic* 10(10):1543-1559.
- Blasi, J., E.R. Chapman, S. Yamasaki, T. Binz, H. Niemann, and R. Jahn. 1993. Botulinum neurotoxin C1 blocks neurotransmitter release by means of cleaving HPC-1/syntaxin. *Embo J* 12(12):4821-4828.
- Bollmann, J.H., and B. Sakmann. 2005. Control of synaptic strength and timing by the release-site Ca<sup>2+</sup> signal. *Nat Neurosci* 8(4):426-434.
- Borisovska, M., Y. Zhao, Y. Tsytsyura, N. Glyvuk, S. Takamori, U. Matti, J. Rettig, T. Sudhof, and D. Bruns. 2005. v-SNAREs control exocytosis of vesicles from priming to fusion. *Embo J* 24(12):2114-2126.
- Boschert, U., C. O'Shaughnessy, R. Dickinson, M. Tessari, C. Bendotti, S. Catsicas, and E.M. Pich. 1996. Developmental and plasticity-related differential expression of two SNAP-25 isoforms in the rat brain. *J Comp Neurol* 367(2):177-193.
- Bowen, M.E., K. Weninger, A.T. Brunger, and S. Chu. 2004. Single molecule

observation of liposome-bilayer fusion thermally induced by soluble N-ethyl maleimide sensitive-factor attachment protein receptors (SNAREs). *Biophys J* 87(5):3569-3584.

Breidenbach, M.A., and A.T. Brunger. 2005. New insights into clostridial neurotoxin-SNARE interactions. *Trends Mol Med* 11(8):377-381.

Brennwald, P., B. Kearns, K. Champion, S. Keranen, V. Bankaitis, and P. Novick. 1994. Sec9 is a SNAP-25-like component of a yeast SNARE complex that may be the effector of Sec4 function in exocytosis. *Cell* 79(2):245-258.

Bronk, P., F. Deak, M.C. Wilson, X. Liu, T.C. Sudhof, and E.T. Kavalali. 2007. Differential effects of SNAP-25 deletion on Ca<sup>2+</sup>-dependent and Ca<sup>2+</sup>-independent neurotransmission. *J Neurophysiol* 98(2):794-806.

Brunger, A.T. 2005. Structure and function of SNARE and SNARE-interacting proteins. *Q Rev Biophys* 38(1):1-47.

Brunger, A.T., K. Weninger, M. Bowen, and S. Chu. 2009. Single-molecule studies of the neuronal SNARE fusion machinery. *Annu Rev Biochem* 78:903-928.

Carafoli, E. 1987. Intracellular calcium homeostasis. *Annu Rev Biochem* 56:395-433.

Chamberlain, L.H., R.D. Burgoyne, and G.W. Gould. 2001. SNARE proteins are highly enriched in lipid rafts in PC12 cells: implications for the spatial control of exocytosis. *Proc Natl Acad Sci U S A* 98(10):5619-5624.

Chamberlain, L.H., and G.W. Gould. 2002. The vesicle- and target-SNARE proteins that mediate Glut4 vesicle fusion are localized in detergent-insoluble lipid rafts present on distinct intracellular membranes. *J Biol Chem* 277(51):49750-49754.

Chen, Y.A., S.J. Scales, and R.H. Scheller. 2001. Sequential SNARE assembly underlies

---

priming and triggering of exocytosis. *Neuron* 30(1):161-170.

Chernomordik, L.V., and M.M. Kozlov. 2008. Mechanics of membrane fusion. *Nat Struct Mol Biol* 15(7):675-683.

Chicka, M.C., E. Hui, H. Liu, and E.R. Chapman. 2008. Synaptotagmin arrests the SNARE complex before triggering fast, efficient membrane fusion in response to Ca<sup>2+</sup>. *Nat Struct Mol Biol* 15(8):827-835.

Chintagari, N.R., N. Jin, P. Wang, T.A. Narasaraaju, J. Chen, and L. Liu. 2006. Effect of cholesterol depletion on exocytosis of alveolar type II cells. *Am J Respir Cell Mol Biol* 34(6):677-687.

de Wit, H., A.M. Walter, I. Milosevic, A. Gulyas-Kovacs, D. Riedel, J.B. Sorensen, and M. Verhage. 2009. Synaptotagmin-1 docks secretory vesicles to syntaxin-1/SNAP-25 acceptor complexes. *Cell* 138(5):935-946.

Delgado-Martinez, I., R.B. Nehring, and J.B. Sorensen. 2007. Differential abilities of SNAP-25 homologs to support neuronal function. *J Neurosci* 27(35):9380-9391.

Devaux, P.F., and R. Morris. 2004. Transmembrane asymmetry and lateral domains in biological membranes. *Traffic* 5(4):241-246.

Dulubova, I., M. Khvotchev, S. Liu, I. Huryeva, T.C. Sudhof, and J. Rizo. 2007. Munc18-1 binds directly to the neuronal SNARE complex. *Proc Natl Acad Sci U S A* 104(8):2697-2702.

Dulubova, I., S. Sugita, S. Hill, M. Hosaka, I. Fernandez, T.C. Sudhof, and J. Rizo. 1999. A conformational switch in syntaxin during exocytosis: role of munc18. *Embo J* 18(16):4372-4382.

Engelman, D.M. 2005. Membranes are more mosaic than fluid. *Nature* 438(7068):578-

580.

- Fasshauer, D., W. Antonin, M. Margittai, S. Pabst, and R. Jahn. 1999. Mixed and non-cognate SNARE complexes. Characterization of assembly and biophysical properties. *J Biol Chem* 274(22):15440-15446.
- Fasshauer, D., W. Antonin, V. Subramaniam, and R. Jahn. 2002. SNARE assembly and disassembly exhibit a pronounced hysteresis. *Nat Struct Biol* 9(2):144-151.
- Fasshauer, D., D. Bruns, B. Shen, R. Jahn, and A.T. Brunger. 1997a. A structural change occurs upon binding of syntaxin to SNAP-25. *J Biol Chem* 272(7):4582-4590.
- Fasshauer, D., and M. Margittai. 2004. A transient N-terminal interaction of SNAP-25 and syntaxin nucleates SNARE assembly. *J Biol Chem* 279(9):7613-7621.
- Fasshauer, D., H. Otto, W.K. Eliason, R. Jahn, and A.T. Brunger. 1997b. Structural changes are associated with soluble N-ethylmaleimide-sensitive fusion protein attachment protein receptor complex formation. *J Biol Chem* 272(44):28036-28041.
- Fasshauer, D., R.B. Sutton, A.T. Brunger, and R. Jahn. 1998. Conserved structural features of the synaptic fusion complex: SNARE proteins reclassified as Q- and R-SNAREs. *Proc Natl Acad Sci U S A* 95(26):15781-15786.
- Fernandez-Chacon, R., A. Konigstorfer, S.H. Gerber, J. Garcia, M.F. Matos, C.F. Stevens, N. Brose, J. Rizo, C. Rosenmund, and T.C. Sudhof. 2001. Synaptotagmin I functions as a calcium regulator of release probability. *Nature* 410(6824):41-49.
- Ficz, G., R. Heintzmann, and D.J. Arndt-Jovin. 2005. Polycomb group protein complexes exchange rapidly in living *Drosophila*. *Development* 132(17):3963-3976.

- 
- Fiebig, K.M., L.M. Rice, E. Pollock, and A.T. Brunger. 1999. Folding intermediates of SNARE complex assembly. *Nat Struct Biol* 6(2):117-123.
- Finley, M.F., S.M. Patel, D.V. Madison, and R.H. Scheller. 2002. The core membrane fusion complex governs the probability of synaptic vesicle fusion but not transmitter release kinetics. *J Neurosci* 22(4):1266-1272.
- Frick, M., K. Schmidt, and B.J. Nichols. 2007. Modulation of lateral diffusion in the plasma membrane by protein density. *Curr Biol* 17(5):462-467.
- Gonzalo, S., W.K. Greentree, and M.E. Linder. 1999. SNAP-25 is targeted to the plasma membrane through a novel membrane-binding domain. *J Biol Chem* 274(30):21313-21318.
- Greaves, J., G.R. Prescott, Y. Fukata, M. Fukata, C. Salaun, and L.H. Chamberlain. 2009. The hydrophobic cysteine-rich domain of SNAP25 couples with downstream residues to mediate membrane interactions and recognition by DHHC palmitoyl transferases. *Mol Biol Cell* 20(6):1845-1854.
- Grishanin, R.N., J.A. Kowalchuk, V.A. Klenchin, K. Ann, C.A. Earles, E.R. Chapman, R.R. Gerona, and T.F. Martin. 2004. CAPS acts at a pre-fusion step in dense-core vesicle exocytosis as a PIP2 binding protein. *Neuron* 43(4):551-562.
- Guan, R., H. Dai, and J. Rizo. 2008. Binding of the Munc13-1 MUN domain to membrane-anchored SNARE complexes. *Biochemistry* 47(6):1474-1481.
- Guzman, R.E., Y.N. Schwarz, J. Rettig, and D. Bruns. 2010. SNARE force synchronizes synaptic vesicle fusion and controls the kinetics of quantal synaptic transmission. *J Neurosci* 30(31):10272-10281.
- Halemani N.D., I. Bethani, S.O. Rizzoli, T. Lang. 2010. Structure and dynamics of a two-helix SNARE complex in live cells. *Traffic* 11:394-404.

- 
- Hanson, P.I., J.E. Heuser, and R. Jahn. 1997. Neurotransmitter release - four years of SNARE complexes. *Curr Opin Neurobiol* 7(3):310-315.
- Hayashi, T., H. McMahon, S. Yamasaki, T. Binz, Y. Hata, T.C. Sudhof, and H. Niemann. 1994. Synaptic vesicle membrane fusion complex: action of clostridial neurotoxins on assembly. *Embo J* 13(21):5051-5061.
- Heidelberger, R., C. Heinemann, E. Neher, and G. Matthews. 1994. Calcium dependence of the rate of exocytosis in a synaptic terminal. *Nature* 371(6497):513-515.
- Hess, D.T., T.M. Slater, M.C. Wilson, and J.H. Skene. 1992. The 25 kDa synaptosomal-associated protein SNAP-25 is the major methionine-rich polypeptide in rapid axonal transport and a major substrate for palmitoylation in adult CNS. *J Neurosci* 12(12):4634-4641.
- Heumann, R., V. Kachel, and H. Thoenen. 1983. Relationship between NGF-mediated volume increase and "priming effect" in fast and slow reacting clones of PC12 pheochromocytoma cells. Role of cAMP. *Exp Cell Res* 145(1):179-190.
- Hong, W. 2005. SNAREs and traffic. *Biochim Biophys Acta* 1744(2):120-144.
- Hurley, J.H., and S. Misra. 2000. Signaling and subcellular targeting by membrane-binding domains. *Annu Rev Biophys Biomol Struct* 29:49-79.
- Jacobson, K., O.G. Mouritsen, and R.G. Anderson. 2007. Lipid rafts: at a crossroad between cell biology and physics. *Nat Cell Biol* 9(1):7-14.
- Jahn, R., T. Lang, and T.C. Sudhof. 2003. Membrane fusion. *Cell* 112(4):519-533.
- Jahn, R., and R.H. Scheller. 2006. SNAREs--engines for membrane fusion. *Nat Rev Mol Cell Biol* 7(9):631-643.



- 
- Jahn, R., and T.C. Sudhof. 1999. Membrane fusion and exocytosis. *Annu Rev Biochem* 68:863-911.
- James, D.J., J. Kowalchuk, N. Daily, M. Petrie, and T.F. Martin. 2009. CAPS drives trans-SNARE complex formation and membrane fusion through syntaxin interactions. *Proc Natl Acad Sci U S A* 106(41):17308-17313.
- Kusumi, A., C. Nakada, K. Ritchie, K. Murase, K. Suzuki, H. Murakoshi, R.S. Kasai, J. Kondo, and T. Fujiwara. 2005. Paradigm shift of the plasma membrane concept from the two-dimensional continuum fluid to the partitioned fluid: high-speed single-molecule tracking of membrane molecules. *Annu Rev Biophys Biomol Struct* 34:351-378.
- Kusumi, A., Y. Sako, and M. Yamamoto. 1993. Confined lateral diffusion of membrane receptors as studied by single particle tracking (nanovid microscopy). Effects of calcium-induced differentiation in cultured epithelial cells. *Biophys J* 65(5):2021-2040.
- Lafont, F., P. Verkade, T. Galli, C. Wimmer, D. Louvard, and K. Simons. 1999. Raft association of SNAP receptors acting in apical trafficking in Madin-Darby canine kidney cells. *Proc Natl Acad Sci U S A* 96(7):3734-3738.
- Lane, S.R., and Y. Liu. 1997. Characterization of the palmitoylation domain of SNAP-25. *J Neurochem* 69(5):1864-1869.
- Lang, T. 2007. SNARE proteins and 'membrane rafts'. *J Physiol* 585(Pt 3):693-698.
- Lang, T. 2008. Imaging Ca<sup>2+</sup>-triggered exocytosis of single secretory granules on plasma membrane lawns from neuroendocrine cells. *Methods Mol Biol* 440:51-59.
- Lang, T., D. Bruns, D. Wenzel, D. Riedel, P. Holroyd, C. Thiele, and R. Jahn. 2001. SNAREs are concentrated in cholesterol-dependent clusters that define docking

- 
- and fusion sites for exocytosis. *Embo J* 20(9):2202-2213.
- Lang, T., M. Margittai, H. Holzler, and R. Jahn. 2002. SNAREs in native plasma membranes are active and readily form core complexes with endogenous and exogenous SNAREs. *J Cell Biol* 158(4):751-760.
- Lang, T., and S.O. Rizzoli. Membrane protein clusters at nanoscale resolution: more than pretty pictures. *Physiology (Bethesda)* 25(2):116-124.
- Laude, A.J., and I.A. Prior. 2004. Plasma membrane microdomains: organization, function and trafficking. *Mol Membr Biol* 21(3):193-205.
- Lippincott-Schwartz, J., N. Altan-Bonnet, and G.H. Patterson. 2003. Photobleaching and photoactivation: following protein dynamics in living cells. *Nat Cell Biol Suppl*:S7-14.
- Liu, T., W.C. Tucker, A. Bhalla, E.R. Chapman, and J.C. Weisshaar. 2005. SNARE-driven, 25-millisecond vesicle fusion in vitro. *Biophys J* 89(4):2458-2472.
- Lommerse, P.H., H.P. Spaink, and T. Schmidt. 2004. In vivo plasma membrane organization: results of biophysical approaches. *Biochim Biophys Acta* 1664(2):119-131.
- Malsam, J., S. Kreye, and T.H. Sollner. 2008. Membrane fusion: SNAREs and regulation. *Cell Mol Life Sci* 65(18):2814-2832.
- Marash, M., and J.E. Gerst. 2001. t-SNARE dephosphorylation promotes SNARE assembly and exocytosis in yeast. *Embo J* 20(3):411-421.
- Margittai, M., D. Fasshauer, S. Pabst, R. Jahn, and R. Langen. 2001. Homo- and heterooligomeric SNARE complexes studied by site-directed spin labeling. *J Biol Chem* 276(16):13169-13177.
-

- 
- Marz, K.E., J.M. Lauer, and P.I. Hanson. 2003. Defining the SNARE complex binding surface of alpha-SNAP: implications for SNARE complex disassembly. *J Biol Chem* 278(29):27000-27008.
- Mayer, A. 2001. What drives membrane fusion in eukaryotes? *Trends Biochem Sci* 26(12):717-723.
- Mayer, A. 2002. Membrane fusion in eukaryotic cells. *Annu Rev Cell Dev Biol* 18:289-314.
- Mayor, S. and B., Sameera. 2007. Fretting about FRET in Cell and Structural Biology. Zuk D, editor. Cell Press, Cambridge, MA.
- McLaughlin, S., and D. Murray. 2005. Plasma membrane phosphoinositide organization by protein electrostatics. *Nature* 438(7068):605-611.
- McMahon, H.T., Y.A. Ushkaryov, L. Edelmann, E. Link, T. Binz, H. Niemann, R. Jahn, and T.C. Sudhof. 1993. Cellubrevin is a ubiquitous tetanus-toxin substrate homologous to a putative synaptic vesicle fusion protein. *Nature* 364(6435):346-349.
- McNew, J.A. 2008. Regulation of SNARE-mediated membrane fusion during exocytosis. *Chem Rev* 108(5):1669-1686.
- McNew, J.A., T. Weber, F. Parlati, R.J. Johnston, T.J. Melia, T.H. Sollner, and J.E. Rothman. 2000. Close is not enough: SNARE-dependent membrane fusion requires an active mechanism that transduces force to membrane anchors. *J Cell Biol* 150(1):105-117.
- Melia, T.J., T. Weber, J.A. McNew, L.E. Fisher, R.J. Johnston, F. Parlati, L.K. Mahal, T.H. Sollner, and J.E. Rothman. 2002. Regulation of membrane fusion by the membrane-proximal coil of the t-SNARE during zippering of SNAREpins. *J Cell*

---

*Biol* 158(5):929-940.

Mima, J., C.M. Hickey, H. Xu, Y. Jun, and W. Wickner. 2008. Reconstituted membrane fusion requires regulatory lipids, SNAREs and synergistic SNARE chaperones. *Embo J* 27(15):2031-2042.

Misura, K.M., R.H. Scheller, and W.I. Weis. 2000. Three-dimensional structure of the neuronal-Sec1-syntaxin 1a complex. *Nature* 404(6776):355-362.

Misura, K.M., R.H. Scheller, and W.I. Weis. 2001. Self-association of the H3 region of syntaxin 1A. Implications for intermediates in SNARE complex assembly. *J Biol Chem* 276(16):13273-13282.

Mohrmann, R., H. de Wit, M. Verhage, E. Neher, and J.B. Sorensen. Fast vesicle fusion in living cells requires at least three SNARE complexes. *Science* 330(6003):502-505.

Mulgrew-Nesbitt, A., K. Diraviyam, J. Wang, S. Singh, P. Murray, Z. Li, L. Rogers, N. Mirkovic, and D. Murray. 2006. The role of electrostatics in protein-membrane interactions. *Biochim Biophys Acta* 1761(8):812-826.

Nagy, G., U. Matti, R.B. Nehring, T. Binz, J. Rettig, E. Neher, and J.B. Sorensen. 2002. Protein kinase C-dependent phosphorylation of synaptosome-associated protein of 25 kDa at Ser187 potentiates vesicle recruitment. *J Neurosci* 22(21):9278-9286.

Nagy, G., I. Milosevic, D. Fasshauer, E.M. Muller, B.L. de Groot, T. Lang, M.C. Wilson, and J.B. Sorensen. 2005. Alternative splicing of SNAP-25 regulates secretion through nonconservative substitutions in the SNARE domain. *Mol Biol Cell* 16(12):5675-5685.

Novick, P., and M. Zerial. 1997. The diversity of Rab proteins in vesicle transport. *Curr Opin Cell Biol* 9(4):496-504.

- 
- Owen, D.M., D. Williamson, C. Rentero, and K. Gaus. 2009. Quantitative microscopy: protein dynamics and membrane organisation. *Traffic* 10(8):962-971.
- Oyler, G.A., G.A. Higgins, R.A. Hart, E. Battenberg, M. Billingsley, F.E. Bloom, and M.C. Wilson. 1989. The identification of a novel synaptosomal-associated protein, SNAP-25, differentially expressed by neuronal subpopulations. *J Cell Biol* 109(6 Pt 1):3039-3052.
- Parlati, F., O. Varlamov, K. Paz, J.A. McNew, D. Hurtado, T.H. Sollner, and J.E. Rothman. 2002. Distinct SNARE complexes mediating membrane fusion in Golgi transport based on combinatorial specificity. *Proc Natl Acad Sci U S A* 99(8):5424-5429.
- Permyakov, E.A., and R.H. Kretsinger. 2009. Cell signaling, beyond cytosolic calcium in eukaryotes. *J Inorg Biochem* 103(1):77-86.
- Pfeffer, S.R. 1999. Transport-vesicle targeting: tethers before SNAREs. *Nat Cell Biol* 1(1):E17-22.
- Pike, L.J. 2006. Rafts defined: a report on the Keystone Symposium on Lipid Rafts and Cell Function. *J Lipid Res* 47(7):1597-1598.
- Predescu, S.A., D.N. Predescu, K. Shimizu, I.K. Klein, and A.B. Malik. 2005. Cholesterol-dependent syntaxin-4 and SNAP-23 clustering regulates caveolae fusion with the endothelial plasma membrane. *J Biol Chem* 280(44):37130-37138.
- Rao, S.S., B.A. Stewart, P.K. Rivlin, I. Vilinsky, B.O. Watson, C. Lang, G. Boulianne, M.M. Salpeter, and D.L. Deitcher. 2001. Two distinct effects on neurotransmission in a temperature-sensitive SNAP-25 mutant. *Embo J* 20(23):6761-6771.
- Reits, E.A., and J.J. Neefjes. 2001. From fixed to FRAP: measuring protein mobility and activity in living cells. *Nat Cell Biol* 3(6):E145-147.

- 
- Rice, L.M., P. Brennwald, and A.T. Brunger. 1997. Formation of a yeast SNARE complex is accompanied by significant structural changes. *FEBS Lett* 415(1):49-55.
- Richmond, J.E., R.M. Weimer, and E.M. Jorgensen. 2001. An open form of syntaxin bypasses the requirement for UNC-13 in vesicle priming. *Nature* 412(6844):338-341.
- Rickman, C., C.N. Medine, A. Bergmann, and R.R. Duncan. 2007. Functionally and spatially distinct modes of munc18-syntaxin 1 interaction. *J Biol Chem* 282(16):12097-12103.
- Rickman, C., C.N. Medine, A.R. Dun, D.J. Moulton, O. Mandula, N.D. Halemani, S.O. Rizzoli, L.H. Chamberlain, and R.R. Duncan. 2010. t-SNARE protein conformations patterned by the lipid micro-environment. *J Biol Chem*.
- Ritchie, K., and J. Spector. 2007. Single molecule studies of molecular diffusion in cellular membranes: determining membrane structure. *Biopolymers* 87(2-3):95-101.
- Rizo, J., and C. Rosenmund. 2008. Synaptic vesicle fusion. *Nat Struct Mol Biol* 15(7):665-674.
- Rizzuto, R., and T. Pozzan. 2006. Microdomains of intracellular Ca<sup>2+</sup>: molecular determinants and functional consequences. *Physiol Rev* 86(1):369-408.
- Rosenmund, C., J. Rettig, and N. Brose. 2003. Molecular mechanisms of active zone function. *Curr Opin Neurobiol* 13(5):509-519.
- Rossi, G., A. Salminen, L.M. Rice, A.T. Brunger, and P. Brennwald. 1997. Analysis of a yeast SNARE complex reveals remarkable similarity to the neuronal SNARE complex and a novel function for the C terminus of the SNAP-25 homolog, Sec9.

---

*J Biol Chem* 272(26):16610-16617.

Sakaba, T., A. Stein, R. Jahn, and E. Neher. 2005. Distinct kinetic changes in neurotransmitter release after SNARE protein cleavage. *Science* 309(5733):491-494.

Sakon, J.J., and K.R. Weninger. Detecting the conformation of individual proteins in live cells. *Nat Methods* 7(3):203-205.

Salaun, C., G.W. Gould, and L.H. Chamberlain. 2005a. Lipid raft association of SNARE proteins regulates exocytosis in PC12 cells. *J Biol Chem* 280(20):19449-19453.

Salaun, C., G.W. Gould, and L.H. Chamberlain. 2005b. The SNARE proteins SNAP-25 and SNAP-23 display different affinities for lipid rafts in PC12 cells. Regulation by distinct cysteine-rich domains. *J Biol Chem* 280(2):1236-1240.

Salaun, C., D.J. James, and L.H. Chamberlain. 2004a. Lipid rafts and the regulation of exocytosis. *Traffic* 5(4):255-264.

Salaun, C., D.J. James, J. Greaves, and L.H. Chamberlain. 2004b. Plasma membrane targeting of exocytic SNARE proteins. *Biochim Biophys Acta* 1693(2):81-89.

Sambrook, J., Russel, D.W. 2001. Molecular cloning: a laboratory manual. Cold Spring Harbor Laboratory Press, Cold Spring Harbor.

Schiavo, G., F. Benfenati, B. Poulain, O. Rossetto, P. Polverino de Laureto, B.R. DasGupta, and C. Montecucco. 1992. Tetanus and botulinum-B neurotoxins block neurotransmitter release by proteolytic cleavage of synaptobrevin. *Nature* 359(6398):832-835.

Schiavo, G., C.C. Shone, O. Rossetto, F.C. Alexander, and C. Montecucco. 1993. Botulinum neurotoxin serotype F is a zinc endopeptidase specific for

---

VAMP/synaptobrevin. *J Biol Chem* 268(16):11516-11519.

Sieber, J.J., K.I. Willig, R. Heintzmann, S.W. Hell, and T. Lang. 2006. The SNARE motif is essential for the formation of syntaxin clusters in the plasma membrane. *Biophys J* 90(8):2843-2851.

Sieber, J.J., K.I. Willig, C. Kutzner, C. Gerding-Reimers, B. Harke, G. Donnert, B. Rammner, C. Eggeling, S.W. Hell, H. Grubmüller, and T. Lang. 2007. Anatomy and dynamics of a supramolecular membrane protein cluster. *Science* 317(5841):1072-1076.

Simons, K., and E. Ikonen. 1997. Functional rafts in cell membranes. *Nature* 387(6633):569-572.

Simons, K., and D. Toomre. 2000. Lipid rafts and signal transduction. *Nat Rev Mol Cell Biol* 1(1):31-39.

Singer, S.J., and G.L. Nicolson. 1972. The fluid mosaic model of the structure of cell membranes. *Science* 175(23):720-731.

Smyth, A.M., R.R. Duncan, and C. Rickman. 2010. Munc18-1 and Syntaxin1: Unraveling the Interactions Between the Dynamic Duo. *Cell Mol Neurobiol*.

Sollner, T., M.K. Bennett, S.W. Whiteheart, R.H. Scheller, and J.E. Rothman. 1993a. A protein assembly-disassembly pathway in vitro that may correspond to sequential steps of synaptic vesicle docking, activation, and fusion. *Cell* 75(3):409-418.

Sollner, T., S.W. Whiteheart, M. Brunner, H. Erdjument-Bromage, S. Geromanos, P. Tempst, and J.E. Rothman. 1993b. SNAP receptors implicated in vesicle targeting and fusion. *Nature* 362(6418):318-324.

Sorensen, J.B. 2009. Conflicting views on the membrane fusion machinery and the



---

fusion pore. *Annu Rev Cell Dev Biol* 25:513-537.

Sorensen, J.B., G. Nagy, F. Varoqueaux, R.B. Nehring, N. Brose, M.C. Wilson, and E. Neher. 2003. Differential control of the releasable vesicle pools by SNAP-25 splice variants and SNAP-23. *Cell* 114(1):75-86.

Spafford, J.D., and G.W. Zamponi. 2003. Functional interactions between presynaptic calcium channels and the neurotransmitter release machinery. *Curr Opin Neurobiol* 13(3):308-314.

Stein, A., G. Weber, M.C. Wahl, and R. Jahn. 2009. Helical extension of the neuronal SNARE complex into the membrane. *Nature* 460(7254):525-528.

Su, Z., Y. Ishitsuka, T. Ha, and Y.K. Shin. 2008. The SNARE complex from yeast is partially unstructured on the membrane. *Structure* 16(7):1138-1146.

Sudhof, T.C. 2004. The synaptic vesicle cycle. *Annu Rev Neurosci* 27:509-547.

Sudhof, T.C., M. Baumert, M.S. Perin, and R. Jahn. 1989. A synaptic vesicle membrane protein is conserved from mammals to *Drosophila*. *Neuron* 2(5):1475-1481.

Sudhof, T.C., and J.E. Rothman. 2009. Membrane fusion: grappling with SNARE and SM proteins. *Science* 323(5913):474-477.

Sutton, R.B., D. Fasshauer, R. Jahn, and A.T. Brunger. 1998. Crystal structure of a SNARE complex involved in synaptic exocytosis at 2.4 Å resolution. *Nature* 395(6700):347-353.

Takahashi, N., H. Hatakeyama, H. Okado, J. Noguchi, M. Ohno, and H. Kasai. 2010. SNARE conformational changes that prepare vesicles for exocytosis. *Cell Metab* 12(1):19-29.

- 
- Toonen, R.F., O. Kochubey, H. de Wit, A. Gulyas-Kovacs, B. Konijnenburg, J.B. Sorensen, J. Klingauf, and M. Verhage. 2006. Dissecting docking and tethering of secretory vesicles at the target membrane. *Embo J* 25(16):3725-3737.
- Tooze, S.A., G.J. Martens, and W.B. Huttner. 2001. Secretory granule biogenesis: rafting to the SNARE. *Trends Cell Biol* 11(3):116-122.
- Tsien, R., and T. Pozzan. 1989. Measurement of cytosolic free Ca<sup>2+</sup> with quin2. *Methods Enzymol* 172:230-262.
- Tucker, W.C., J.M. Edwardson, J. Bai, H.J. Kim, T.F. Martin, and E.R. Chapman. 2003. Identification of synaptotagmin effectors via acute inhibition of secretion from cracked PC12 cells. *J Cell Biol* 162(2):199-209.
- Ungar, D., and F.M. Hughson. 2003. SNARE protein structure and function. *Annu Rev Cell Dev Biol* 19:493-517.
- van den Bogaart, G., M.G. Holt, G. Bunt, D. Riedel, F.S. Wouters, and R. Jahn. 2010. One SNARE complex is sufficient for membrane fusion. *Nat Struct Mol Biol* 17(3):358-364.
- van Meer, G., D.R. Voelker, and G.W. Feigenson. 2008. Membrane lipids: where they are and how they behave. *Nat Rev Mol Cell Biol* 9(2):112-124.
- Veit, M., T.H. Sollner, and J.E. Rothman. 1996. Multiple palmitoylation of synaptotagmin and the t-SNARE SNAP-25. *FEBS Lett* 385(1-2):119-123.
- Verhage, M., A.S. Maia, J.J. Plomp, A.B. Brussaard, J.H. Heeroma, H. Vermeer, R.F. Toonen, R.E. Hammer, T.K. van den Berg, M. Missler, H.J. Geuze, and T.C. Sudhof. 2000. Synaptic assembly of the brain in the absence of neurotransmitter secretion. *Science* 287(5454):864-869.

- 
- von Heijne, G. 1991. Proline kinks in transmembrane alpha-helices. *J Mol Biol* 218(3):499-503.
- Wang, L., M.A. Bittner, D. Axelrod, and R.W. Holz. 2008. The structural and functional implications of linked SNARE motifs in SNAP25. *Mol Biol Cell* 19(9):3944-3955.
- Washbourne, P., P.M. Thompson, M. Carta, E.T. Costa, J.R. Mathews, G. Lopez-Bendito, Z. Molnar, M.W. Becher, C.F. Valenzuela, L.D. Partridge, and M.C. Wilson. 2002. Genetic ablation of the t-SNARE SNAP-25 distinguishes mechanisms of neuroexocytosis. *Nat Neurosci* 5(1):19-26.
- Weber, T., B.V. Zemelman, J.A. McNew, B. Westermann, M. Gmachl, F. Parlati, T.H. Sollner, and J.E. Rothman. 1998. SNAREpins: minimal machinery for membrane fusion. *Cell* 92(6):759-772.
- Weninger, K., M.E. Bowen, U.B. Choi, S. Chu, and A.T. Brunger. 2008. Accessory proteins stabilize the acceptor complex for synaptobrevin, the 1:1 syntaxin/SNAP-25 complex. *Structure* 16(2):308-320.
- Wickner, W. Membrane fusion: five lipids, four SNAREs, three chaperones, two nucleotides, and a Rab, all dancing in a ring on yeast vacuoles. *Annu Rev Cell Dev Biol* 26:115-136.
- Willig, K.I., Keller, J., Bossi, M. & Hell, S.W. 2006. STED microscopy resolves nanoparticle assemblies. *New J. Phys.* 8:106.
- Woodbury, D.J., and K. Rognlien. 2000. The t-SNARE syntaxin is sufficient for spontaneous fusion of synaptic vesicles to planar membranes. *Cell Biol Int* 24(11):809-818.
- Xiao, W., M.A. Poirier, M.K. Bennett, and Y.K. Shin. 2001. The neuronal t-SNARE

---

complex is a parallel four-helix bundle. *Nat Struct Biol* 8(4):308-311.

- Xu, T., B. Rammner, M. Margittai, A.R. Artalejo, E. Neher, and R. Jahn. 1999. Inhibition of SNARE complex assembly differentially affects kinetic components of exocytosis. *Cell* 99(7):713-722.
- Yang, B., L. Gonzalez, Jr., R. Prekeris, M. Steegmaier, R.J. Advani, and R.H. Scheller. 1999. SNARE interactions are not selective. Implications for membrane fusion specificity. *J Biol Chem* 274(9):5649-5653.
- Zacharias, D.A., J.D. Violin, A.C. Newton, and R.Y. Tsien. 2002. Partitioning of lipid-modified monomeric GFPs into membrane microdomains of live cells. *Science* 296(5569):913-916.
- Zerial, M., and H. McBride. 2001. Rab proteins as membrane organizers. *Nat Rev Mol Cell Biol* 2(2):107-117.
- Zhang, F., Y. Chen, D.H. Kweon, C.S. Kim, and Y.K. Shin. 2002. The four-helix bundle of the neuronal target membrane SNARE complex is neither disordered in the middle nor uncoiled at the C-terminal region. *J Biol Chem* 277(27):24294-24298.
- Zhong, P., Y.A. Chen, D. Tam, D. Chung, R.H. Scheller, and G.P. Miljanich. 1997. An alpha-helical minimal binding domain within the H3 domain of syntaxin is required for SNAP-25 binding. *Biochemistry* 36(14):4317-4326.
- Zilly, F.E., J.B. Sorensen, R. Jahn, and T. Lang. 2006. Munc18-Bound Syntaxin Readily Forms SNARE Complexes with Synaptobrevin in Native Plasma Membranes. *PLoS Biol* 4(10):e330.
- Zilly, F.E., N.D. Halemani, D. Walrafen, L. Spitta, A. Schreiber, R. Jahn and T. Lang. 2011. Ca<sup>2+</sup> induces clustering of membrane proteins in the plasma membrane via electrostatic interactions. *EMBO J.* 30, 1209–1220.

Zimmerberg, J., and K. Gawrisch. 2006. The physical chemistry of biological membranes. *Nat Chem Biol* 2(11):564-567.

---

**6. List of abbreviations used**

<b>3D</b>	three dimensional
<b>Å</b>	Angstrom
<b>AA</b>	Aminoacid
<b>AOTF</b>	Acousto-Optical Tunable Filter
<b>ATP</b>	Adenosine triphosphate
<b>a.u.</b>	Arbitrary units
<b>BP</b>	Bandpass
<b>BSA</b>	Bovine Serum-Albumin
<b>BHK</b>	Baby Hamster Kidney
<b>BoNT</b>	Botulinum Neurotoxin
<b>CAPS</b>	Ca <sup>2+</sup> - dependent activator protein for secretion
<b>CCD</b>	Charge coupled device
<b>CFP</b>	Cyan Flourescent protein
<b>CMV</b>	Cytomegalo virus
<b>CNT</b>	Clostridial neurotoxin
<b>C-t/C-term.</b>	C-terminal
<b>DAPI</b>	4',6-diamidino-2-phenylindol
<b>DHHC</b>	(Asp-His-His-Cys)
<b>DMEM</b>	Dulbecco's modified Eagle medium
<b>DNA</b>	Deoxyribonucleic acid
<b>DPTA</b>	1,3-diamino-2-propanol-N,N,N',N' - tetra acetic acid
<b>DRM</b>	Detergent-resistant-membrane
<b>DTT</b>	Dithiothreitol
<b>E.coli</b>	Escherichia coli
<b>EGFP</b>	Enhanced Green Fluorescent protein
<b>EGTA</b>	Ethyleneglycol-bis-(2-aminoethylether) - N,N,N',N' - tetraacetic acid
<b>EPR</b>	Electron paramagnetic resonance
<b>FCS</b>	Fluorescence Correlation Spectroscopy
<b>FLIM</b>	Flourescence Life time Imaging
<b>FRAP</b>	Flourescence Recovery After Photobleaching
<b>FRET</b>	Förster Resonance Energy Transfer

---

<b>GTP</b>	Guanosine triphosphate
<b>kDa</b>	Kilo Dalton
<b>KGlu</b>	Potassium glutamate
<b>LP</b>	Long pass
<b>M<math>\beta</math>CD</b>	Methyl- $\beta$ -cyclodextrin
<b>mEGFP</b>	monomeric EGFP
<b>Munc13</b>	<i>mamalian</i> Unc-13
<b>Munc18</b>	<i>mamalian</i> Unc-18
<b>NA</b>	Numerical Aperture
<b>NEM</b>	N-ethyl-maleimide
<b>NSF</b>	N-ethylmaleimide-sensitive factor
<b>N-t/N-term.</b>	N-terminal
<b>PAGE</b>	Polyacrylamide gel electrophoresis
<b>PBS</b>	Phosphate buffered saline
<b>PFA</b>	Paraformaldehyde
<b>pH</b>	Negative logarithm of H <sup>+</sup> concentration
<b>PC12</b>	Phaeochromocytoma
<b>PCR</b>	Polymerase-Chain-Reaction
<b>PM</b>	Plasma membrane
<b>PIP2</b>	Phosphatidyl-Inositol-Bis-Phosphate
<b>PSF</b>	Point Spread Function
<b>RIM</b>	Rab3-interacting molecule
<b>ROI</b>	Regions-of-Interest
<b>RT</b>	Room temperature
<b>S</b>	second
<b>SDS</b>	Sodium dodecyl sulfate
<b>SD</b>	Standard deviation
<b>SEM</b>	Standard error of the mean
<b>SM-Family</b>	Sec1/Munc18-Family
<b>SNAP</b>	Soluble-NSF-attachment protein
<b>SNAP-25</b>	Synaptosome associated protein of 25 kDa
<b>SN25</b>	SNAP-25

<b>SNARE</b>	Soluble N-ethylmaleimide Sensitive Factor (NSF) Attachment Protein Receptor
<b>STED</b>	Stimulated-Emission-Depletion
<b>Syx</b>	Syntaxin
<b>TMA-DPH</b>	1-(4- trimethyl-ammonium phenyl)-6-phenyl-1,3,5-hexatriene <i>p</i> -toluenesulfonate
<b>TeNT</b>	Tetanus Neurotoxin
<b>t-SNARE</b>	Target SNARE (used interchangeably with Q-SNAREs)
<b>v-SNARE</b>	vesicle SNARE
<b>Unc</b>	uncoordinated locomotion
<b>VAMP</b>	Vesicle associated membrane protein



## 7. List of Figures

<b>Figure 1.</b> Models for membrane structure	03
<b>Figure 2.</b> Stages of membrane fusion	05
<b>Figure 3.</b> Proteolytic cleavage of neuronal SNAREs	11
<b>Figure 4.</b> The primary structure diagram for SNAP-25	11
<b>Figure 5.</b> The primary structure diagram for syntaxin1	13
<b>Figure 6.</b> The primary structure diagram for synaptobrevin	14
<b>Figure 7.</b> The SNARE conformational cycle during vesicle docking and fusion	15
<b>Figure 8.</b> The neuronal ternary SNARE complex	22
<b>Figure 9.</b> Domain structure of GFP-SNAP-25 constructs	40
<b>Figure 10.</b> Immunoblot analysis expression of GFP-SNAP-25 and its mutant constructs in PC12 cells	42
<b>Figure 11.</b> FRAP micrographs and recovery traces	44
<b>Figure 12.</b> Restriction of SNAP-25 mobility involves its N-terminal SNARE-motif	45
<b>Figure 13.</b> Confocal micrographs monitoring the basal plasma membrane of a PC12 cell expressing GFP-labelled SNAP25 and syntaxin 1-CFP	47
<b>Figure 14.</b> Half times of recovery as a function of syntaxin 1-CFP levels shown for SNAP-25, SN25-N <sub>L</sub> 0, SN25-0 <sub>L</sub> C and SN25-0 <sub>L</sub> 0	48
<b>Figure 15.</b> Restriction of SNAP-25 mobility involves its N-terminal SNARE-motif and syntaxin	49
<b>Figure 16.</b> Half times of recovery as a function of syntaxin 1-CFP levels shown for SNAP-25, SN25-N <sub>L</sub> N, SN25-C <sub>L</sub> C and SN25-0 <sub>L</sub> N	51
<b>Figure 17.</b> Positional specificity of the N-terminus of SNAP-25 for its interaction with syntaxin	52
<b>Figure 18.</b> Illustration of N-terminal SNARE motif amino acid deletion constructs	53
<b>Figure 19.</b> Half times of recovery as a function of syntaxin 1-CFP levels shown for SNAP-25 and deletion constructs, including deletion from residues -7 to -5, -7 to -2 and from -7 to +3	54
<b>Figure 20.</b> SNAP-25 interaction with syntaxin requires N-terminal amino acids	54
<b>Figure 21.</b> Illustration of amino acid substitution constructs	56

---

<b>Figure 22.</b> Half times of recovery as a function of syntaxin 1-CFP levels shown for SNAP-25 and the AA substitution constructs – M32P-V36P, I60P-M64P and G43D	57
<b>Figure 23.</b> Effect of amino acid substitution in N-terminal SNARE motif on SNAP-25 / syntaxin 1 interactions	57
<b>Figure 24.</b> Correlation of expression levels and maximal recovery or half time of recovery	59
<b>Figure 25.</b> SNAP-25 interacts with non-cognate Q <sub>a</sub> - SNARE syntaxin 4 in PC12 cells	61
<b>Figure 26.</b> SNAP-25 - syntaxin interactions require no neuronal co-factors	63
<b>Figure 27.</b> Representative images of binding of soluble syntaxin 1 with membrane sheets expressing either SNAP-25 or SN25-0 <sub>L</sub> 0	66
<b>Figure 28.</b> Soluble syntaxin 1 readily reacts with the N-terminal SNARE motif of SNAP-25	67
<b>Figure 29.</b> Enhanced reactivity mediated by the N-terminal position does not require parallel oriented syntaxin	68
<b>Figure 30.</b> SNAP-25 or SN25-0 <sub>L</sub> 0 signal distribution characterized by autocorrelation analysis	71
<b>Figure 31.</b> Representative images of co-localisation studies of SNAP-25/SN-25-0 <sub>L</sub> 0 and syntaxin 1 clusters	73
<b>Figure 32.</b> Co-localisation analysis of syntaxin 1 and STED-resolved SNAP-25 and SN25-0 <sub>L</sub> 0 images	74
<b>Figure 33.</b> Representative images of co-localisation studies of SNAP-25/SN25-0 <sub>L</sub> 0 and syntaxin 4 clusters	76
<b>Figure 34.</b> Co-localisation analysis of syntaxin 4 and STED-resolved SNAP-25 and SN25-0 <sub>L</sub> 0 images	77
<b>Figure 35.</b> Overlap between syntaxin 1 and SNAP-25/SN25-0 <sub>L</sub> 0 upon incubation without synaptobrevin 2	79
<b>Figure 36.</b> Quantification of the overlap between syntaxin 1 and SNAP-25/SN25-0 <sub>L</sub> 0 upon incubation without synaptobrevin 2	80
<b>Figure 37.</b> Overlap between syntaxin 1 and SNAP-25/SN25-0 <sub>L</sub> 0 upon incubation with synaptobrevin 2	81

---

<b>Figure 38.</b> Quantification of the overlap between syntaxin 1 and SNAP-25/SN25-0L0 upon incubation with synaptobrevin 2	82
<b>Figure 39.</b> Effect of cholesterol depletion on syntaxin 1 cluster morphology	84
<b>Figure 40.</b> An increase in intracellular calcium diminishes membrane protein immunostaining intensities	86
<b>Figure 41.</b> Influence of the incubation process and Mg <sup>2+</sup> ions on the membrane protein immunostaining intensities	88
<b>Figure 42.</b> Effect of calcium on plasma membrane proteins	90
<b>Figure 43.</b> Confocal micrographs of bovine chromaffin cells stimulated by depolarisation with high potassium	92
<b>Figure 44.</b> Quantification of depolarisation induced decrease in the membrane protein immunostaining	93
<b>Figure 45.</b> SNARE complexes forming <i>in vitro</i> and <i>in vivo</i>	98
 <b>Figures from Appendix</b>	
<b>Figure 1.</b> Co-immunoprecipitation (IP) of SNAP-25 with syntaxin 1 or syntaxin 4 antibodies from PC12 cell extracts	133
<b>Figure 2.</b> Co-immunoprecipitation of GFP-labeled SNAP-25 / SNAP-25 constructs by anti-syntaxin 1 antibody	134

**8. List of Tables**

<b>Table 1.</b> Free calcium in the buffer solution	28
---	----

## 9. Curriculum Vitae (in brief)

### NAGARAJ D HALEMANI

#### Education

- 1) Currently pursuing **Ph.D** at the Membrane Biochemistry Unit (Prof Thorsten Lang), LIMES institute, Uni. Bonn, Bonn, Germany and formerly at the Dept.of Neurobiology (Prof. Reinhard Jahn), Max Planck Institute of Biophysical Chemistry (MPIBPC), Göttingen since 01 March 2006.
- 2) **MSc** (Master of Science) in Molecular Genetics - Dept. of Genetics, University of Leicester, Leicester. UK. Sept. 2004 to Sept. 2005.
- 3) **M.B, B.S** (Bachelor of Medicine and Bachelor of Surgery – equivalent to European medical degree M.D), Mysore Medical College, Mysore, India. August 1995 to Sept 2001.
- 4) **High School** - Jawahar Navodaya Vidyalaya, Kuknoor, Koppal, Karnataka, India. -August 1989 to March 1995.

#### Employment details

- 1) 2002 June to 2002 August – Chinmaya Mission Hospital, Bangalore, India - Junior Resident Doctor.
- 2) 2002 August to 2003 April – MIND (Manipal Institute for Neurological Disorders), Manipal Hospital Bangalore, India. – Junior Resident Doctor in department of Neurology.
- 3) 2003 May to 2004 March - Voluntary Community Healthcare Services at my resident village in India.
- 4) April 2004 to August 2004 – MIND, Manipal Hospital Bangalore, India - Clinical Research Assistant in department of Neurosurgery – Antisense gene therapy (TGFbeta2 antisense therapy) for malignant gliomas.

## 10. Appendix

### 10.1 Co-immunoprecipitation (IP) of SNAP-25 with syntaxin 1 and syntaxin 4

In order to clarify to what extent SNAP-25 physically associates with syntaxin 1 and syntaxin 4, IP studies were performed. With syntaxin 1 antibodies approx.20% of SNAP-25 was pulled down but only 2% when syntaxin 4 were used (see Figure 1 below) reflecting the measured microscopic cluster overlap (see Figures 32 & 34 of main text).

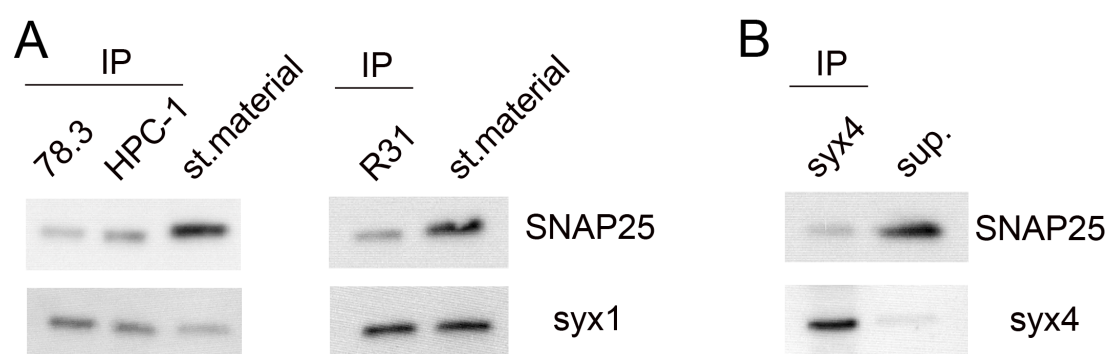


**Figure 1. Co-immunoprecipitation (IP) of SNAP-25 with (A) syntaxin1 or (B) syntaxin 4 antibodies from PC12 cell extracts.** (A) PC12 cells were solubilized in Triton X-100 and for co-IP of SNAP-25 three different anti-syntaxin 1 antibodies were used (rabbit polyclonal R31 and mouse monoclonals 78.3 and HPC-1). For immunoblot analysis, 10% from the immunoprecipitate and 1.66% from the starting material were loaded. For immunoblotting, SNAP-25 and syntaxin were detected using either polyclonal antibodies (Casanova for SNAP-25 and R31 for syntaxin 1 when for IP a monoclonal antibody was used) or monoclonal antibodies (71.1 for SNAP-25 and 78.3 for syntaxin 1 when a polyclonal antibody was used for immunoprecipitation). The percentage of SNAP-25 in the precipitate was calculated and multiplied by the efficiency (1 = 100%) of the IP as judged from the percentage of precipitated syntaxin. For each syntaxin antibody, three independent experiments were performed. On average, 19% (15.4%, 15.2% and 26.5% for R31, 78.3 and HPC-1, respectively) of SNAP-25 co-immunoprecipitated with syntaxin. (B) Co-IP from Triton X-100 solubilized PC12 cells using an anti-syntaxin 4 antibody. For immunoblotting SNAP-25 (using monoclonal 71.1 as antibody), 10 % of the immunoprecipitate and 0.8 % of the supernatant were loaded; for the syntaxin 4 (using polyclonal anti-syntaxin 4 antibody) blot, 10% of the immunoprecipitate and 2.4% of the supernatant were loaded. The percentage of SNAP-25 in the precipitate was calculated and multiplied by the efficiency (1 = 100%) of the IP as judged from the percentage of precipitated syntaxin 4. On average (n=3 experiments), 2.04% of SNAP-25 coimmunoprecipitated with syntaxin 4. [The figure is taken from \(Halemani et al., 2010\).](#)

## 10.2 Co-immunoprecipitation (IP) of GFP-SNAP-25 constructs with syntaxin 1

To check to what extent overexpressed GFP-SNAP-25 constructs are physically associated with endogenous syntaxin 1 IP studies for syntaxin were performed and the following values were obtained: 2.09% of GFP-SNAP-25, 2.29% of GFP-SN25-N<sub>L</sub>0, 0.28% of GFP-SN25-0<sub>L</sub>C and -0.25% of GFP- SN25-0<sub>L</sub>0 co-immunoprecipitated with syntaxin1 (see Figure 2 A).

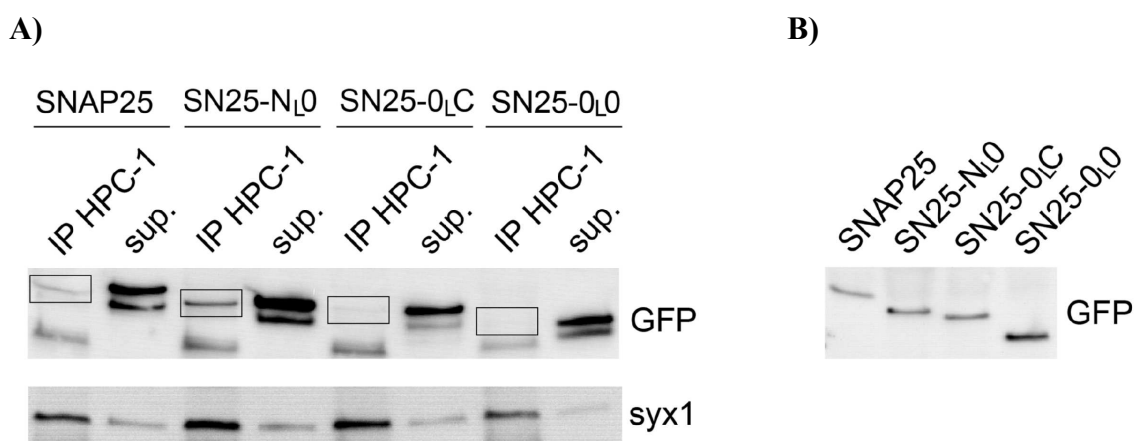


**Figure 2. Co-immunoprecipitation of GFP-labeled SNAP-25 / SNAP-25 constructs by anti-syntaxin 1 antibody.** (A) PC12 cells expressing either GFP-SNAP-25, GFP-SN25-N<sub>L</sub>0, GFP-SN25-0<sub>L</sub>C or GFP-SN25-0<sub>L</sub>0 were lysed (using 1% Triton X-100) and it was analyzed if GFP-labelled constructs co-immunoprecipitate with syntaxin 1 using a monoclonal anti-syntaxin 1 antibody (HPC-1). For immunoblotting of GFP (using a polyclonal anti-GFP antibody) and syntaxin 1 (using monoclonal antibody 78.3), 24% of the immunoprecipitate and 0.8 % of the supernatant were loaded. Boxes mark areas where co immunoprecipitated bands should appear. For each construct, the percentage of GFP in the precipitate was calculated and multiplied by the efficiency (1 = 100%) of the IP as judged from the percentage of precipitated syntaxin 1 in each case. From duplicate blots we determined that 2.09% of GFP-SNAP-25, 2.29% of GFP- SN25-N<sub>L</sub>0, 0.28% of GFP-SN25-0<sub>L</sub>C and -0.25% of GFP-SN25-0<sub>L</sub>0 co-immunoprecipitated with syntaxin1. (B) Control experiment - Directly blotting the freshly lysed cells eliminates the occurrence of degradation bands evident in panel A (especially in the supernatants) showing that the degradation occurs during IP processing. [The figure is taken from \(Halemani et al., 2010\).](#)